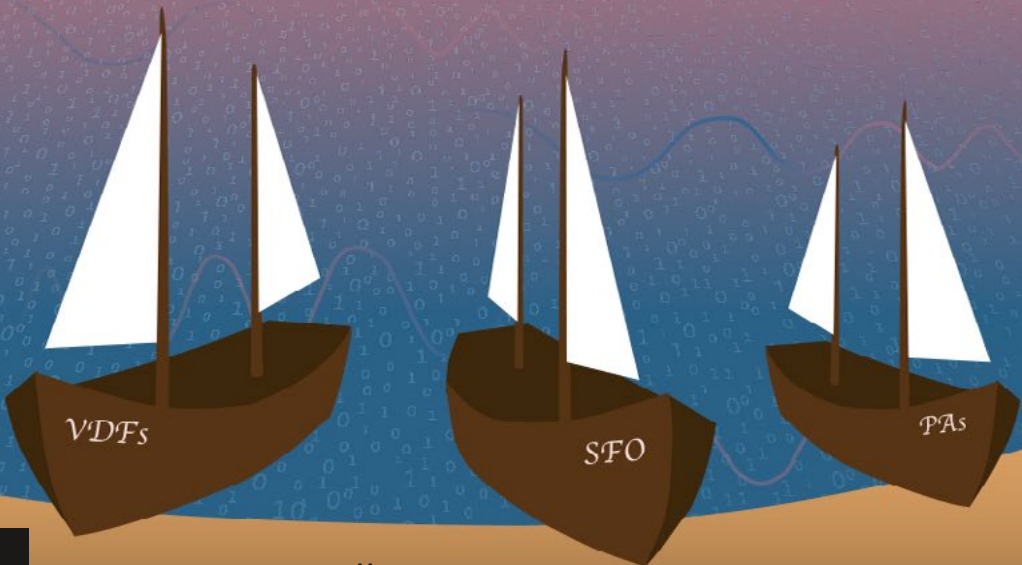


Linköping Studies in Science and Technology
Dissertations, No. 2517

Efficient Signal Processing Algorithms for Reconfigurable Digital Filtering, Synchronization, and Power Amplifier Linearization

Oksana Moryakova



Linköping Studies in Science and Technology
Dissertations, No. 2517

Efficient Signal Processing Algorithms for Reconfigurable Digital Filtering, Synchronization, and Power Amplifier Linearization

Oksana Moryakova



Division of Communication Systems
Department of Electrical Engineering (ISY)
Linköping University, 581 83, Linköping, Sweden
<https://liu.se/organisation/liu/isy/ks>

Linköping 2026

This is a Swedish Doctor of Philosophy thesis.
The Doctor of Philosophy degree comprises 240 ECTS credits of
postgraduate studies.

Cover: The main contributions of the thesis are represented by three boats in the world of digital communication systems. The boats, labeled VDFs, SFO, and PAs, symbolize variable digital filters, sampling frequency synchronization, and power amplifiers. Their position at the shore illustrates that they are ready to depart into the practical world of communication systems. The design is inspired by the quote, “*We cannot direct the wind, but we can adjust the sails,*” reflecting the idea that real communication systems cannot be fully controlled and that signals are inevitably affected by channel conditions, hardware nonidealities, and other impairments. The sea represents this challenging practical environment, while the boats symbolize the methods developed in the thesis to address these challenges. Just as sails are adjusted to adapt to the wind and make effective use of it, the contributions of this thesis employ efficient and reconfigurable signal processing algorithms to address the various challenges encountered in communication systems. The sunset symbolizes the end of my PhD journey, while also hinting at a new day and new opportunities ahead.

Efficient Signal Processing Algorithms for Reconfigurable Digital Filtering, Synchronization, and Power Amplifier Linearization

© 2026 Oksana Moryakova, unless otherwise stated.

ISBN 978-91-8118-536-2(print)

ISBN 978-91-8118-537-9(PDF)

ISSN 0345-7524

URL <https://doi.org/10.3384/9789181185379>

Printed in Sweden by LiU-Tryck, Linköping 2026



Except where otherwise noted, this work is licensed under a
Creative Commons Attribution 4.0 International License.

<https://creativecommons.org/licenses/by/4.0/>

To my family

*“We cannot direct the wind,
but we can adjust the sails.”*

—Unknown

Abstract

Complexity reduction and reconfigurability are challenges in the design of modern communication system front-ends. Each new generation of communication standards brings more stringent requirements on data rates, bandwidth, synchronization, and spectral efficiency, which in turn can lead to increased power consumption and chip area. To meet these requirements and at the same time prevent a rapid growth in power consumption and silicon area, it is necessary to develop more sophisticated digital signal processing (DSP) algorithms that simultaneously can achieve high performance, flexibility, and low implementation cost, particularly in hardware-constrained receiver and transmitter front-ends. This thesis investigates efficient signal processing techniques for reconfigurable communication system front-ends and presents contributions in three directions: design and implementation of variable digital filters (VDFs), efficient synchronization techniques, particularly sampling frequency offset (SFO) estimation and compensation using VDFs, and analysis and optimization of cascaded power amplifiers (PAs), specifically their accumulated nonlinearities.

Since digital filters form the core of DSP algorithms, a key candidate for efficient reconfigurability in digital front-ends is the class of VDFs, which are capable of real-time frequency response tuning without the need for online filter design. The main advantage of VDFs is that they require only an adjustment of one or a few parameters to change their characteristics, while the majority of filter coefficients remain fixed after the initial design. This property eliminates the need for extensive online computations and makes VDFs particularly attractive for modern adaptive communication technologies, enabling efficient hardware implementation. In this area, various aspects of design and implementation of VDFs are presented in the thesis, including: (i) implementations and systematic design procedures based on minimax optimization for reconfigurable finite-impulse-response (FIR) filters for simultaneous equalization and lowpass filtering; (ii) an analysis of chip area and power consumption for application-specific integrated circuit (ASIC)

implementation of the reconfigurable lowpass equalizer with simultaneously variable bandwidth; (iii) low-complexity frequency-domain implementations of VDFs based on the assumption that these filters have been designed using a common time-domain design approach based on optimizing the impulse response coefficients; (iv) efficient frequency-sampling-based design approaches (minimax based and closed-form least-squares) for a variable-bandwidth FIR filter implemented in the frequency domain, allowing for direct optimization of the DFT coefficients considering the filter frequency-domain implementation and thereby resulting in a substantial reduction in implementation complexity.

Further, accurate synchronization is essential for reliable operation of communication systems, as synchronization errors can significantly degrade overall system performance. Among these impairments, SFO is critical, especially in modern wideband and high-speed communication systems, where even tiny differences between sampling clocks lead to a noticeable cumulative timing drift, resulting in inter-carrier and inter-symbol interference. While the SFO compensation is commonly carried out in the time domain, most existing SFO estimation methods are formulated in the frequency domain, which are generally quite computationally demanding, and it results in a separation between estimation and compensation stages. In contrast to these traditional approaches, this thesis presents two contributions in this area, specifically: (i) a joint SFO estimation and compensation framework based on a variable-fractional-delay filter, that results in reduced implementation complexity of the SFO estimation and is applicable to arbitrary bandlimited signals; (ii) a generalized accumulator-based approach for efficient computation of time-index powered weighted sums, which is employed in the proposed SFO estimation algorithms to implement computation of time-index and time-index-squared weighted sums in an efficient way leading to eliminating considerable parts of multiplications.

Finally, recent advances in wireless communication systems have shown the need for a reconfigurable number of cascaded power amplifiers (PAs). While PAs generally constitute one of the main sources of nonlinearities in a transceiver that distort the transmitted signal and degrade the overall system performance, in cascaded PAs, the distortions from each amplifier accumulate with those from the preceding stages, leading to severe nonlinear behavior. Considering the requirements on high efficiency and a maximally linear operation regime, this thesis investigates the effect of total nonlinearities occurring in cascaded PAs by providing results on modeling, analysis, linearization, and optimization of cascaded amplifiers.

Populärvetenskaplig Sammanfattning

Komplexitetsreduktion och avstämbarhet är utmaningar i konstruktion av moderna kommunikationssystem så kallade front-ends. Varje ny generation av kommunikationsstandard medför strängare krav på datahastigheter, bandbredd, synkronisering och spektral effektivitet, vilket i sin tur kan leda till ökad strömförbrukning och chiparea i en hårdvaruimplementering. För att möta dessa krav och samtidigt förhindra ökning av strömförbrukning och kiselarea är det nödvändigt att utveckla mer sofistikerade algoritmer för digital signalbehandling (DSB) som samtidigt kan uppnå en hög prestanda, flexibilitet och låg implementeringskostnad, särskilt i hårdvarubegränsade mottagar- och sändar-front-ends. Denna avhandling studerar effektiva signalbehandlingstekniker och presenterar tre olika bidrag: konstruktion och implementering av avstämbara digitala filter (VDF), effektiva synkroniseringstekniker, särskilt estimering och kompensation av samplingsfrekvensoffsetet (SFO) med hjälp av VDF, och analys och optimering av kaskadkopplade effektförstärkare (så kallade PA), särskilt deras ackumulerade olinjäriteter.

Eftersom digitala filter utgör kärnan i DSB-algoritmer är en nyckelkan- didat för effektiv avstämbarhet i digitala front-ends klassen av VDF:er som kan finjustera frekvenskaraktistiken i realtid utan behov av online-filterdesign. Den största fördelen med VDF:er är att de endast kräver en justering av en eller några få parametrar för att ändra sina egenskaper, medan majoriteten av filterkoefficienterna förblir fixa efter den initiala designen. Denna egenskap eliminerar behovet av omfattande online-beräkningar och gör VDF:er särskilt attraktiva för moderna adaptiva kommunikationstekniker, vilket möjliggör effektiv hårdvaruimplementering. Inom detta område presenterar avhandlingen tre olika tekniker för design och implementering av VDF: (i) implementeringar och systematiska designprocedurer baserade på minimaxoptimering för avstämbara så kallade FIR-filter för

samtidig frekvensgångsutjämning och lågpassfiltrering; (ii) implementering av den avstämbara lågpassutjämnaren med samtidigt variabel bandbredd, inklusive analys av chiparea och effektförbrukning i applikationsspecifika integrerade kretsar; (iii) effektiva frekvensdomän-implementeringar av VDF:er som konstruerats via filterdesign i tidsdomänen; (iv) effektiva frekvenssamplingsbaserade designmetoder (minimax och minstakvadrat) för FIR-filer med avstämbar bandbredd implementerat i frekvensdomänen, vilket möjliggör direkt optimering av DFT-koefficienterna med hänsyn till filtrets frekvensdomänimplementering och därigenom resulterar i en signifikant minskning av implementeringskomplexiteten.

Vidare är noggrann synkronisering avgörande för tillförlitlig drift av kommunikationssystem, eftersom synkroniseringsfel kan försämra systemets totala prestanda avsevärt. Bland dessa försämringar är SFO kritisk, särskilt i moderna bredbandiga och höghastighetskommunikationssystem, där även små skillnader mellan samplingsklockor leder till en märkbar kumulativ tidsdrift, vilket resulterar i interferens mellan bärvågor och symboler. Medan SFO-kompensationen vanligtvis utförs i tidsdomänen är de flesta befintliga SFO-estimeringsmetoder formulerade i frekvensdomänen, vilka i allmänhet är ganska beräkningskrävande, och det resulterar i en separation mellan estimering och kompensation. I motsats till dessa traditionella metoder presenterar denna avhandling två bidrag inom detta område: (i) ett gemensamt ramverk för SFO-estimering och kompensation baserat på ett avstämbar fördröjningsfilter, vilket resulterar i minskad implementeringskomplexitet för SFO-estimeringen och är tillämpligt på godtyckliga bandbegränsade signaler; (ii) en generaliserad ackumulatorbaserad metod för effektiv beräkning av viktade summor, som används i de föreslagna SFO-estimeringsalgoritmerna för att implementera beräkning av tidsindex-viktade och tidsindexkvadratviktade summor på ett effektivt sätt, vilket leder till att de flesta av multiplikationerna elimineras.

Slutligen har nya framsteg inom trådlösa kommunikationssystem visat behovet av ett avstämbar antal kaskadkopplade PA-steg. Medan en PA i allmänhet är en av de huvudsakliga källorna till olinjäriteter i en sändarmottagare som förvränger den sända signalen och försämrar systemets totala prestanda, ackumuleras felen i kaskadkopplade PA-steg, vilket leder till större olinjäriteter. Med hänsyn till kraven på hög effektivitet och ett maximalt linjärt driftsområde studerar denna avhandling effekten av totala olinjäriteter som uppstår i kaskadkopplade PA-steg genom modellering, analys, linjärisering och optimering.

Acknowledgements

Pursuing a PhD abroad is more than an academic challenge; it is also a deeply personal journey. It is shaped not only by research, but also by the need to adapt to a new country, build a sense of belonging, and grow through uncertainty and self-doubt. It is a journey with both achievements and setbacks, moments of confidence and moments of difficulty. More than anything, however, it is shaped by the people around us, who create the environment that helps us grow, remain strong, and move forward.

First and foremost, I would like to express my sincere gratitude to my supervisor, Prof. Håkan Johansson, for giving me the opportunity to pursue my PhD under his supervision. I am deeply thankful for his invaluable guidance, support, patience, and kindness, as well as for the time he devoted to discussing research problems and giving detailed feedback on my work. I would also like to thank my co-supervisor, Assoc. Prof. Oscar Gustafsson, for his valuable insights, useful discussions, and collaborations.

I would like to extend my thanks to all other co-authors of the papers included in this thesis. In particular, I am grateful to Assoc. Prof. Yinan Wang and Prof. Thomas Eriksson for sharing their expertise, contributing ideas, and providing valuable comments throughout our collaborative work. Many thanks also go to Narges for our collaboration on the implementation aspects of variable digital filters, and to Deijany for our collaborations on synchronization algorithms. I am thankful for the chance to work with all of you and to learn through our collaborations.

I truly appreciate being part of the Division of Communication Systems and the welcoming and inspiring environment it offers through invited lectures, workshops, and other academic activities organized for PhD students. I would also like to express my appreciation to the head of division, Prof. Erik G. Larsson, for his leadership and for the many opportunities made available within the division. I am grateful to all my colleagues, past and present, for the many technical and non-technical discussions, for our bi-weekly division meetings that gave us the chance to learn more about each other's work, and

for our traditional Friday fika with coffee, Princess cakes, and many other treats, as well as the after-work gatherings and sports activities that helped us build stronger relationships and create lasting memories. Thank you also for the kindness and friendliness that made this journey more pleasant. Being surrounded by people from different parts of the world has been a truly valuable experience, and I feel fortunate to have shared this time with you as colleagues. Some of you have also become very close friends of mine.

Additionally, I appreciate the opportunities I was given to attend and present at various conferences and project meetings, which certainly served as an additional source of motivation and inspiration. I am especially grateful to have been part of several research projects, which gave me a broader view of the research problems and opened many doors for networking. My sincere thanks also go to Prof. Liesbet Van der Perre for the invitation to spend one month with her research group at KU Leuven, Belgium. That stay was both inspiring and enriching, and it gave me the opportunity to view the PhD journey from a different perspective.

My heartfelt thanks go to all my friends who have supported me throughout this journey. I would especially like to thank my friend Yana, who was always there for me, encouraging me, believing in me, and standing by my side, especially during the most stressful moments. I am also deeply grateful to my friends who, despite being far away from Sweden, continued to offer their support and care.

Finally, and most importantly, I would like to express my heartfelt gratitude to my family—my husband, Aleksandr, and my parents, Svetlana and Aleksei—for their unwavering belief in me. Their love, care, patience, and constant encouragement reminded me, even through many difficult and stressful days, that *while we cannot direct the wind, we can adjust the sails*. I am deeply grateful for their presence in my life and for the strength they have given me throughout this journey.

Oksana Moryakova
Linköping, April 2026

Contents

List of Abbreviations	xiii
I Background	1
1 Introduction and Motivation	3
1.1 Communication Transceiver Front-Ends	3
1.1.1 Variable Digital Filters	4
1.1.2 Sampling Clocks Synchronization	5
1.1.3 Cascaded Power Amplifiers	6
1.2 Contributions of the Thesis	7
1.2.1 Included Papers	8
1.2.2 Excluded Papers	13
1.3 Thesis Outline	14
2 Basics of Digital Filters and Filter Banks	15
2.1 FIR Filters	15
2.1.1 Linear-Phase FIR Filters	16
2.1.2 Digital Filter Design and Implementation Steps	17
2.1.3 Design of FIR Filters	18
2.1.4 Realizations of FIR Filters	24
2.1.5 Finite Word Length Effects	28
2.1.6 Digital Differentiators	30
2.2 Multirate Systems and Filter Banks	31
2.2.1 Basic Multirate Operations	31
2.2.2 Filter Banks	34
3 Variable Digital Filters	39
3.1 Introduction	39
3.2 Farrow-Based Variable Digital Filters	40

3.2.1	Variable-Fractional-Delay Filters	42
3.2.2	Variable Equalizers	43
3.2.3	Variable-Bandwidth Filters	45
3.3	Filter-Bank-Based Variable Digital Filters	47
3.3.1	Fast Filter Banks	47
3.3.2	Fast-Convolution-Based Filter Banks	48
4	Sampling Clocks Synchronization	51
4.1	Overview of Synchronization Errors	51
4.2	Sampling Frequency Offset	52
4.2.1	Sampling Frequency Offset Impact	53
4.2.2	Estimation Methods	57
4.2.3	Compensation Methods	58
4.3	Joint Impact of Sampling and Carrier Frequency Offsets	58
4.3.1	Carrier Frequency Offset Impact	59
4.3.2	Joint Impact of SFO and CFO	61
5	Power Amplifier Nonlinearities	63
5.1	Power Amplifier Challenges	63
5.1.1	Behavioral Modeling	64
5.1.2	Linearization Techniques	67
5.1.3	Performance Metrics	68
5.2	Cascaded Power Amplifiers Challenges	69
6	Concluding Remarks and Thesis Contributions	71
	Bibliography	72
II	Included Papers	87
A	Low-Complexity Reconfigurable FIR Lowpass Equalizers for Polynomial Channel Models	89
1	Introduction	91
1.1	Contributions	92
1.2	Outline	94
2	Problem Statement	94
3	Proposed Reconfigurable Equalizers	96
3.1	Cascaded Structure	96
3.2	Cascaded-Parallel Structure	99
3.3	Parallel Structure	100

4	Design Procedures	101
4.1	Minimax Design	101
4.2	Cascaded and Cascaded-Parallel Structures	102
4.3	Parallel Structure	105
4.4	Fast RLPE Design	106
5	Filter Order Estimation	106
5.1	Order-Estimation Expression of Lowpass Filters	108
5.2	Order-Estimation Expressions of Differentiators	108
6	Complexity	110
6.1	Implementation Complexity	110
6.2	Design Complexity	113
7	Design Examples	114
7.1	Simulation Results	114
7.2	Comparison and Analysis	124
8	Conclusion	125

B Low-Complexity Implementation of Real-Time Reconfigurable

	Low-Pass Equalizers	129
1	Introduction	131
2	Background	134
2.1	FIR Filters	134
2.2	Implementation of FIR Filters	135
2.3	Structure of the RLPE	136
3	Implementation of the RLPE	138
3.1	Implementation of the VBW Filter $G(z, b)$	138
3.2	Implementation of Polynomial Evaluation in the VBW Filter	140
3.3	Implementation of the VE	142
3.4	Pipelining of the Baseline Implementation	143
3.5	Reformulating the Problem to Break the Polynomial Section	144
4	Word Length Optimization	146
4.1	Coefficients Quantization	147
4.2	Data Quantization	148
4.3	Required Bits for Integer Part of the Data Quantization	150
5	Considered Implementation of a General FIR Equalizer	151
6	Results	152
6.1	Finite Word Length/Quantization Results	153
6.2	Architectural Results	154
6.3	Implementation Results	158

7	Conclusion	161
C	Frequency-Domain Implementations of Variable Digital FIR Filters Using the Overlap-Save Technique	165
1	Introduction	167
2	Overlap-Save Method	168
3	Proposed Frequency-Domain Implementations of Variable Filters	169
3.1	Proposed VDF Structures	169
3.2	Implementation Complexity	170
3.3	Design Complexity	174
4	Design Examples	174
4.1	Example A: VBW Filter	174
4.2	Example B: VBWFD Filter	176
5	Conclusions	178
D	Efficient Design and Implementation of Fast-Convolution Based Variable-Bandwidth Filters	181
1	Introduction	183
2	Overlap-Save Method	185
3	Proposed Approach to Design a VBW Filter Implemented Using the OLS method	186
3.1	VBW Filter Implemented Using the OLS method	186
3.2	Proposed HFSO Approach	188
3.3	Minimax Design	189
3.4	Implementation and Design Complexity	190
3.5	Design Procedure Minimizing the Overall Complexity	191
4	Example	191
5	Conclusions	193
E	Closed-Form Least-Squares Design of Fast-Convolution Based Variable-Bandwidth FIR Filters	197
1	Introduction	199
2	Overlap-Save Method	202
3	Proposed Closed-Form Design of a VBW Filter Implemented Using the OLS Method	203
3.1	VBW Filter Implemented Via the OLS Method	203
3.2	Proposed Approach to Closed-Form Design	206
3.3	Specification in Terms of Frequency Bins	211
3.4	Complexity Analysis	212
4	Design Examples	214

4.1	Example 1	214
4.2	Example 2	216
4.3	Example 3	218
4.4	Example 4	218
5	Extension to Continuous VBW Filters	219
6	Conclusion	220

F Joint Sampling Frequency Offset Estimation and Compensation Algorithms Based on the Farrow Structure 225

1	Introduction	227
1.1	Contributions	229
1.2	Outline	230
2	Problem Statement and Proposed SFO Time-Domain Estimation Utilizing the Farrow Structure	231
2.1	SFO Model	231
2.2	SFO Compensation Using the Farrow Structure	231
2.3	Proposed SFO Estimation Principle Using the Farrow Structure	233
3	Proposed SFO Estimator Using Newton’s Method	234
3.1	Low-Complexity Implementation	236
4	Proposed SFO Estimator Using An Iterative Least-Squares Algorithm	240
4.1	Low-Complexity Implementation	244
5	Numerical Examples	245
5.1	Accuracy of Proposed Estimators	245
5.2	VFD Filter Complexity Influence on Estimation Accuracy	253
5.3	Number of Samples Required for the Estimation	255
6	Proposed Estimators Using a Simplified Farrow Structure ($L = 1$)	257
6.1	Numerical Example: First-Degree Farrow Based Estimator	259
7	Conclusions	262

G Efficient Computation of Time-Index Powered Weighted Sums Using Cascaded Accumulators 269

1	Introduction	271
2	Cascaded Accumulator’s Output	273
3	Proposed Computation of Time-Index Powered Weighted Sums via Cascaded Accumulators	275
3.1	Derivation of $\{c_k\}$ in Closed Form via Stirling Numbers	276

4	Complexity Analysis	280
4.1	Hardware Cost	281
5	Conclusion	281

H Modeling, Analysis, and Optimization of Cascaded Power Amplifiers		285
1	Introduction	287
2	System Model	289
3	Analysis of Nonlinearities in the Cascaded Structure	291
3.1	Cascaded Nonlinearities in the Noise-Free Case	291
3.2	Cascaded Nonlinearities in the Presence of Noise	292
3.3	Analysis of the Approximating Expressions	292
4	Optimization Problem	293
4.1	Problem Formulation	293
4.2	Performance Metrics	293
5	Simulation Results	294
5.1	The Choice of the Starting Point for the Optimization	294
5.2	Optimization of the Parameters in the Cascaded Structures	296
6	Conclusions	298

List of Abbreviations

ACLR	Adjacent channel leakage ratio
ADC	Analog-to-digital converter
AFE	Analog frond-end
AM/AM	Amplitude-to-amplitude modulation
AM/PM	Amplitude-to-phase modulation
ASIC	Application specific integrated circuit
CFO	Carrier frequency offset
CP	Cyclic prefix
DAC	Digital-to-analog converter
DFE	Digital front-end
DFT	Discrete Fourier transform
DPD	Digital predistortion
DSP	Digital signal processing
EVM	Error vector magnitude
FB	Filter bank
FC	Fast convolution
FCFB	Fast-convolution filter bank
FFB	Fast filter bank
FFT	Fast Fourier transform
FIR	Finite impulse response
FPGA	Field programmable gate array
ICI	Inter-carrier interference
IDFT	Inverse discrete Fourier transform

IFFT	Inverse fast Fourier transform
IIR	Infinite-impulse-response
IoT	Internet of things
ISAC	Integrated sensing and communication
ISI	Inter-symbol interference
LPTV	Linear periodically time-varying
LS	Least-squares
MIMO	Multiple input multiple output
NMSE	Normalized mean squared error
OFDM	Orthogonal frequency division multiplexing
OLA	Overlap-add
OLS	Overlap-save
PA	Power amplifier
PAPR	Peak-to-average power ratio
PO	Phase offset
ppm	Parts per million
PR	Perfect reconstruction
PTVIR	Periodically time-varying impulse response
QAM	Quadrature amplitude modulation
RF	Radio frequency
RLPE	Reconfigurable lowpass equalizer
SFO	Sampling frequency offset
SNR	Signal-to-noise ratio
STO	Sampling time offset
VBW	Variable bandwidth
VDF	Variable digital filter
VE	Variable equalizer
VFD	Variable fractional delay
WASN	Wireless acoustic sensor networks
WLS	Weighted least squares

Part I

Background

Chapter 1

Introduction and Motivation

In the era of digital transformation, our way of life is constantly changing, attracting more digital technologies every day. As a result, demands for constant access to the Internet and various digital devices are growing. The basis of these technologies is digital signal processing (DSP), a fundamental technology that has revolutionized the way signals are processed in various fields. DSP involves the sophisticated manipulation of digital signals using mathematical algorithms and computational techniques to extract, analyze, and interpret information embedded within the signals. One of the most significant applications of signal processing is in communication systems, where this technology enables not only voice transmission but also multimedia streaming, data exchange and beyond. From wireless to fiber-optic communications, signal processing algorithms form the core of seamless, efficient and reliable signal transmission, reception, and processing.

1.1 Communication Transceiver Front-Ends

Modern communication transceivers consist of both analog and digital processing stages. While the analog front-end (AFE) is an essential part for performing signal amplification and frequency conversion in the analog domain, the digital front-end (DFE) is responsible for a wide range of signal processing tasks to enable reliable communication and achieve optimal performance in terms of signal quality and spectral efficiency. A high-level block diagram of a communication transceiver with AFE and DFE is illustrated in Fig. 1.1. The transmitter chain typically includes the stages of waveform generation and spectral shaping in the digital domain, digital-to-analog conversion with subsequent amplification of the radio frequency (RF) signal. At

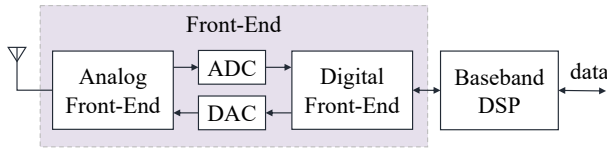


Figure 1.1: A high-level block diagram of a communication transceiver.

the receiver, the signal is converted back to the digital domain, so that DFE can perform synchronization, filtering, equalization, and other DSP tasks needed for reliable signal detection [1–4]. While DFE algorithms typically constitute the main part in determining the overall complexity and efficiency at the receiver side, at the transmitter, power amplifiers (PAs) play a critical role in determining the overall power consumption and linearity [5].

With each new generation of communication technologies, there exists a persistent drive towards achieving higher data rates, lower latency, and improved accuracy positioning [6–9] that together necessitate the development of more sophisticated signal processing algorithms implemented in the DFE. Additionally, recent communication standards have introduced new requirements on flexibility and reconfigurability to support different standards and operate for different needs of the systems [7–9]. Moreover, the diversification and fragmentation of communication markets have led to situations where similar system designs must be developed, adapted, and validated multiple times for different standards or application domains. This repeated design and validation process increases development and production costs, that shows the need for the design of reconfigurable systems [5, 10]. At the same time, many practical transceiver implementations are constrained by power consumption and silicon area requirements. Consequently, the development of efficient and reconfigurable signal processing techniques for communication system front-ends is one of the research challenges nowadays.

1.1.1 Variable Digital Filters

Among the DFE components, digital filters play a crucial role in many DSP tasks. This is still an active research area, where more advanced solutions for efficient filter design and implementation are proposed every year [11–17]. Moreover, considering the demands for flexible and adaptive systems [8, 9, 18–21], reconfigurable digital filtering techniques are essential for the development of flexible communication systems.

At first sight, these requirements can be fulfilled by means of regular digital

filters having all coefficients general, the values of which can be updated after online filter design based on new specification requirements from time to time. This type of filters can be implemented in general-purpose digital signal processors or field programmable gate arrays (FPGAs). However, the reconfiguration time is relatively long and the filters cannot be reconfigured dynamically, i.e., while processing. Moreover, this approach usually leads to high implementation complexity and thereby high power consumption, which is one of the main limitation, for example, in mobile terminals and internet of things (IoT) devices [22, 23].

This problem has lead many researchers to variable digital filters (VDFs) and increased interest in their design and implementation techniques [24–74]. The main feature of VDFs is the ability to vary their frequency response "on-the-fly" by adjusting only one or a few parameters without online redesign. In these filters, most of coefficients are fixed once the filter has been designed, and thus, they can be efficiently implemented in hardware, for example, in FPGAs or application specific integrated circuits (ASICs) using various techniques [11–13, 17, 75], while preserving both flexibility and low implementation complexity. This is the main advantage over regular digital filters, which have all coefficients being general (i.e., variable) and require redesign for every new specification using, e.g., the least-squares (LS) method or minimax optimization [76]. This means that the overall complexity of regular digital filters consists of implementation of general multipliers and obtaining new values for them, whereas the overall complexity of VDFs contains mainly implementation of constant multipliers, which requires significantly less computational resources than the general ones.

1.1.2 Sampling Clocks Synchronization

Another important function of the DFE is synchronization. In practical transceiver implementations, perfect synchronization is difficult to achieve without additional corrections due to hardware imperfections and varying channel conditions. Importantly, even small mismatches can result in significant degradation of the overall system performance [77, 78].

Among various synchronization impairments encountered in receivers, sampling frequency offset (SFO) is particularly important to mitigate in many applications and becomes more crucial in modern high-speed and wide-band communication systems, where the use of large signal bandwidths necessitates very high sampling rates [77]. For such systems, even tiny differences between sampling clocks lead to a noticeable accumulative timing drift, which in turn distorts the received signal and leads to inter-symbol

interference (ISI), while in multi-carrier systems it can also cause inter-carrier interference (ICI) [77–84]. Consequently, efficient techniques for estimating and compensating SFO are essential for maintaining reliable communication.

Various techniques have been proposed to mitigate the effects of SFO. While the estimation algorithms are more often implemented in the frequency domain [77, 80, 83–91], the compensation is typically carried out in the time domain by interpolating the received signal employing VDF structures, specifically, a variable fractional delay (VFD) filter [92–95]. By exploiting the flexibility of the VFD filters, synchronization algorithms can account for a time-varying fractional delay, corresponding to SFO, while maintaining low implementation complexity.

1.1.3 Cascaded Power Amplifiers

Among the transmitter-side components, PAs, which constitute a part of the AFE, are particularly important in many communication systems. They are responsible for increasing the power of the transmitted signal to ensure that the receiver can recognize the presence of the signal. However, PAs are typically the most power-hungry elements and constitute one of the main sources of nonlinearities that distort the transmitted signal. This is especially problematic in systems with stringent requirements on consumed power and operating on signals with high peak-to-average power ratio (PAPR). In order to design high-performance transmitters ensuring a balance between high efficiency and linearity of PAs, the behavioral modeling of PAs has received considerable attention over the last few decades, as it is an essential step in understanding PA limitations and developing efficient DSP algorithms for optimizing their performance [96–104].

To support the demands for reconfigurability, recent advances in wireless communication systems have introduced a system with a reconfigurable number of PAs placed in cascade, where each PA amplifies the incoming signal to compensate for the losses incurred in the preceding fiber [105, 106]. A similar problem but with a fixed number of PAs has been considered in optical free-space communications [107] and optical communications [94, 108–110] to overcome the impact of the attenuation for long distances. Additionally, multiple amplification stages can be employed to improve power efficiency and minimize chip size [111, 112]. In such cascaded structures, the nonlinear behavior of each PA is accumulated throughout the transmitter chain, resulting in a more complex and severe overall nonlinear effect, which requires to be analyzed and mitigated.

1.2 Contributions of the Thesis

This doctoral thesis comprises research publications that have been produced as a result of research work at the Communication Systems Division, Department of Electrical Engineering, Linköping University, Sweden. The papers have been peer-reviewed and published, or submitted for possible publication.

The thesis investigates the aforementioned areas, specifically, efficient design and implementation techniques for VDFs, low-complexity SFO estimation algorithms, and analysis and optimization of the cascaded structure of PAs to minimize the overall nonlinearities, and provides the contributions to these three research directions.

Variable Digital Filters

The problem of efficient signal processing techniques in the area of reconfigurable digital filtering is addressed by presenting the following contributions to the low-complexity design and implementation algorithms for VDFs.

- Paper A proposes implementations and systematic design procedures for a reconfigurable lowpass equalizer (RLPE) based on minimax optimization, while Paper B provides an analysis of chip area and power consumption for an ASIC implementation of the RLPE. These studies highlight that VDF structures allow to reduce the implementation complexity, power consumption, and chip area compared to regular digital filters.
- Paper C presents low-complexity frequency-domain implementations of VDFs based on the assumption that these filters have been designed using a common time-domain design approach based on optimizing the impulse response coefficients. The filter's discrete Fourier transform (DFT) coefficients are proposed to be implemented as fixed, hybrid, or variable weights, where each of the realizations can find their application in practice depending on the overall system requirements.
- Efficient frequency-sampling-based design approaches for a variable-bandwidth finite impulse response (FIR) filter implemented in the frequency domain are introduced in Paper D using minimax optimization and in Paper E by providing a closed-form least-squares solution. The proposed methods allow for direct optimization of the DFT coefficients considering the filter frequency-domain implementation and thereby offer a significant reduction in implementation complexity.

Sampling Clocks Synchronization

In contrast to the traditional approaches preserving a separation between SFO estimation and compensation stages, this thesis contributes to the area of sampling clocks synchronization by presenting a joint SFO estimation and compensation framework based on a VFD filter. The contributions are as follows.

- Paper F proposes the estimation algorithms which rely on two complementary methods, specifically, Newton's method and iterative least-squares formulation. Both algorithms result in reduced implementation complexity of the SFO estimation and are applicable to arbitrary band-limited signals.
- Paper G introduces a generalized accumulator-based approach for efficient computation of time-index powered weighted sums, which is employed in the proposed SFO estimation algorithms to implement computation of time-index and time-index-squared weighted sums in an efficient way leading to eliminating considerable parts of multiplications.

Cascaded Power Amplifiers

In the area of PA nonlinearities, this thesis contributes by studying modeling, analysis, and optimization of cascaded PA parameters to mitigate the severe effect of the accumulated distortions. The results of the optimized configurations using nonlinear LS optimization demonstrate potential ways of linearizing the cascaded PA structure. This is presented in Paper H.

1.2.1 Included Papers

Paper A: Low-Complexity Reconfigurable FIR Lowpass Equalizers for Polynomial Channel Models

Authored by: Oksana Moryakova, Yinan Wang, and Håkan Johansson

Published in Journal Digital Signal Processing, vol. 150, pp. 1–13, Jul. 2024.

Abstract: This paper introduces realizations of a reconfigurable FIR filter for simultaneous equalization and lowpass filtering for high-order polynomial channel models. The main advantage of the proposed solutions is computational complexity reduction compared to existing solutions for a given performance, which leads to reduced hardware complexity. The proposed structures employ properties of both a variable bandwidth (VBW) filter and

a variable equalizer (VE) with variable coefficients. The overall transfer function of the proposed RLPE is a weighted linear combination of fixed subfilters where the weights are directly determined by the bandwidth and one or several parameters of the channel needed to be equalized. The paper provides design procedures based on minimax optimization and introduces a fast design method for the filter with several variable parameters that can substantially decrease the design time. Filter order estimation expressions as well as complexity expressions are presented for all proposed realizations. Design examples include comparison of the RLPE structures and a common approach of using a regular FIR equalization filter requiring online redesign when the bandwidth or channel characteristics are changed. It is shown that the number of general multiplications can be reduced up to 91% using the proposed RLPE.

Paper B: Low-Complexity Implementation of Real-Time Reconfigurable Low-Pass Equalizers

Authored by: Narges Mohammadi Sarband, Oksana Moryakova, Håkan Johansson, and Oscar Gustafsson

Published in IEEE Transactions on Very Large Scale Integration (VLSI) Systems, vol. 33, Sep. 2025, pp. 246–2473.

Abstract: Implementation techniques and results for a recently proposed real-time RLPE consisting of a variable bandwidth filter and a variable equalizer are presented. Both components utilize fixed FIR filters combined with a few general multipliers, resulting in lower area and power consumption compared to a general FIR filter, despite requiring more multiplications. This is because the constant multipliers in the fixed FIR filters of the RLPE can be optimized for implementation. An additional advantage is that the proposed RLPE do not require online design. Various implementation alternatives for fixed FIR filters, including ways to increase the frequency, are evaluated to optimize the implementation of the RLPE. Several versions of the proposed RLPE as well as a general FIR filter for comparison are implemented using a 28 nm fully depleted silicon on insulator (FD-SOI) standard cell library. The results demonstrate that the RLPE baseline design requires less power and area than the general equalizer and although the frequency of the baseline implementation is lower, the design can reach the same frequency while still having significantly less power and area. Furthermore, an approach is introduced to break the chain in the polynomial section of the variable bandwidth filter by using less additional registers compared to standard

pipelining. Instead, this method reformulates the constant multiplication problem to produce correct results. For the considered case, the power consumption is reduced between 49 and 70% for different frequencies, with an area decrease in the range of 64 to 67%, by using the proposed RLPE compared to a general FIR filter.

Paper C: Frequency-Domain Implementations of Variable Digital FIR Filters Using the Overlap-Save Technique

Authored by: Oksana Moryakova and Håkan Johansson

Published in proceedings of 24th International Conference on Digital Signal Processing (DSP), Rhodes, Greece, Jun. 11–13, 2023, pp. 1–5.

Abstract: The paper introduces frequency-domain implementations of variable digital filters using the overlap-save method. Expressions for implementation and design complexities are derived for real-valued impulse responses. Design examples include implementations of a VBW filter alone as well as a cascade of a VBW filter and a VFD filter. Compared to a time-domain implementation and a filter bank approach, the proposed structures can reduce the implementation complexity significantly and achieve savings up to 95% in the multiplication rate and up to 89% in the addition rate.

Paper D: Efficient Design and Implementation of Fast-Convolution-Based Variable-Bandwidth Filters

Authored by: Oksana Moryakova and Håkan Johansson

Published in proceedings of 32nd European Conference on Signal Processing (EUSIPCO), Lyon, France, Aug. 26–30, 2024, pp. 1–5.

Abstract: This paper introduces a frequency-domain design approach of a fast-convolution-based VBW filter. The proposed approach is based on a hybrid of frequency sampling and optimization, that offers significant computational complexity reduction compared to existing solutions for a given performance. The paper provides a design procedure based on minimax optimization to obtain the minimum complexity of the overall filter. A design example includes comparison of the proposed-design based VBW filter and time-domain designed VBW filters implemented in the time domain and in the frequency domain. It is shown that not only the implementation complexity can be reduced but also the design complexity by excluding any computations when the bandwidth of the filter is adjusted. Moreover, memory

requirements are also decreased compared to the existing frequency-domain implementations.

Paper E: Closed-Form Least-Squares Design of Fast-Convolution Based Variable-Bandwidth FIR Filters

Authored by: Oksana Moryakova and Håkan Johansson

Published in IEEE Open Journal of Signal Processing, vol. 7, Jan. 2026, pp. 54-63.

Abstract: This paper introduces a closed-form LS design approach for fast convolution (FC) based VBW FIR filters. The proposed LS design utilizes frequency sampling and the VBW filter frequency-domain implementation using the overlap-save (OLS) method, that together offer significant savings in implementation and online bandwidth reconfiguration complexities. Since combining frequency-domain design and OLS implementation leads to a linear periodically time-varying (LPTV) behavior of the VBW filter, a set of the corresponding time-invariant impulse responses is considered in the proposed design. Through numerical examples, it is demonstrated that the proposed approach enables not only closed-form design of FC-based VBW filters with substantial complexity reductions compared to existing solutions for a given performance, but also allows the variable bandwidth range to be extended without any increase in complexity. Moreover, a way of reducing the maximum approximation error energy over the whole set of the time-invariant filters of the LPTV system is shown by introducing appropriate weighting functions in the design.

Paper F: Joint Sampling Frequency Offset Estimation and Compensation Algorithms Based on the Farrow Structure

Authored by: Deijany Rodriguez Linares, Oksana Moryakova, and Håkan Johansson

Submitted to IEEE Open Journal of Signal Processing.

Abstract: This paper presents joint SFO estimation and compensation algorithms based on the Farrow structure. Unlike conventional approaches that treat estimation and compensation separately, the proposed framework exploits the interpolator structure to enable a low-complexity, fully time-domain solution applicable to arbitrary bandlimited signals, without imposing constraints on the waveform or requiring Fourier transform based processing. The estimation stage can operate on a real-valued component of a complex

signal and supports the simultaneous estimation of SFO and sampling time offset, while being inherently robust to other synchronization impairments such as carrier frequency offset. The proposed estimation algorithms rely on two complementary methods, specifically, Newton's method and iterative least-squares formulation. The implementations of the estimators are presented and the overall computational complexity is analyzed, showing that the complexity scales only linearly with the number of samples employed. Numerical results for real and complex multisine and bandpass-filtered white noise signals demonstrate accurate estimation and effective compensation over a wide range of operating conditions, confirming the flexibility and efficiency of the proposed approach. Moreover, the influence of the Farrow structure approximation error on the SFO estimation accuracy is investigated.

Paper G: Efficient Computation of Time-Index Powered Weighted Sums Using Cascaded Accumulators

Authored by: Deijany Rodriguez Linares, Oksana Moryakova, and Håkan Johansson

Published in IEEE Signal Processing Letters, Feb. 2026, pp. 893–897.

Abstract: This letter presents a novel approach for efficiently computing time-index powered weighted sums of the form $\sum_{n=0}^{N-1} n^K v[n]$ using cascaded accumulators. Traditional direct computation requires $K \times N$ general multiplications, which become prohibitive for large N , while alternative strategies based on lookup tables or signal reversal require storing entire data blocks. By exploiting accumulator properties, the proposed method eliminates the need for such storage and reduces the multiplicative cost to only $K+1$ constant multiplications, enabling efficient real-time implementation. The approach is particularly useful when such sums need to be efficiently computed in sample-by-sample processing systems.

Paper H: Modeling, Analysis, and Optimization of Cascaded Power Amplifiers

Authored by: Oksana Moryakova, Thomas Eriksson, and Håkan Johansson

Published in proceedings of 33rd European Conference on Signal Processing (EUSIPCO), Palermo, Sicily, Italy, Sep. 8–12, 2025, pp. 2692–2696.

Abstract: This paper deals with modeling, analysis, and optimization of PAs placed in a cascaded structure, particularly the effect of cascaded nonlinearities is studied by showing potential ways to minimize the total

nonlinearities. The nonlinear least-squares algorithm is proposed to optimize the PA parameters along with the input power level, and thereby minimize the total nonlinearities in the cascaded structure. The simulation results demonstrate that the performance of the optimized configurations for up to five PAs using the proposed framework can improve the linearity properties of the overall cascade.

1.2.2 Excluded Papers

The following paper are excluded as they are preliminary versions of the included Papers A and F in the thesis.

Paper P.1: Reconfigurable FIR Lowpass Equalizers

Authored by: Oksana Moryakova, Yinan Wang, and Håkan Johansson

Published in proceedings of 2022 IEEE Workshop on Signal Processing Systems (SiPS), Rennes, France, Nov. 2–4, 2022, pp. 1–6.

Abstract: This paper introduces realizations of a reconfigurable FIR filter for simultaneous equalization and lowpass filtering. The proposed structures employ properties of both a VBW filter and a VE with an adjustable coefficient using the Farrow structure, therefore they consist of weighted combinations of fixed subfilters. Design procedures using minimax optimization technique are provided. The paper includes a design example and complexity comparisons between the proposed structures of the RLPE and a common approach of using a regular FIR equalization filter requiring online redesign.

Paper P.2: Joint Sampling Frequency Offset Estimation and Compensation Based on the Farrow Structure

Authored by: Deijany Rodriguez Linares, Oksana Moryakova, and Håkan Johansson

Published in proceedings of 25th International Conference on Digital Signal Processing (DSP), Costa Navarino, Greece, Jun. 25–27, 2025, pp. 1–5.

Abstract: This paper introduces a SFO estimation method based on the Farrow structure, which is typically utilized for the SFO compensation and thereby enables a reduction of the implementation complexity of the SFO estimation. The proposed method is implemented in the time domain and works for arbitrary bandlimited signals, thus with no additional constraints on the waveform structure. Moreover, it can operate on only the real or

imaginary part of a complex signal, which further reduces the estimation complexity. Furthermore, the proposed method can simultaneously estimate the SFO and additional sampling time offset (STO) and it is insensitive to other synchronization errors, like carrier frequency offset. Both the derivations of the proposed method and its implementation are presented, and through simulation examples, it is demonstrated that it can accurately estimate both SFO and STO for different types of bandlimited signals.

1.3 Thesis Outline

This thesis consists of two parts. Part I provides the necessary background and context for the three main research areas addressed in the thesis: VDFs, sampling clocks synchronization, and PAs nonlinearities. Following the introduction presented in this chapter, the background starts from the basics of digital filters and filter banks presented in Chapter 2. Specifically, it discusses FIR filters, which are commonly used as the basic building blocks in VDFs, and the basic elements of multirate systems and filter banks (FBs), which can help the reader to acquire an overall understanding of FB-based VDFs, presented in Chapter 3 along with commonly used Farrow-based VDFs. Further, Chapter 4 gives an overview on the sampling clocks synchronization errors, in particular, SFO impact and its estimation and compensation methods. Chapter 5 provides common challenges in the area of PAs and gives an introduction to cascaded PAs. Chapter 6 concludes Part I of the thesis. Part II comprises the published papers, the layout of which has been changed and a few typos have been corrected.

Chapter 2

Basics of Digital Filters and Filter Banks

In this chapter, relevant basics of digital filters and filter banks are provided. Generally, FIR filters are used as basic building blocks in VDFs, which are discussed in Papers A–F. Therefore, their design and implementation are important to recall here. The main focus is on linear-phase FIR filters and digital differentiators since those two types are used in the contributions to this thesis. Additionally, many DSP applications, for example, communications and audio processing, utilize multirate techniques because their use can simplify and reduce computational complexity. Similarly, VDFs can be efficiently implemented using these techniques. Thus, this chapter also covers the basics of multirate systems and filter banks, which can be used to analyze and design time-varying systems as discussed in Papers D and E.

2.1 FIR Filters

There are two major classes of digital filters, namely, FIR filters and infinite-impulse-response (IIR) filters. Advantages of the former over the latter are that stability of the filters can be guaranteed and a linear-phase response can be obtained. Additionally, a drawback of IIR filters is that they have a bound on the data rate [113]. Therefore, FIR filters are commonly used in applications where linear phase response and stability are important, e.g., in channel equalization and anti-aliasing filtering, especially, in high data rate applications. FIR filters usually have a higher order and, correspondingly, greater group delay compared to IIR filters [76, 114–116]. This is why it is of interest to reduce the complexity of FIR filter implementations [11, 13, 17].

The impulse response $h(n)$ of a causal FIR filter of order N is nonzero only for $0 \leq n \leq N$, while the transfer function and frequency response are defined as

$$H(z) = \sum_{n=0}^N h(n)z^{-n} \quad (2.1)$$

and

$$H(e^{j\omega T}) = \sum_{n=0}^N h(n)e^{-j\omega T n}, \quad (2.2)$$

respectively, where ωT indicates the discrete-signal frequency¹ for the sampling period T . The frequency response in (2.2) can be represented as

$$H(e^{j\omega T}) = |H(e^{j\omega T})|e^{j\Phi(\omega T)}, \quad (2.3)$$

where $|H(e^{j\omega T})|$ is the magnitude response and $\Phi(\omega T)$ is the phase response.

The FIR filter output can be expressed in the time domain as linear convolution of an input sequence $x(n)$ and the filter impulse response as

$$y(n) = \sum_{k=0}^N h(k)x(n-k). \quad (2.4)$$

In the frequency domain, it corresponds to the product of the corresponding Fourier transforms, i.e.,

$$Y(e^{j\omega T}) = H(e^{j\omega T})X(e^{j\omega T}), \quad (2.5)$$

where $X(e^{j\omega T})$ and $Y(e^{j\omega T})$ are the Fourier transforms of the input and output sequences, respectively.

2.1.1 Linear-Phase FIR Filters

Linear-phase FIR filters are of particular interest in the class of FIR filters. The phase response of these filters is linear, and the impulse response is symmetric or antisymmetric depending on the type of the filter as follows [116]:

$$\begin{aligned} \text{Type I } (N \text{ even}): & \quad h(n) = h(N-n), \\ \text{Type II } (N \text{ odd}): & \quad h(n) = h(N-n), \\ \text{Type III } (N \text{ even}): & \quad h(n) = -h(N-n), \\ \text{Type IV } (N \text{ odd}): & \quad h(n) = -h(N-n). \end{aligned}$$

¹In literature, the discrete-signal frequency is alternatively denoted as ω or Ω .

This means that the number of multiplications in filter implementations can be halved. The frequency response of linear-phase FIR filters can be expressed with the help of a real function $H_R(\omega T)$, called *zero-phase frequency response*, as

$$H(e^{j\omega T}) = H_R(\omega T)e^{-j\left(\omega T\frac{N}{2}-c\right)}, \quad (2.6)$$

where $c = 0$ for filters of Types I and II and $c = \pi/2$ for filters of Types III and IV. The zero-phase frequency response $H_R(\omega T)$ depends on the linear-phase filter type as follows [116]:

$$H_R(\omega T) = \begin{cases} h\left(\frac{N}{2}\right) + \sum_{n=1}^{N/2} 2h\left(\frac{N}{2} - n\right) \cos(\omega T n), & \text{(Type I)} \\ \sum_{n=1}^{\frac{N+1}{2}} 2h\left(\frac{N+1}{2} - n\right) \cos\left(\omega T \left[n - \frac{1}{2}\right]\right), & \text{(Type II)} \\ \sum_{n=1}^{N/2} 2h\left(\frac{N}{2} - n\right) \sin(\omega T n), & \text{(Type III)} \\ \sum_{n=1}^{\frac{N+1}{2}} 2h\left(\frac{N+1}{2} - n\right) \sin\left(\omega T \left[n - \frac{1}{2}\right]\right). & \text{(Type IV)} \end{cases} \quad (2.7)$$

Then, the phase response of a linear-phase filter $H(z)$ is

$$\Phi(\omega T) = \begin{cases} -\omega T\frac{N}{2} + c, & H_R(\omega T) > 0, \\ -\omega T\frac{N}{2} + c \pm \pi, & H_R(\omega T) < 0, \end{cases} \quad (2.8)$$

while the group delay is²

$$\tau_g(\omega T) = -\frac{\partial\Phi(\omega T)}{\partial(\omega T)} = \frac{N}{2}. \quad (2.9)$$

To achieve an integer group delay, the filter order must be even, i.e., one should consider Type I or Type III linear-phase FIR filters.

2.1.2 Digital Filter Design and Implementation Steps

The design process of digital filters generally follows³ the structure shown in Fig. 2.1 [117]. It starts from defining the desired specification of the filter, followed by optimizing the filter coefficients to satisfy the frequency response specification. The resulting coefficients are typically obtained in a floating-point form first. Therefore, the next steps of the filter design process include a choice of the filter realization and an analysis of the finite word length effects. These steps are primarily covered in this thesis. Further, the steps including

²This is the group delay ignoring the phase discontinuity at $H_R(\omega T) = 0$.

³This is an overall principle, but it can be slightly modified in many practical cases depending on the specific application.

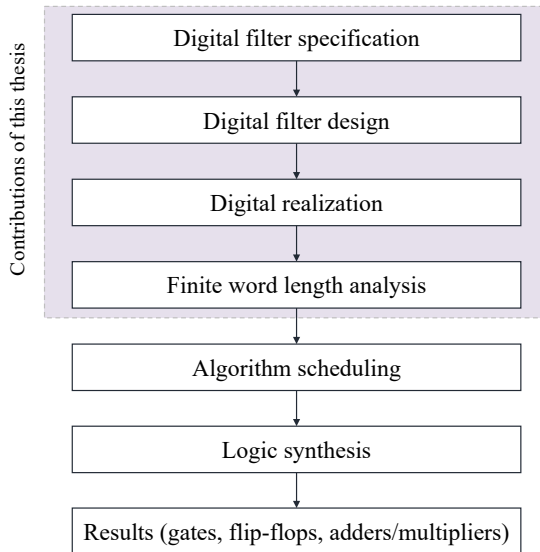


Figure 2.1: Design and implementation steps for a digital filter.

an analysis of the hardware specification such as algorithm scheduling and resource allocation, logic synthesis of the architectural components (processing elements, memory, control units, etc.), and circuit description in terms of basic building blocks (gates, adders, flip-flops, etc.) [117], are not covered here but are analyzed in Paper B for a cascaded structure of a VDF.

2.1.3 Design of FIR Filters

For a given specification, filter design generally involves two stages, namely, filter order estimation and obtaining the filter coefficients by approximation of the desired response for an order around the estimated value, where the last step is often iterative until the minimum-order filter is obtained. For an FIR filter, it generally amounts to determine the impulse response values $h(n)$, for which the filter frequency response satisfies the given specification. This type of filter design is common for an FIR filter implemented in the time domain. An alternative way is to obtain the filter DFT coefficients during the second step of the design procedure to meet the desired frequency response specification. This type of filter design can be used for efficient filter implementations in the frequency domain. This section discusses the procedures in detail for both design approaches for frequency-selective filters.

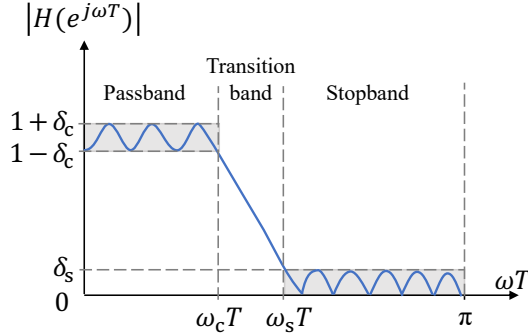


Figure 2.2: Frequency-response specification of a lowpass filter.

Specification

Among all types of frequency-selective filters, here, we will consider a linear-phase lowpass FIR filter since it is mainly used as the basic element in the contributions to this thesis.

The desired frequency response of a causal lowpass FIR filter of order N is given by

$$H_{\text{des}}(e^{j\omega T}) = \begin{cases} e^{-j\omega T \frac{N}{2}}, & \omega T \in [0, \omega_c T], \\ 0, & \omega T \in [\omega_s T, \pi], \end{cases} \quad (2.10)$$

where the frequencies $\omega_c T$ and $\omega_s T$ indicate the passband and stopband edges, respectively. The specification of a lowpass filter $H(e^{j\omega T})$ is shown in Fig. 2.2 and commonly given as

$$\begin{aligned} 1 - \delta_p \leq |H(e^{j\omega T})| \leq 1 + \delta_p, & \quad \omega T \in [0, \omega_c T], \\ |H(e^{j\omega T})| \leq \delta_s, & \quad \omega T \in [\omega_s T, \pi], \end{aligned} \quad (2.11)$$

where δ_p and δ_s denote the passband and stopband ripples. There are no requirements on the magnitude response in the transition band, which is generally referred as a *don't-care band*. For a linear-phase FIR filter, the specification in (2.11) can be defined in terms of the zero-phase frequency response $H_R(\omega T)$ introduced in (2.7) according to

$$\begin{aligned} 1 - \delta_p \leq H_R(\omega T) \leq 1 + \delta_p, & \quad \omega T \in [0, \omega_c T], \\ -\delta_s \leq H_R(\omega T) \leq \delta_s, & \quad \omega T \in [\omega_s T, \pi]. \end{aligned} \quad (2.12)$$

Filter Order Estimation

Compared to IIR filters, there are no closed-form expressions determining the minimum filter order for FIR filters. However, there are many approximation formulas available, which have been derived empirically [114, 115, 118, 119]. For a given specification, one can estimate the order of a linear-phase lowpass FIR filter using, for example, the expression given by [114]

$$\hat{N} = -\frac{4\pi \log_{10}(10\delta_p\delta_s)}{3(\omega_s T - \omega_c T)}. \quad (2.13)$$

Thus, the narrower the transition band, the higher is the filter order required to meet the desired specification.

Design Methods

There are four common methods to design FIR filters, namely, the windowing method, minimax optimization, LS method, and frequency-sampling method.

Design by the Windowing Method. In the windowing method, the impulse response $h(n)$ of an FIR filter is obtained by multiplying the ideal impulse response $h_I(n)$ by a window sequence $w_I(n)$, i.e.,

$$h(n) = h_I(n)w_I(n), \quad (2.14)$$

where $h_I(n)$ is the infinite-duration impulse response of an ideal filter obtained using the inverse Fourier transform of the ideal frequency response $H_I(e^{j\omega T})$, i.e., when $\omega_c T = \omega_s T$ in (2.10). In the frequency domain, the response $H(e^{j\omega T})$ is a convolution of the ideal frequency response $H_I(e^{j\omega T})$ with the window's Fourier transform $W_I(e^{j\omega T})$. A variety of windows are available, including rectangular, Hamming, Hanning, Blackman-Harris, and Kaiser windows [76, 120].

Although this method is straightforward and simple, the drawback of it is that the order of the designed FIR filters is higher compared to other available methods, which leads to relatively high implementation complexity. Moreover, the windowing approach does not allow an explicit control of the band edges or error weighting.

Minimax Design. Optimization-based design methods allow to obtain an optimal solution in terms of filter parameters and meet the desired specification. One common method is the Parks-McClellan algorithm, which is used for designing linear-phase FIR filters using minimax (Chebyshev) optimization by minimizing the maximum error between the desired and actual frequency responses [121]. For lowpass FIR filter design, the following

problem needs to be solved. For a given filter of order N , find $N + 1$ impulse response values $h(n)$ as well as δ to

$$\begin{aligned} & \text{minimize } \delta \\ & \text{subject to } |E(\omega T)| \leq \delta, \end{aligned} \quad (2.15)$$

where $E(\omega T)$ is a *weighted error function*, given by

$$E(\omega T) = W(\omega T)[H(e^{j\omega T}) - H_{\text{des}}(e^{j\omega T})], \quad (2.16)$$

with $H(e^{j\omega T})$ as in (2.2), $H_{\text{des}}(e^{j\omega T})$ as in (2.10), and the *weighting function* $W(\omega T)$ given by

$$W(\omega T) = \begin{cases} 1, & \omega \in [0, \omega_c T], \\ \delta_p / \delta_s, & \omega \in [\omega_s T, \pi]. \end{cases} \quad (2.17)$$

The specification is met if δ after the optimization satisfies $\delta \leq \delta_p$. The resulting filter is optimal in the minimax (Chebyshev) sense, meaning that it is not possible to find another filter of equal or lower order with a smaller value of the error $E(\omega T)$ in (2.16).

Least-Squares Design. In the applications where requirements on the error energy are given, it is appropriate to design a filter by minimizing the total squared error between the desired filter response $H_{\text{des}}(e^{j\omega T})$ and the actual filter response $H(e^{j\omega T})$ [76]. Thus, the design problem is stated as L_2 -norm minimization as follows. For a given filter order N , find $N + 1$ impulse values $h(n)$ to

$$\text{minimize } \|E\|_2^2, \quad (2.18)$$

where

$$\|E\|_2^2 = \frac{1}{2\pi} \int_{\omega T \in \Omega} |H(e^{j\omega T}) - H_{\text{des}}(e^{j\omega T})|^2 d(\omega T) \quad (2.19)$$

with $H(e^{j\omega T})$ as in (2.2), $H_{\text{des}}(e^{j\omega T})$ as in (2.10), and $\Omega = [-\pi, -\omega_s T] \cup [-\omega_c T, \omega_c T] \cup [\omega_s T, \pi]$.

For a linear-phase FIR filter, (2.18) can be expressed as

$$\text{minimize } \frac{1}{\pi} \int_{\omega T \in \Omega_p} |H_R(\omega T) - H_{R,\text{des}}(\omega T)|^2 d(\omega T), \quad (2.20)$$

where $H_{R,\text{des}}(\omega T)$ is the desired zero-frequency response with one in the passband and zero in the stopband, and $\Omega_p = [0, \omega_c T] \cup [\omega_s T, \pi]$. For a Type I linear-phase filter, the response $H_R(\omega T)$ in (2.7) can be written as

$$H_R(\omega T) = \sum_{n=0}^{N/2} b(n) \cos(\omega T n) = \mathbf{b}^T \mathbf{c}(\omega T), \quad (2.21)$$

where

$$\mathbf{b} = [h(N/2), 2h(N/2 - 1), \dots, 2h(0)]^T, \quad (2.22)$$

$$\mathbf{c}(\omega T) = [1, \cos(\omega T), \dots, \cos(\omega T N/2)]^T. \quad (2.23)$$

Then the solution of the problem (2.20) is given by

$$\mathbf{b} = \mathbf{Q}^{-1} \mathbf{p}, \quad (2.24)$$

where \mathbf{Q} is a symmetric positive-definite $(N/2 + 1) \times (N/2 + 1)$ matrix [122] with the elements $Q(n, m)$ given by

$$Q(n, m) = \frac{1}{\pi} \int_0^{\omega_c T} \cos(\omega T n) \cos(\omega T m) d(\omega T) + \frac{1}{\pi} \int_{\omega_s T}^{\pi} \cos(\omega T n) \cos(\omega T m) d(\omega T). \quad (2.25)$$

Further, \mathbf{p} represents a vector of length $N/2 + 1$ with the elements $p(m)$ given by

$$p(m) = \frac{1}{\pi} \int_0^{\omega_c T} \cos(\omega T m) d(\omega T). \quad (2.26)$$

If a weighted error function $W(\omega T)$ is desired, the problem in (2.20) is modified as

$$\mathbf{minimize} \quad \frac{1}{\pi} \int_{\omega T \in \Omega_p} W(\omega T) |H_R(\omega T) - H_{R,\text{des}}(\omega T)|^2 d(\omega T), \quad (2.27)$$

where $W(\omega T)$ has the gain α for $\omega T \in [0, \omega_c T]$ and $1 - \alpha$ for $\omega T \in [\omega_s T, \pi]$. Then, the solution is obtained as in (2.24) with \mathbf{Q} and \mathbf{p} including the corresponding weights in the passband and stopband regions [76, 122].

Frequency-Sampling-Based Design. This design method is based on deriving the filter DFT coefficients for the passband and stopband directly by sampling the desired frequency response in (2.10) and optimizing the

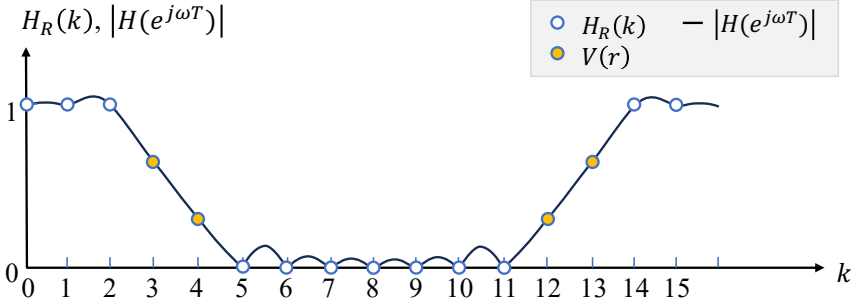


Figure 2.3: Concept of the frequency-sampling-based FIR filter design.

transition band values, which are generally not specified, to minimize the error between the actual and the desired frequency responses.

Let $H_{\text{des}}(k) = H_{\text{des}}(e^{j\omega_k T})$ be the samples of the desired frequency response for a filter of order $N - 1$, uniformly spaced in the interval $[0, 2\pi)$, where $\omega_k T = 2\pi k/N$, $k = 0, \dots, N - 1$. Thus, the coefficients $H(k)$ can be expressed as

$$H(k) = H_R(k)e^{-j\frac{\pi k(N-1)}{N}} \quad (2.28)$$

with the magnitude response samples $H_R(k)$ given by

$$H_R(k) = \begin{cases} 1, & k \in [0, k_1 - 1] \cup [N - k_1 + 1, N - 1], \\ V(k - k_1), & k \in [k_1, k_2] \cup [N - k_2, N - k_1], \\ 0, & k \in [k_2 + 1, N - k_2 - 1], \end{cases} \quad (2.29)$$

where k_1 and k_2 are the first and the last sample indices of the transition band⁴. An example of the magnitude response samples $H_R(k)$ with the transition band samples $V(r)$, $r = k - k_1 = 0, \dots, k_2 - k_1$, is shown in Fig. 2.3 for $N = 16$.

Further, the impulse response coefficients, obtained by the IDFT, are given by [76]

$$h(n) = \frac{1}{N} \sum_{k=0}^{N-1} H(k)e^{j2\pi kn/N}. \quad (2.30)$$

Substituting (2.30) in (2.2), the frequency response of the actual filter is

⁴The expression in (2.29) assumes $k_1 > 1$. For $k_1 = 1$, (2.29) is modified for the passband, which consists of only one sample for $k = 0$.

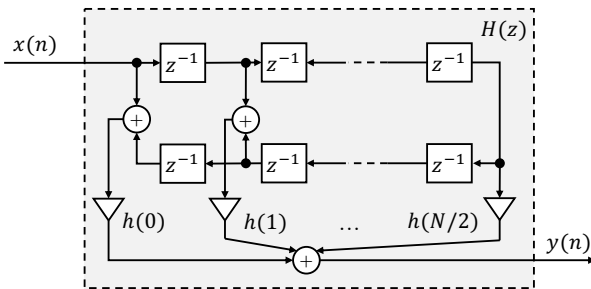


Figure 2.4: Time-domain implementation of a Type I linear-phase FIR filter.

obtained as

$$H(e^{j\omega T}) = \frac{1}{N} \sum_{n=0}^{N-1} \sum_{k=0}^{N-1} H(k) e^{j2\pi kn/N} e^{-j\omega T n}. \quad (2.31)$$

Therefore, the error between the responses $H_{\text{des}}(e^{j\omega T})$ and $H(e^{j\omega T})$ can be minimized by determining values of $V(r)$, that can be carried out using iterative optimization algorithms [123–125] or the LS method [126].

2.1.4 Realizations of FIR Filters

Time-Domain Realizations

A time-domain realization of a Type I linear-phase FIR filter is shown in Fig. 2.4. Since the impulse responses of linear-phase filters are either symmetric or antisymmetric, the number of multiplications can be reduced by approximately a factor of two compared to regular FIR filters, however the number of additions and delay elements remain the same.

Complexity of Time-Domain Realization. Implementation complexity can be measured by the number of multiplications C_m^{TD} , number of additions C_a^{TD} , and number of delay elements C_d^{TD} . For the time-domain filter implementations, these numbers can also be viewed as complexity per output sample. For a linear-phase FIR filter, implementation complexity expressions are given in Table 2.1.

Frequency-Domain Realizations

As mention in Section 2.1, the linear convolution in (2.4) corresponds to the multiplication of DFT coefficients in the frequency domain as in (2.5). It can

Table 2.1: Complexity expressions for linear-phase FIR filters realized in the time domain.

	Type I	Type II	Type III	Type IV
C_m^{TD}	$N/2 + 1$	$(N + 1)/2$	$N/2$	$(N + 1)/2$
C_a^{TD}	N	N	$N - 1$	N
C_d^{TD}	N	N	N	N

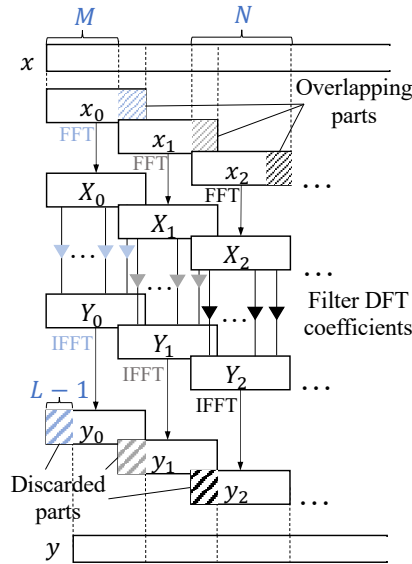


Figure 2.5: Overlap-save method.

be efficiently implemented using FC with much lower complexity than in the time-domain [13, 127–129]. The most widely-used techniques are the OLS and overlap-add (OLA) methods which employ the DFT and IDFT [3]. The number of multiplications per sample is the same for both methods, but the former requires slightly less additions per sample than the latter. Thus, the OLS method is more common to implement.

The main idea of the OLS method, shown in Fig. 2.5, is that the input signal is divided into overlapping segments $x_m(n) = x(n + mM)$, $n = 0, 1, \dots, N - 1$, where m is a segment index and the overlapping part is $N - M$. Then, for each segment, the following computations are carried out.

1. The segment x_m is transformed via an N -point DFT.
2. The DFT coefficients $X_m(k)$ are multiplied by the filter DFT bins $H(k)$.

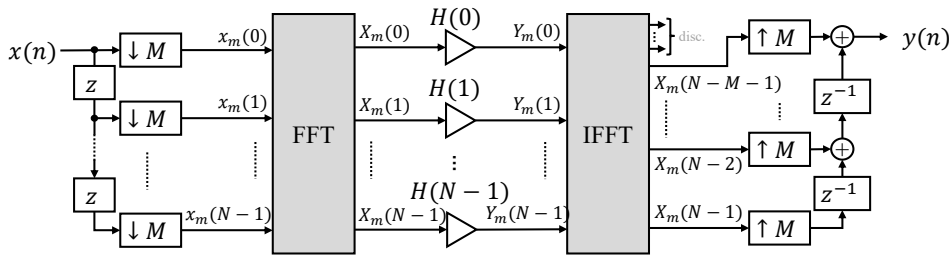


Figure 2.6: FIR filter frequency-domain implementation using the OLS method.

3. An N -point inverse discrete Fourier transform (IDFT) is computed.
4. The first $N - M$ samples of the resulting block are discarded, so that the output segments of length M are no longer overlapping.
5. The output sequence is obtained by concatenating the resulting segments as $y(n) = \sum_{m=0}^{\infty} y_m(n - mM)$.

The FIR filter frequency-domain implementation using the OLS method is shown in Fig. 2.6.

In classical OLS filtering, the system is intended to be time-invariant, i.e., the aliasing error is zero. In this case, the DFT coefficients $H(k)$ of an FIR filter correspond to the N -point DFT of the impulse response $h(n)$ of length L , designed by any of the available methods [4]. This means $h(n) = 0$ for $n = L, \dots, N - 1$, where $L = N - M + 1$.

However, for the frequency-sampling-based design method, the filter DFT coefficients $H(k)$ are directly obtained by sampling the desired frequency response, and the impulse response $h(n)$ is obtained by the IDFT of $H(k)$, resulting in a non-zero tail for $n = L, \dots, N - 1$. In this case, the overall system becomes time-varying, and an aliasing error occurs [50, 129]. This error cannot be cancelled but can be controlled during the design process by optimizing the transition band samples $V(r)$, $r = k - k_1 = 0, \dots, k_2 - k_1$, to meet the desired specification. This is discussed in Papers D and E for VDFs.

Complexity of Frequency-Domain Realizations. The total implementation complexity of FIR filter frequency-domain implementations is typically expressed as the number of computations per output sample and consists of two parts, namely, DFT/IDFT computing and the multiplications by the filter DFT coefficients. For the OLS technique with M output samples,

the complexity is given in terms of multiplication rate R_m^{FD} and addition rate R_a^{FD} per output sample as

$$R_m^{\text{FD}} = \frac{2C_m^{\text{DFT}} + C_m^{\text{W}}}{M}, \quad (2.32)$$

$$R_a^{\text{FD}} = \frac{2C_a^{\text{DFT}} + C_a^{\text{W}}}{M}, \quad (2.33)$$

respectively, where C_m^{DFT} and C_a^{DFT} are the numbers of multiplications and additions for the DFT/IDFT, and C_m^{W} and C_a^{W} are the numbers of multiplications and additions for weighting by the DFT filter coefficient $H(k)$, $k = 0, 1, \dots, N - 1$.

The DFT and IDFT can be efficiently implemented using the fast Fourier transform (FFT) and its inverse (IFFT). The complexity of FFT/IFFT depends on two factors, namely, the type of the FFT algorithm and whether the complex multiplications are implemented with three real multiplications and three real additions (referred as the 3/3 algorithm) or with four real multiplications and two real additions (referred as the 4/2 algorithm) [130]. A complex addition requires two real additions. Then, assuming the split-radix FFT algorithm is implemented together with the 3/3 algorithm for a real-valued sequence $x_m(n)$ of length $N = 2^Q$, the complexity of FFT/IFFT is given by

$$C_m^{\text{DFT}} = (1/2)N \log_2 N - (3/2)N + 2, \quad (2.34)$$

$$C_a^{\text{DFT}} = (3/2)N \log_2 N - (5/2)N + 4. \quad (2.35)$$

Further, considering that $h(n)$ is real-valued, the DFT coefficients of $x_m(n)$ and $h(n)$ are conjugate symmetric, and thus only half of the multiplications needs to be carried out. Then, weighting by $H(k)$ requires⁵ $C_m^{\text{W}} = C_a^{\text{W}} = 3N/2$, and thus the total implementation complexity of an OLS-based FIR filter is

$$R_m^{\text{FD}} = \frac{N \log_2 N - (3/2)N + 4}{M}, \quad (2.36)$$

$$R_a^{\text{FD}} = \frac{3N \log_2 N - (7/2)N + 8}{M}. \quad (2.37)$$

⁵For real-valued sequences, Hermitian symmetry reduces the number of independent frequency bins to $\lfloor N/2 \rfloor + 1$. Using the 3/3 algorithm, this gives approximately $3N/2$ real multiplications and additions, with minor deviation depending on whether N is even or odd, which is negligible when computing the complexity per output sample for relatively big M .

2.1.5 Finite Word Length Effects

In practical digital filters, their coefficients and the processed signals must be represented with a finite number of bits. Therefore, floating-point coefficients are quantized and the internal word length of the filters is analyzed to ensure that the quantization errors, roundoff noise, and possible overflow effects remains within acceptable limits. This phase in the digital filter design process is commonly referred to as finite word length analysis [116, 117].

Fixed-Point Representation

Many implementation strategies generally assume fixed-point two's complementary number representation due to its advantages in hardware implementation, including handling signed numbers and temporary overflow. This representation is given by

$$x = -x_0 + \sum_{i=1}^{W-1} x_i 2^{-i}, \quad (2.38)$$

where W is the word length, i.e., the number of bits used to represent the number, x_0 represents the sign bit, x_i are the fractional bits, $i = 1, \dots, W - 1$, and $x \in [-1, 1 - 2^{-W-1}]$ is the normalized (fractional) two's complement representation.⁶

Coefficient Quantization

The use of fixed-point arithmetic requires quantizing all coefficients and data sequence values within a finite word length. Generally, one needs to obtain as few total bits as possible to reduce the power consumption of the resulting system [116].

Compared to infinite-precision frequency response $H(e^{j\omega T})$ discussed in Section 2.1.3, quantization of FIR filter coefficients primarily results in slight deviations of the passband and stopband characteristics, i.e., in a modified frequency response $H_q(e^{j\omega T})$ and corresponding transfer function $H_q(z)$ [122]. Therefore, it is common to set a level of the specification degradation due to the quantization of the filter coefficients. Then, following the optimization problem in (2.15), the filter coefficients word length can be obtained to meet the specified criteria

$$\begin{aligned} |H_q(e^{j\omega T}) - H_{\text{des}}(e^{j\omega T})| &\leq k\delta_p, & \omega T &\in [0, \omega_c T], \\ |H_q(e^{j\omega T})| &\leq k\delta_s, & \omega T &\in [\omega_s T, \pi], \end{aligned} \quad (2.39)$$

⁶For convenience, numbers are typically normalized to the range $[-1, 1)$.

with the desired passband and stopband ripples defined as $k\delta_p$ and $k\delta_s$, respectively, and k being the degradation tolerance.⁷

Integer Linear Programming

An alternative approach to the analysis of the finite word length effect after designing a floating-point filter is to directly design the filter coefficients as integers. This approach is commonly referred to as integer linear programming [131]. The main idea is to formulate the filter design problem as an optimization problem with integer constraints on the filter coefficients. This approach can simplify the design process, allowing for the direct control of the coefficients' word length. However, this approach possesses high computational complexity and cannot be used for cascaded filters. Thus, in many cases, including the one in Paper B, the word length analysis is carried out using the approach presented in Fig. 2.1, i.e., by first designing a floating-point filter and then analyzing the finite word length effect through coefficients rounding.

Data Quantization

Data quantization generally involves quantization of the input signal and results of the internal operations. The former is commonly analyzed based on analog-to-digital converter (ADC) quantization noise, and the latter is evaluated using roundoff noise [116].

ADC quantization noise: The input signal to a digital filter can be represented as

$$x_q(n) = x(n) + e(n), \quad (2.40)$$

where $x(n)$ refers to the original (non-quantized) signal and $e(n)$ denotes the error due to the quantization in the preceding ADC. Typically, the quantization noise is modeled as white noise with the variance σ_e^2 and zero mean if uniform quantizer is considered [116]. For an ADC with Q_{ADC} bits, $\sigma_e^2 = 2^{-2(Q_{\text{ADC}}-1)}/12$. By propagation through the filter, the ADC noise power at the output can be obtained as

$$\sigma_{\text{ADC}}^2 = \frac{\sigma_e^2}{2\pi} \int_{-\pi}^{\pi} |H(e^{j\omega T})|^2 d(\omega T). \quad (2.41)$$

⁷In general, the degradation tolerance for the passband and stopband can be different.

Roundoff noise: During filter computations using fixed-point implementations, arithmetic operations such as multiplications, additions, and subtractions may produce results that must be quantized using rounding or truncation to fit the available word length. Errors caused by either of the quantization method are often referred to as rounding errors and appear as roundoff noise [116]. Similar to the ADC quantization noise, any quantization operation here can be represented as a sum of the corresponding input signal and a noise source, modeled as white noise with zero mean and variance σ_e^2 . Since there are typically several quantization operations inside the filter, the total roundoff noise at the output is obtained by summing the contributions from all noise sources due to data quantization. This means that the variance of the total noise is given by

$$\sigma_R^2 = \sum_{m=1}^M \sigma_m^2, \quad (2.42)$$

where m is the index of the quantization operation, M is the total number of quantization operations, and σ_m^2 represents the contribution of the m th quantization operation. It can be computed as

$$\sigma_m^2 = \sigma_e^2 \sum_{n=0}^{\infty} |g_m(n)|^2, \quad (2.43)$$

with $g_m(n)$ being the impulse response from the point where the quantization is introduced to the output of the filter.

Thus, the total noise power at the filter output is

$$\sigma_y^2 = \sigma_{\text{ADC}}^2 + \sigma_R^2. \quad (2.44)$$

The impact of data quantization depends on many factors, such as filter structure and selected word length. If not properly controlled, these quantization errors result in a severe degradation of the signal-to-noise ratio (SNR) at the output of the filter. For this reason, an analysis on the finite word length effect is an important step in digital filter design process.

2.1.6 Digital Differentiators

Digital differentiators find their applications in various domains including communication systems and speech processing. This type of digital filters can be used as a part of systems for bandwidth extension and signal quality enhancement by compensating channel distortion and mitigating intersymbol interference [116, 132].

The desired frequency response for a causal digital differentiator of order N_D is given by [133]

$$D_{\text{des}}(j\omega T) = e^{-j\omega T N_D/2} (j\omega T)^k \quad (2.45)$$

for $|\omega T| \leq \omega_c T < \pi$ with k determining the degree of the differentiator.

For design of a digital differentiator, linear-phase FIR filters can be used. Thus, the frequency response of the differentiator can be written as [133]

$$H(e^{j\omega T}) = \begin{cases} e^{-j\omega T N_D/2} H_R(\omega T), & \text{for Type I and II,} \\ j e^{-j\omega T N_D/2} H_R(\omega T), & \text{for Type III and IV,} \end{cases} \quad (2.46)$$

where the function $H_R(\omega T)$ is real-valued. Using (2.45) and (2.46), one can design a digital differentiator by minimizing the error between the desired and actual responses in the minimax sense or LS sense using a similar approach as for a linear-phase FIR filter design mentioned in Section 2.1.3.

2.2 Multirate Systems and Filter Banks

In multirate systems, the sampling rate is changed during the signal processing. Many DSP applications, for example communications and audio processing, utilize multirate techniques because their use can simplify and reduce computational complexity. Variable digital filters can also be efficiently implemented using these techniques. Thus, this chapter gives an introduction to basic elements of multirate systems and filter banks, which can be used to analyze and design time-varying systems as discussed in Papers D and E.

2.2.1 Basic Multirate Operations

Generally, different parts of multirate systems operate at different sampling frequencies, and thus an essential part of these systems is sampling rate conversion, which employs the fundamental operations of multirate DSP, namely interpolation and decimation.

Interpolation. Interpolation generates a new sequence with a higher sampling frequency, while maintaining the original signal information. For interpolation with an integer factor L , this is a two-stage process, which consists of upsampling following by filtering as shown in Fig. 2.7a. The first stage, upsampling by a factor of L , inserts $L - 1$ zeros between each input sample pair, i.e., a new signal $x_1(m)$ formed from $x(n)$ is expressed as [122]

$$x_1(m) = \begin{cases} x\left(\frac{m}{L}\right), & m = 0, \pm L, \pm 2L, \dots, \\ 0, & \text{otherwise,} \end{cases} \quad (2.47)$$

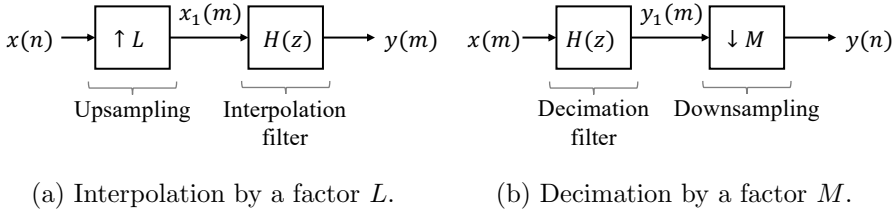


Figure 2.7: Principle of interpolation and decimation.

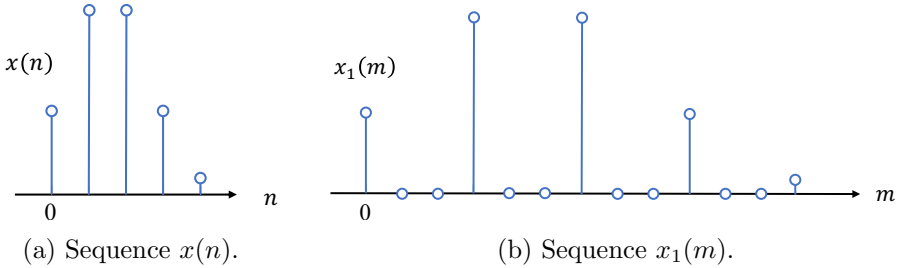


Figure 2.8: Illustration of upsampling by a factor $L = 3$ in the time domain.

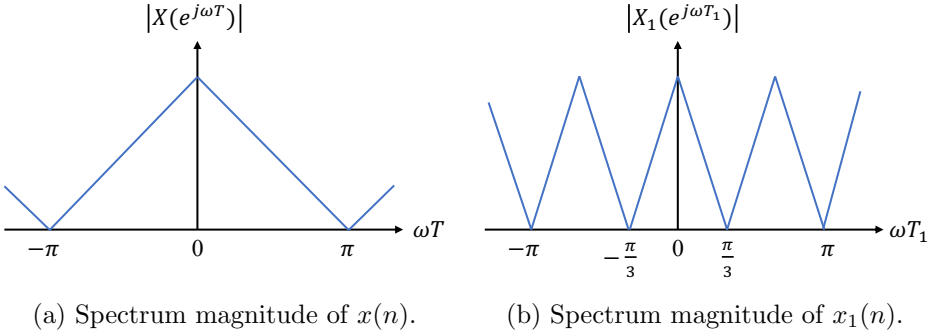


Figure 2.9: Illustration of upsampling by a factor $L = 3$ in the frequency domain.

where $L > 1$. In the frequency domain, the Fourier transform of $x_1(m)$ is given by

$$X_1(e^{j\omega T_1}) = X_1(e^{j\omega T/L}) = X(e^{j\omega T}) = X(e^{j\omega T_1 L}), \quad (2.48)$$

where T and $T_1 = T/L$ are the sampling periods before and after upsampling, respectively. The corresponding z -transform is

$$X_1(z) = X(z^L). \quad (2.49)$$

Illustrations of upsampling by a factor of $L = 3$ in the time domain and in the frequency domain are shown in Figs. 2.8 and 2.9, respectively.

In the second stage, an interpolation filter is used to remove images created due to upsampling. Ideally, it is a lowpass with cutoff frequency π/L . The output signal $y(n)$ is obtained as a convolution between $x_1(n)$ and the filter impulse response $h(n)$.

Decimation. Decimation by an integer factor M , shown in Fig. 2.7b, is also a two-stage process, consisting of filtering followed by downsampling. The filter, which is ideally a lowpass with cutoff frequency π/M , ensures that the signal being decimated is bandlimited to avoid aliasing. Further, downsampling reduces the sampling rate by a factor of M by extracting every M th value of the signal, i.e., the output signal $y(n)$ is obtained from $y_1(m)$, which is a result of convolution between the input signal $x(n)$ and the filter impulse response $h(n)$, as

$$y(n) = y_1(Mn). \quad (2.50)$$

In the frequency domain, downsampling is expressed as

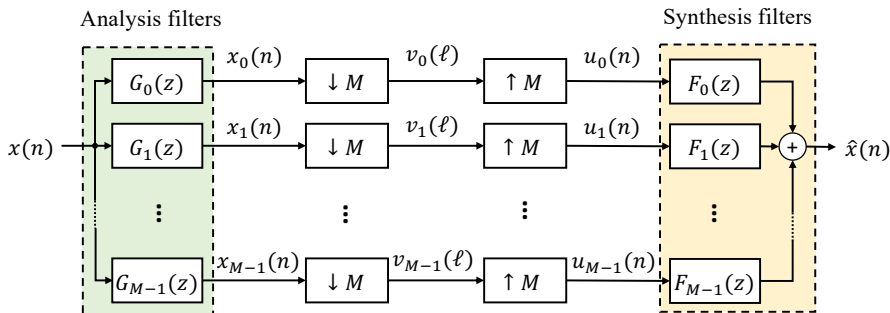
$$\begin{aligned} Y(e^{j\omega T}) &= \frac{1}{M} \sum_{m=0}^{M-1} Y_1(e^{j(\omega T - 2\pi m)/M}) \\ &= \frac{1}{M} \sum_{m=0}^{M-1} Y_1(e^{j(\omega T_1 - 2\pi m/M)}), \end{aligned} \quad (2.51)$$

where T_1 and $T = MT_1$ are the sampling periods before and after downsampling, respectively. The corresponding z -transform is

$$Y(z) = \frac{1}{M} \sum_{m=0}^{M-1} Y_1(z^{1/M} W_M^m), \quad (2.52)$$

where $W_M^m = e^{-j2\pi m/M}$ [122]. Thus, the output signal spectrum is the sum of M stretched and shifted versions of $Y_1(e^{j\omega T_1})$.

Sampling rate conversion by a rational factor L/M , where both L and M are integers, can be realized by combining interpolation and decimation [116, 122]. However, when L and M are large, i.e., the rational factor is close to unity, this approach can be computationally inefficient. In this case, the Farrow-structure-based interpolators are typically used [92, 93, 95], which will be discussed in Chapter 3.


 Figure 2.10: M -channel maximally decimated filter bank.

2.2.2 Filter Banks

A system of digital filters with a common input and/or common output, capable of processing various bands of a signal separately, is referred to as a FB. One special type of FBs is an M -channel maximally decimated FB, which is shown in Fig. 2.10. It contains the analysis bank of M filters $G_k(z)$, which splits the input signal $x(n)$ into M subband signals $x_k(n)$, $k = 0, \dots, M - 1$, downsamplers by M , upsamplers by M , and the synthesis bank of M filters $F_k(z)$, which recombine the signals to produce $\hat{x}(n)$. The downsampled signals $v_k(\ell)$ can be processed individually, which is required in many applications, for instance, subband coding in audio processing [122], channelization in wireless communication systems [40, 50, 124, 134], and hearing aid devices [29, 37, 135]. The z -transform of $v_k(\ell)$ is given by

$$V_k(z) = \frac{1}{M} \sum_{m=0}^{M-1} G_k(z^{1/M} W^m) X(z^{1/M} W^m), \quad (2.53)$$

while the output of the FB is expressed as

$$\hat{X}(z) = \frac{1}{M} \sum_{m=0}^{M-1} X(zW^m) \sum_{k=0}^{M-1} G_k(zW^m) F_k(z). \quad (2.54)$$

This input-output relation can be expressed as

$$\hat{X}(z) = \sum_{m=0}^{M-1} A_m(z) X(zW^m), \quad (2.55)$$

where

$$A_m(z) = \frac{1}{M} \sum_{k=0}^{M-1} G_k(zW^m)F_k(z), \quad (2.56)$$

with $A_0(z)$ being the distortion function and $A_m(z)$ being the aliasing functions for $m = 1, \dots, M - 1$. The term $X(zW^m)$ is referred to as the m th aliasing term with the gain $A_m(z)$ [122]. For a perfect reconstruction (PR) FB, i.e., when $\hat{x} = cx(n - n_0)$ for some constant $c \neq 0$ and delay n_0 , the distortion and aliasing functions must satisfy

$$A_0(z) = cz^{-n_0}, \quad A_m(z) = 0 \quad \text{for } m = 1, \dots, M - 1. \quad (2.57)$$

For non-maximally decimated FBs, the number of subbands is greater than the downsampling and upsampling factors ($N > M$), and the functions $A_m(z)$ in (2.55) are given by [122]

$$A_m(z) = \frac{1}{M} \sum_{k=0}^{N-1} G_k(zW^m)F_k(z). \quad (2.58)$$

This is commonly used when realizing a so called fast-convolution filter bank (FCFB) [21, 50, 136], as will be discussed in Section 3.3.

For modulated FBs, design starts from design of a prototype filter, for example using the techniques described in Section 2.1.3. Then all the filters involved in the FB can be expressed in terms of the prototype filter to satisfy certain criteria [122].

Linear Periodically Time-Varying Systems. In practice, the filters $G_k(z)$ and $F_k(z)$ are not ideal, i.e., the transition band and stopband gain are non-zero, therefore this can result in aliasing. Unless it is canceled, a general FB with N channels and M -fold downsamplers and upsamplers corresponds to an LPTV system with period M [122, 137]. The output of such a system is given by

$$y(n) = \sum_{q=0}^{Q-1} h_n(q)x(n - q), \quad (2.59)$$

where Q is the length of the M -periodic impulse response $h_n(q) = h_{n+M}(q)$, $n = 0, \dots, M - 1$.

Design of LPTV systems has to include measuring distortion function and aliasing functions, or analysis of periodically time-varying impulse

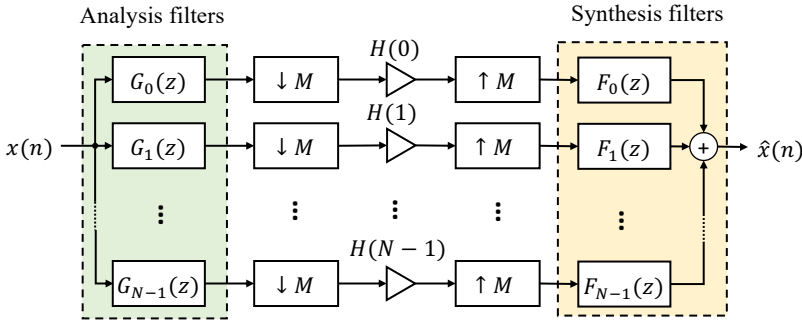


Figure 2.11: Multirate FB representation of the system in Fig. 2.6.

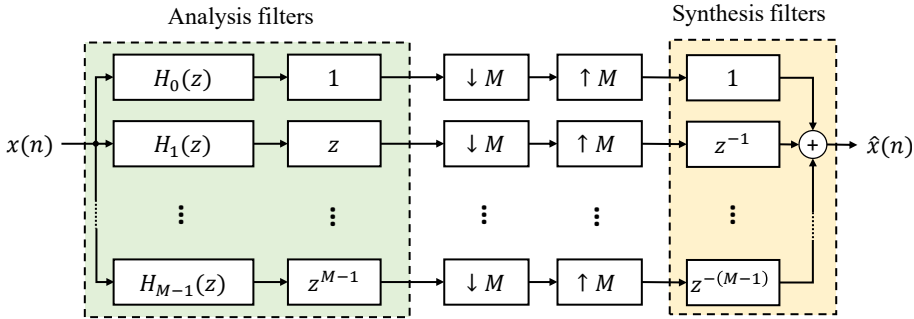


Figure 2.12: PTVIR representation of the system in Fig. 2.11.

response (PTVIR) representation which corresponds to a set of M time-invariant impulse responses $h_n(q)$ and their corresponding frequency responses $H_n(e^{j\omega T})$ [129, 137–139].

For the first approach, one should ensure that $A_m(z) = 0$ for $m = 1, \dots, M - 1$ in (2.58). To achieve PR, the aliasing and distortion functions must satisfy (2.57). The second approach is commonly used for design of LPTV FIR filters, when aliasing cannot be canceled but can be suppressed to any desired level through a proper design. In this case, the system in Fig. 2.6 can be represented as an equivalent N -channel FB with the multiplication by $H(k)$ between the M -fold downsampler and upsampler in every branch k , $k = 0, \dots, N - 1$, as shown in Fig. 2.11. Then, the frequency responses of

the analysis and synthesis filters are given as [129]

$$G_k(e^{j\omega T}) = \sum_{n=0}^{M-1} e^{j2\pi(n+1)k/N} e^{-j\omega T n} \quad (2.60)$$

and

$$F_k(e^{j\omega T}) = \frac{1}{N} \sum_{n=0}^{N-1} e^{j2\pi(n-M)k/N} e^{-j\omega T n}, \quad (2.61)$$

respectively. This N -channel FB with M -fold downsampling and upsampling can be represented as an equivalent PTVIR system, shown in Fig. 2.12, with the M time-invariant filters $H_n(e^{j\omega T})$, given by [129]

$$H_n(z) = z^{-n} \sum_{k=0}^{N-1} H(k) G_k(z) F_{kn}(z^M), \quad (2.62)$$

where $F_{kn}(z)$ is the so called *polyphase component* of $F_k(z)$ being defined as [122]

$$F_k(z) = \sum_{n=0}^{M-1} z^{-n} F_{kn}(z^M). \quad (2.63)$$

The distortion and aliasing functions in (2.55) can be expressed in terms of $H_n(z)$ as [129]

$$A_m(z) = \frac{1}{M} \sum_{n=0}^{M-1} H_n(zW^m) W_M^{mn}. \quad (2.64)$$

This means that the distortion function $A_0(z)$ is the average of the M filter transfer functions $H_n(z)$ while each aliasing function is the average of frequency-shifted and rotated versions of $H_n(z)$. Thus, to design an LPTV FIR filter (or a corresponding multirate FB representation) by suppressing aliasing to a desired level, each of the responses $H_n(e^{j\omega T})$ should approximate the desired frequency response $H(e^{j\omega T})$ of the overall system.

Chapter 3

Variable Digital Filters

This chapter gives an introduction to VDFs and presents a review of the most common types of VDFs.

3.1 Introduction

Due to the increasing demand for computational complexity reduction while preserving flexibility, reconfigurable systems are getting more attention in the contemporary world of technologies. For instance, recent communication standards require flexible, adaptive systems capable of real-time frequency-domain tuning [140, 141]. Such requirements can be fulfilled by means of VDFs. The key feature of VDFs is that they require only an adjustment of one or a few parameters to change their characteristics, without the need for extensive additional computations. Compared to regular digital filters, which require recomputing all coefficients for every new specification, i.e., online filter design using one of the methods mentioned in Section 2.1.3, generally leading to high computational complexity, most coefficients in VDFs are fixed after the initial design. This allows efficient hardware implementation and makes VDFs essential for many modern adaptive technologies, for example in communication systems [30, 31, 33, 39, 45, 47, 48, 50, 142] and medicine [26, 37, 44, 143].

Research on VDFs emerged in the 1970s [65]. The first methods for designing VDFs were mainly for lowpass digital filters with variable cutoff and center frequencies based on spectral transformations applied to a prototype linear-phase lowpass FIR filter [67, 72, 74]. Further, this approach was developed and extended to bandpass filters [69, 71]. For design of variable IIR filters, allpass transformations were utilized to transform a lowpass prototype

filter to the desired frequency-selective filters [70, 73, 144]. However, in most cases, transformation-based methods appeared to suffer from some inherent limitations and high computational cost.

Alternative methods, which are more general and based on spectral parameter approximation, were introduced later [63, 64, 66]. The main idea consists of representing the impulse responses or the poles and zeros as polynomials of the variable spectral parameters and a set of constant coefficients. This approach allowed continuous tuning of VDFs directly by the spectral parameters with the reduced implementation complexity compared to the transformation-based methods. Further, it was shown that VDFs can be efficiently implemented based on the Farrow structure [68]. This has led to the growth of research works on FIR VDFs due to their simple design procedures and good filter properties [61, 62, 145], especially digital FIR filters with adjustable fractional delay received considerable attention [27, 28, 31, 32, 38, 41, 53, 54, 61, 145–147]. Later, the Farrow structure was also utilized in digital filters with adjustable bandwidth [30, 39, 44, 46, 58] and for simultaneously variable bandwidth and fractional delay [51, 59].

In addition to the transformation-based and spectral parameter approximation based methods, many other approaches have been proposed for some specific applications. Among these, frequency response masking techniques and filter banks were utilized to design VDFs with a sharp transition band or a channelizer with the ability to control different bands separately in real time [29, 33, 37, 39, 40, 45, 49, 50, 52, 56].

In the thesis contributions, the proposed FIR VDFs are mainly based on the Farrow structure and/or are compared to existing solutions based on this structure or FB-based structures. Therefore, these two types of VDFs are discussed in more detail below.

3.2 Farrow-Based Variable Digital Filters

The Farrow structure [68] has received great attention in realizing VDFs as it allows to achieve an efficient realization of fine tunability with small computational overhead, especially for filters with VFD [27, 31–33, 38, 41, 51, 53, 54, 61, 145] and VBW [24, 30, 34, 39, 43–46, 51, 58, 143, 148]. In this technique, the overall transfer function is expressed as a weighted linear combination of $L + 1$ fixed filters, commonly referred to as *subfilters*. A realization of a Farrow-based VDF is shown in Fig. 3.1. Due to fewer multiplications and inherent stability, linear-phase FIR filters are generally the basic elements of

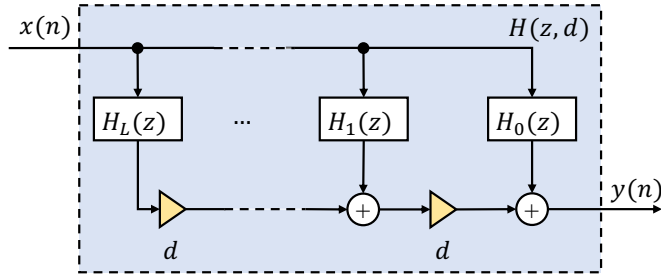


Figure 3.1: Farrow-based realization of a VDF with the variable parameter d .

VDFs. Thus, the overall frequency response is given by

$$H(e^{j\omega T}, d) = \sum_{k=0}^L d^k H_k(e^{j\omega T}), \quad (3.1)$$

where $H_k(e^{j\omega T})$ are typically linear-phase FIR filters of order N_{H_k} and d is a variable parameter that can directly determine, for example, the fractional delay or bandwidth.

Design of Farrow-based VDFs with the overall frequency response $H(e^{j\omega T}, d)$ can be carried out by approximating the desired frequency response, for example, in the minimax sense [24, 58, 145] or in the LS sense [57].

The implementation complexity of Farrow-based VDFs consists of the complexity of the fixed part, represented by $L + 1$ subfilters $H_k(z)$ with constant coefficients, and the variable part, i.e., L general multiplications by the variable coefficient d . Further, to compute the output $y(n)$ after the multiplications by d , L additions are needed. Thus, the total complexity can be expressed in terms of fixed multiplications C_{mf} , variable multiplications C_{mv} , and additions C_{a} given by

$$C_{\text{mf}} = \sum_{k=0}^L C_{\text{mf},k}, \quad (3.2)$$

$$C_{\text{mv}} = L, \quad (3.3)$$

$$C_{\text{a}} = L + \sum_{k=0}^L C_{\text{a},k}, \quad (3.4)$$

where $C_{\text{mf},k}$ and $C_{\text{a},k}$ are the numbers of fixed multiplications and additions

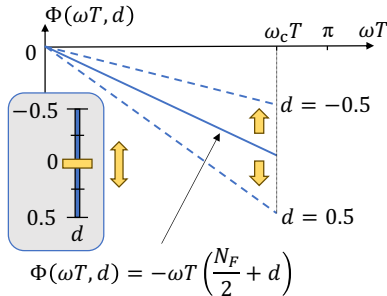


Figure 3.2: Illustration of the VFD filter phase response.

per subfilter k , which depend on the linear-phase FIR filter type as follows

$$C_{\text{mf},k} = \begin{cases} N_k/2 + 1, & \text{Type I,} \\ (N_k + 1)/2, & \text{Type II or IV,} \\ N_k/2, & \text{Type III,} \end{cases} \quad (3.5)$$

$$C_{\text{a},k} = \begin{cases} N_k, & \text{Type I, II, or IV,} \\ N_k - 1, & \text{Type III.} \end{cases} \quad (3.6)$$

Further complexity reduction can be carried out by implementing constant multiplications very efficiently using various techniques for constant multiplications [11–13, 17, 75].

3.2.1 Variable-Fractional-Delay Filters

Digital filters capable of dynamically adjusting a delay that is a fraction of a sample period are referred to as VFD filters. They find applications in telecommunications, audio processing, control systems, and other fields [27, 28, 31–33, 38, 41, 54, 61, 149, 150].

The desired frequency response and phase response of a VFD filter are given by [145]

$$F_{\text{des}}(e^{j\omega T}, d) = e^{-j\omega T(N_F/2+d)}, \quad |\omega T| \leq \omega_c T < \pi \quad (3.7)$$

and

$$\Phi_{\text{des}}(\omega T, d) = -\omega T(N_F/2 + d), \quad |\omega T| \leq \omega_c T < \pi \quad (3.8)$$

respectively, where $\omega_c T$ is the passband edge, N_F is the filter order, and $d \in [-1/2, 1/2]$ is a variable fractional delay. Illustration of the phase response of a VFD filter, controllable by the variable parameter d , is shown in Fig. 3.2.

Farrow-based VFD filters are typically realized as a linear combination of differentiators [38, 51, 54, 61]. This realization, which is shown in Fig. 3.1, has received great attention due to low implementation complexity. The frequency response of a Farrow-structure-based VFD filter is expressed as in (3.1), where each $H_k(e^{j\omega T})$ approximates a differentiator of k th degree and order N_{H_k} , which should preferably be even since this choice results in a lower implementation complexity for the overall VFD filter due to a pure delay in the first branch compared to the odd-order case [145]. Thus, the subfilters $H_k(e^{j\omega T})$ are of Type I or Type III linear-phase filters with symmetric (for even k) or antisymmetric (for odd k) impulse responses $h_k(n)$, i.e., $h_k(n) = h_k(N_{H_k} - n)$ and $h_k(n) = -h_k(N_{H_k} - n)$ for even and odd k , respectively. They can be of different orders, therefore an additional delay $(N_F - N_{H_k})/2$ has to be introduced in a corresponding branch k with lower order to have the same delay $N_F/2$ in every branch, where the overall filter order N_F is given by

$$N_F = \max_k \{N_{H_k}\}. \quad (3.9)$$

The subfilters' frequency responses can be written as

$$H_k(e^{j\omega T}) = \begin{cases} e^{-j\omega T N_{H_k}/2} F_{Rk}(\omega T), & k \text{ even,} \\ j e^{-j\omega T N_{H_k}/2} F_{Rk}(\omega T), & k \text{ odd,} \end{cases} \quad (3.10)$$

where $F_{Rk}(\omega T)$ should approximate the desired function $F_{Rk,\text{des}}(\omega T)$, given by

$$F_{Rk,\text{des}}(\omega T) = \begin{cases} \frac{(-j\omega T)^k}{k!}, & k \text{ even,} \\ -j \frac{(-j\omega T)^k}{k!}, & k \text{ odd.} \end{cases} \quad (3.11)$$

The frequency response $H(e^{j\omega T}, d)$ in (3.1) should approximate the desired response $F_{\text{des}}(e^{j\omega T}, d)$ in (3.7).

The implementation complexity is here computed as in (3.2)–(3.4), considering that the differentiators can be of different orders N_{H_k} . To further reduce the complexity, different modifications of the Farrow structure have been introduced [27, 32, 53, 54]. VFD filters can be designed using the windowing method [151], weighted least squares (WLS) method [32, 38, 54, 57], and minimax optimization algorithms [38, 53, 145].

3.2.2 Variable Equalizers

Variable equalizers (VEs) allow to adjust the equalization frequency response by controlling one or a few parameters. This type of digital filters has been

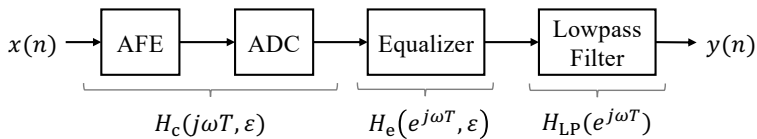


Figure 3.3: Principle of frequency response equalization using a variable equalizer.

utilized mainly in acoustic signal processing for audio equalization with gain as a variable parameter [152, 153]. Although an equalizer is an essential part of communication systems, to the best of the author's knowledge, VEs have not been extensively explored in this context.

The basic principle of the AFE equalization in communication systems is illustrated in Fig. 3.3. The analog input signal is assumed to be bandlimited to $\omega_e < \pi/T$, where T denotes the sampling period. The channel frequency response of the AFE circuits and the following ADC⁸ generally distort and attenuate the signal within the band of interest $[0, \omega_e T]$.

The desired frequency response after channel equalization is given by

$$H_{ce,des}(e^{j\omega T}) = \begin{cases} e^{-j\omega T \frac{N_E}{2}}, & \omega T \in [0, \omega_e T], \\ 0, & \omega T \in [\omega_s T, \pi], \end{cases} \quad (3.12)$$

where N_E is the equalizer order. To recover the original input signal and achieve the desired response in (3.12), it is needed to equalize the channel frequency response $H_c(j\omega T, \epsilon)$, which can vary depending on the variable parameter⁹ $\epsilon \in [\epsilon_{\min}, \epsilon_{\max}]$. Generally, a lowpass filter is combined with the equalizer in order to remove out-of-band noise and aliasing after the ADC [154, 155]. Thus, to design a VE with the frequency response $H_e(e^{j\omega T}, \epsilon)$, the resulting response $H_{ce}(e^{j\omega T}, \epsilon)$, given by

$$H_{ce}(j\omega T, \epsilon) = H_c(j\omega T, \epsilon)H_e(e^{j\omega T}, \epsilon)H_{LP}(e^{j\omega T}), \quad (3.13)$$

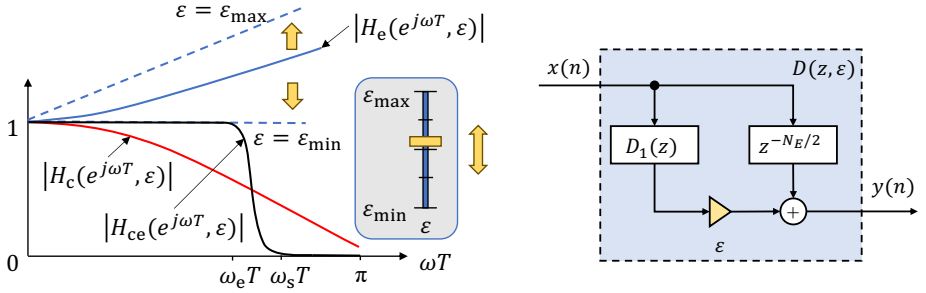
with a lowpass filter response $H_{LP}(e^{j\omega T})$, should approximate $H_{ce,des}(e^{j\omega T})$.

A VE can be realized based on the Farrow structure using digital differentiators as proposed in Paper A. Then, the VE frequency response in the simplest case [34] is given by

$$H_e(e^{j\omega T}, \epsilon) = e^{-j\omega T N_E/2} + \epsilon D_1(e^{j\omega T}), \quad (3.14)$$

⁸Some papers include the ADC in the AFE while some papers do not. Here, the AFE and ADC are considered as separate blocks.

⁹For a higher-order polynomial channel models, several variable parameters for the corresponding VE may be required as proposed in Paper A.



(a) Illustration of the VE magnitude response.

(b) VE Farrow-based realization.

Figure 3.4: Illustration of the VE magnitude response and its Farrow-based realization, controllable by the variable parameter ϵ .

with $D_1(e^{j\omega T})$ being a fixed Type III linear-phase FIR filter with antisymmetric impulse response that should approximate the first-degree differentiator frequency response $D_{1,\text{des}}(j\omega T) = j\omega T e^{-j\omega T N_E/2}$. The illustration of the variable equalization and the VE Farrow-based realization are shown in Figs. 3.4a and 3.4b, respectively.

VE can be designed in a similar way as VFD filters as their realization also can consist of digital differentiators of different degrees. This is explained in Paper A.

3.2.3 Variable-Bandwidth Filters

Digital filters whose bandwidth can be controlled by tuning a single parameter b are referred to as VBW filters. They are required in many DSP applications, for example, spectrum sensing in cognitive radio [39] and adjusting the bandwidth of interest for amplification in hearing aid devices [46]. The desired frequency response of a VBW lowpass filter is given by

$$G_{\text{des}}(e^{j\omega T}, b) = \begin{cases} e^{-j\omega T N_G/2}, & \omega T \in [0, b - \Delta/2], \\ 0, & \omega T \in [b + \Delta/2, \pi], \end{cases} \quad (3.15)$$

where the filter order N_G is preferably even¹⁰, $b \in [b_l, b_u]$ is the center of the fixed transition band Δ , whereas $\omega_c T = b - \Delta/2$ and $\omega_s T = b + \Delta/2$ represent variable passband and stopband edges, respectively.

¹⁰The assumption on an even filter order gives an integer group delay, as outlined in Section 2.1.1.

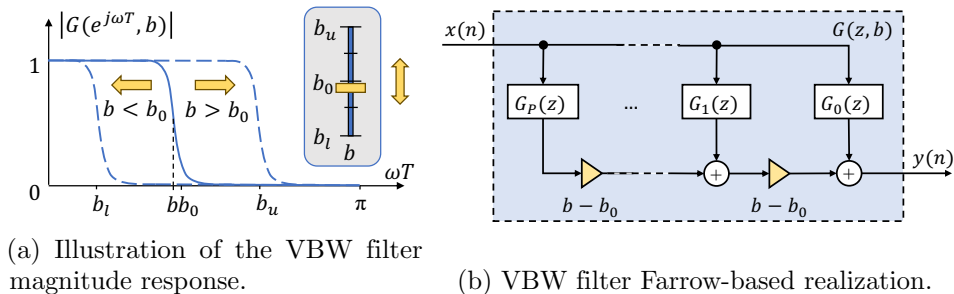


Figure 3.5: Illustration of the VBW lowpass filter magnitude response and its Farrow-based realization, controllable by the variable parameter b .

The overall frequency response $G(e^{j\omega T}, b)$ of a Farrow-based VBW filter is given by

$$G(e^{j\omega T}, b) = \sum_{p=0}^P (b - b_0)^p G_p(e^{j\omega T}), \quad (3.16)$$

where the subfilters $G_p(e^{j\omega T})$ are generally Type I linear-phase FIR filters (see Footnote 10) of order N_{G_p} . Typically, the subfilters for a VBW filter are chosen to have the same order, i.e., $N_{G_p} = N_G$, since the use of different orders will not bring significant reduction in complexity but complicate the design [60]. For obtaining a more balanced structure with smaller filter coefficients, the selection $b_0 = (b_l + b_u)/2$ tends to make the filter coefficients smaller in magnitude as well as enables one to find a lower bound on the filter order required to meet a given specification [156]. Moreover, for $b = b_0$, $G(e^{j\omega T}, b_0) = G_0(e^{j\omega T})$ is a regular lowpass filter with passband and stopband edges at $b_0 - \Delta/2$ and $b_0 + \Delta/2$, respectively. The frequency response $G(e^{j\omega T}, b)$ in (3.16) should approximate the desired response $G_{\text{des}}(e^{j\omega T}, b)$ in (3.15). An illustration of a VBW lowpass filter magnitude response and its Farrow-based realization are shown in Figs. 3.5a and 3.5b, respectively.

VBW filters are typically designed using minimax optimization [156] or using the WLS method [63]. The implementation complexity of a Farrow-based VBW filter is computed as in (3.2)–(3.4), considering that the subfilters $G_p(z)$ are of the same order N_G .

3.3 Filter-Bank-Based Variable Digital Filters

For some applications, e.g., when a sharp transition band is required and Farrow-based VDFs may cause high computational complexity per sample or for flexible channelization of wireless communication systems, VDFs can be realized based on a FB. There are two common FB-based approaches that have received great attention: based on a fast filter bank (FFB) and based on a FCFB.

3.3.1 Fast Filter Banks

FFBs are referred to as an efficient realization of filter banks based on the sliding FFT [157], which itself is a recursive realization of the DFT [118]. FFBs are typically organized in a tree structure FB, i.e., a multistage FB, where the filters in each stage split the signal further into two or three channels [56, 157].

In FFB-based VDFs, an input signal is split into subbands by an analysis FFB as shown in Fig. 3.6, and each band can be processed independently. For example, a discretely tunable bandwidth can be realized in a simple way by combining different bands or discarding the bands outside the desired passband as shown in Fig. 3.7 for $N = 8$ channels [56]. Additionally, to make continuous variability of the bandwidth, shaping bandpass filters need to be introduced in the realizations [49, 52, 56, 134]. Thus, the overall computational complexity of an FFB-based VBW filter consists of the FFB implementation, shaping filter implementation, and implementation of band shifting [56]. A variable fractional delay can be realized as a variable phase shift in each subband, resulting in the desired phase shift [52].

In this technique, one can implement simultaneously many filters with different center frequencies, resulting in reduced computational complexity per subband. This approach significantly reduces computational costs, particularly when compared to Farrow-based structures for very sharp transition bands [56, 134] and for two variable parameters [49, 52]. FFB-based VDFs are generally designed based on a prototype filter for every stage and a shaping filter [49, 52, 56, 134].

Applications of the FFB-based VDFs also include spectrum sensing and channelization of wireless communication systems, where compatibility of channelizers with different standards is required [134].

This type of VDFs is used in Paper C for comparison with the proposed frequency-domain implementations.

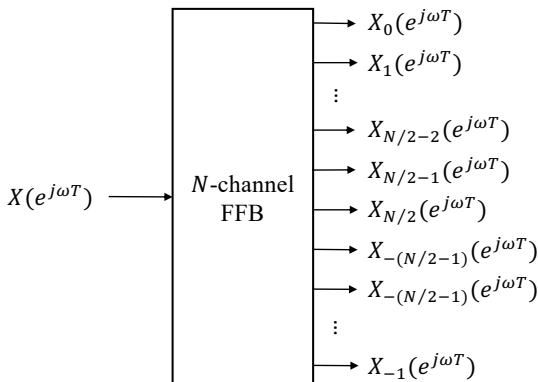


Figure 3.6: N -channel FFB.

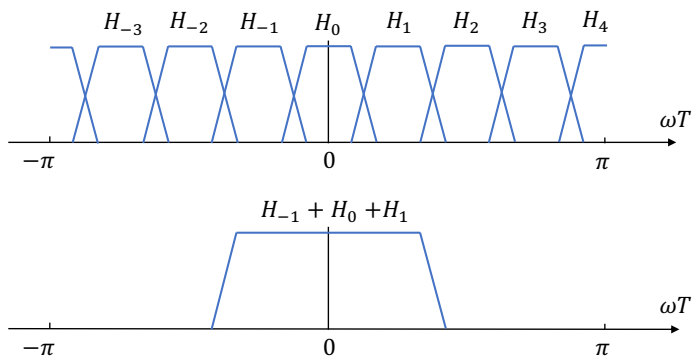


Figure 3.7: Magnitude response of a discretely tunable FFB-based VBW filter.

3.3.2 Fast-Convolution-Based Filter Banks

Another approach for efficient implementation of VDFs is based on FCFB [50], which is widely applied in realizing multiplexers for spectrum sensing and dynamic spectrum allocation in wireless communication systems [40, 158, 159]. The main idea of this method is based on combination of the frequency-domain implementation of FIR filters based on the OLS technique, described in Section 2.1.4, and individual subband processing using FBs, mentioned in Section 2.2.2, that together form a multirate version of fast convolution. In the structure shown in Fig. 3.8 [50], after taking the FFT of an input signal of length N with overlapped block processing, the signal frequency bins are split into blocks of length L_k , $k = 1, \dots, M$, and each of them is multiplied by the corresponding band weights (filter DFT coefficients). Each subband

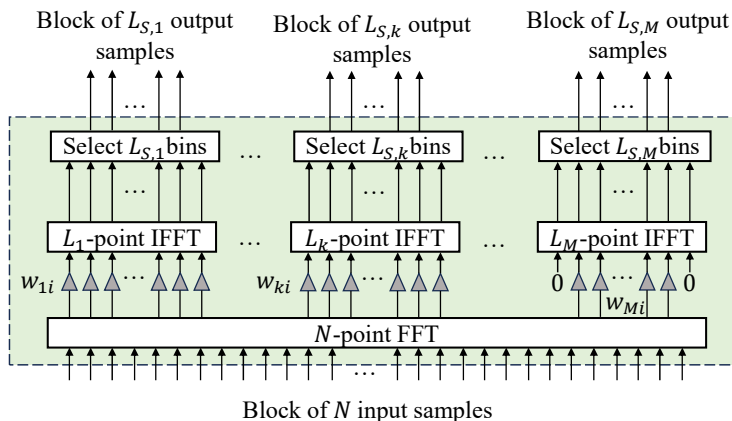


Figure 3.8: Fast-convolution based flexible analysis FB [50].

can be easily configured for unequal bandwidths, different center frequencies, and adjustable sampling rates $R_k = N/L_k$, determined by changing the IFFT length L_k and the corresponding subband filter bandwidth. The latter can be easily performed without additional computations, because the fact that these filters are designed based on the frequency sampling method, when the passband and stopband values are set as ones and zeros, respectively, and only the transition band values need to be optimized during the FB design, allows to vary the passband and stopband width by inserting or removing ones or zeros, respectively, while keeping the transition band fixed [50].

Based on the idea from FCFB-based VDFs, an approach for VBW filter design by optimizing the frequency bins directly in the frequency domain is proposed in Papers D and E. Paper D investigates a hybrid of frequency sampling and minimax optimization method, while Paper E proposes a closed-form LS solution.

Chapter 4

Sampling Clocks Synchronization

This chapter discusses synchronization errors occurring in communication systems, primarily the problem of sampling clocks synchronization is highlighted.

4.1 Overview of Synchronization Errors

In practical implementations of digital communication systems, perfect synchronization between the transmitter and receiver cannot be guaranteed because each device is driven by its own independent internal clock. Consequently, to ensure reliable signal transmission, accurate synchronization techniques of the overall system are essential. In general, synchronization problems can be categorized into global transmitter-receiver synchronization and intra-node synchronization. The first category deals with mismatches between transmitter and receiver clocks for a point-to-point scenario [77, 79, 81, 85, 87, 91, 160, 161] or in distributed systems where the synchronization problem is escalated to multi-node synchronization (e.g., in bistatic integrated sensing and communication (ISAC) systems [83, 84] or wireless acoustic sensor networks (WASN) [162, 163]). The second category of the synchronization problems addresses relative mismatches between parallel branches within a single receiver, e.g., relative timing, phase, and frequency-response misalignment between branches, affecting further multi-channel processing algorithms. This problem can occur, for example, in multiple RF chains in multiple input multiple output (MIMO) systems [164, 165].

Many applications utilize orthogonal frequency division multiplexing

(OFDM), especially in wireless communications. Although OFDM systems have many advantages including their high spectral efficiency, flexibility in resource allocation, and capability of performing simple channel equalization, these systems are sensitive to synchronization errors. For this reason, many research directions have been investigating the synchronization issues of OFDM systems [77–79, 81–91, 93, 164, 166–178]. However, the problem of timing and frequency synchronization is also a key challenge in systems utilizing other waveforms, e.g., in FB multi-carrier systems [94] and single-carrier systems [174, 179, 180].

The synchronization process at the receiver is typically split into two major stages, namely, initial (coarse) synchronization and refinement of the residual offsets [167, 181]. While the first stage consists of detecting the presence of the signal and frame synchronization, fine synchronization deals with estimation and compensation of the residual error. In practice, these residual impairments originate from different sources. Mismatches between the transmitter and receiver carrier generators produce a carrier frequency offset (CFO), while mismatches between sampling clocks leads to a SFO. In addition to these deterministic discrepancies, both impairments are further influenced by oscillator fluctuations such as phase noise and clock jitter, leading to frequency offsets varying with time. The impact of these mismatches has been analyzed in [77, 78, 92, 178, 182, 183], highlighting the overall system performance degradation and the need for estimation and compensation of these discrepancies.

The focus of this thesis is particularly SFO, and thus, the major part of this chapter is devoted to estimation and compensation techniques for this discrepancy. However, many research works study SFO together with CFO due to their interrelated effects, especially for OFDM systems [77, 86–91]. Therefore, a brief introduction to CFO is also given here.

4.2 Sampling Frequency Offset

In communication systems, the sampling clock differences can occur between the transmitter and receiver, i.e., between digital-to-analog converter (DAC) and ADC, or within a single receiver, e.g., between parallel ADCs. Regardless of the scenario, the mismatches between sampling frequencies result in a SFO problem, which requires two signals to be synchronized.

SFO is particularly important to mitigate in many applications, especially in modern high-speed and wide-band communication systems, where the use of large signal bandwidth necessitates very high sampling rates, and thus even

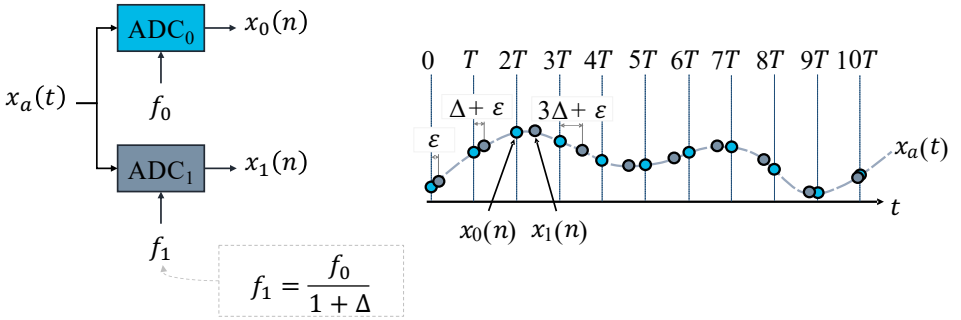


Figure 4.1: SFO problem for two ADCs sampled as slightly different frequencies.

tiny differences between sampling clocks lead to a noticeable accumulative timing drift resulting in inter-carrier and inter-symbol interferences. In the literature, the offset between sampling frequencies is also called sampling clock offset [184], sampling timing offset [87], and sampling frequency deviation [169].

4.2.1 Sampling Frequency Offset Impact

Let f_0 and f_1 be two slightly different sampling frequencies such that

$$f_1 = \frac{f_0}{1 + \Delta} \quad (4.1)$$

with f_0 being the reference frequency and Δ being the SFO, commonly reported in parts per million (ppm), i.e., $\Delta \text{ ppm} = \Delta \times 10^{-6}$. Then, for a general bandlimited continuous-time signal $x_a(t)$ sampled at these frequencies, i.e., $t = n/f_0$ and $t = n/f_1$, the sampled signals can be expressed as

$$x_0(n) = x_a(nT), \quad (4.2)$$

$$x_1(n) = x_a(n(1 + \Delta)T + \varepsilon), \quad (4.3)$$

where $T = 1/f_0$ and $T_1 = (1 + \Delta)T$ are the sampling periods of the reference and distorted signals, respectively. Additionally, the fractional fixed STO, ε , is considered here because its presence may also affect the overall performance [174], and it is generally difficult to maintain a perfect alignment of the initial samples. An illustration of the SFO problem occurring in the case of two ADCs is shown in Fig. 4.1. It is important to emphasize here that Δ is typically fixed over time, but the time deviation $n\Delta T$ in $x_1(n)$ grows linearly with time relative to the reference instances in $x_0(n)$. Furthermore, for many

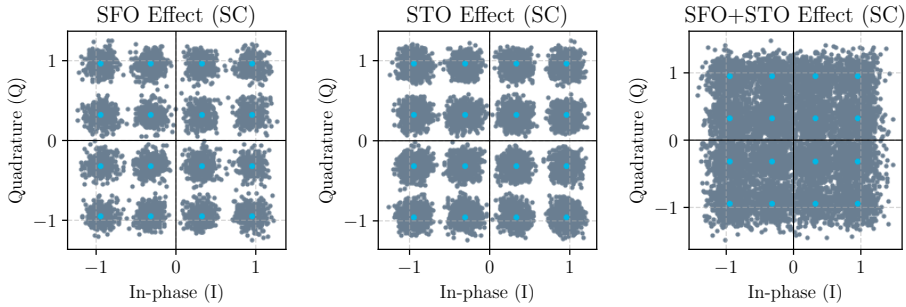


Figure 4.2: The impact of SFO and STO on the constellation diagrams of 1024 received 16-QAM symbols using a single carrier transmission with 80% occupied bandwidth. Here, the SFO and STO are $\Delta = 100$ ppm and $\varepsilon = 0.1$, respectively.

samples or for a relatively large value of Δ , the overall time-domain deviation may result in ISI [180]. Figure 4.2 shows the impact of SFO and STO on the constellation diagrams of 16-quadrature amplitude modulation (QAM) symbols using a single carrier transmission with 80% occupied bandwidth.

For multi-carrier systems, the sampling clock differences result in ICI [185, 186]. For example, an OFDM baseband signal sampled with the frequency f_1 instead of f_0 is given by [185]

$$x(n) = \frac{1}{\sqrt{N}} \sum_{k=-N/2}^{N/2-1} s_k e^{j \frac{2\pi k}{N} (1+\Delta)n} \quad (4.4)$$

with N being the number of subcarriers within the OFDM symbol, s_k being the complex symbol of the k th subcarrier, and it is assumed that cyclic prefix (CP) has been removed.¹¹ After taking the DFT of the received signal, the ℓ th subcarrier can be expressed as [185]

$$\begin{aligned} X(\ell) &= \frac{1}{\sqrt{N}} \sum_{n=0}^{N-1} x(n) e^{-j \frac{2\pi}{N} n \ell} \\ &= \frac{1}{N} \sum_{k=-N/2}^{N/2-1} s_k \sum_{n=0}^{N-1} e^{-j \frac{2\pi}{N} n (\ell - k(1+\Delta))} \\ &\stackrel{(a)}{=} s_\ell \mathcal{C}_{\ell, \ell} + \sum_{\substack{k=-N/2 \\ k \neq \ell}}^{N/2-1} s_k \mathcal{C}_{\ell, k}, \end{aligned} \quad (4.5)$$

¹¹The presence of the channel and noise influence is omitted here.

where $c_{\ell,\ell}$ is the scaling and phase rotation coefficient for the ℓ th subcarrier given by

$$c_{\ell,\ell} = \frac{\sin(\pi\ell\Delta)}{N \sin\left(\frac{\pi\ell\Delta}{N}\right)} e^{j\pi\frac{N-1}{N}\ell\Delta}, \quad (4.6)$$

and $c_{\ell,k}$ represents the ICI caused by SFO and given by

$$c_{\ell,k} = \frac{\sin(\pi(\ell - k(1 + \Delta)))}{N \sin\left(\frac{\pi}{N}(\ell - k(1 + \Delta))\right)} e^{-j\pi\frac{N-1}{N}(\ell - k(1 + \Delta))}. \quad (4.7)$$

Note that in (a), the geometric sum property is applied [185].

In many research works on SFO estimation, only the SFO is considered, without taking into account imperfect synchronization of the first sample. Even though a fixed fractional time offset can be compensated later in the equalization stages, the effect of STO is not negligible during the sampling clock synchronization stage [166], including SFO estimation. An STO alone introduces a phase shift $2\pi k\varepsilon/T_u$ for each k th subcarrier of an OFDM signal [166], where

$$T_u = \frac{1}{\Delta f_{\text{sub}}} = NT \quad (4.8)$$

is the useful data duration with Δf_{sub} being the subcarrier spacing and $T = 1/f_0$ being the sampling period. In the presence of both SFO and STO considered, the received OFDM signal and its ℓ th subcarrier can be expressed, respectively, as

$$x_1(n) = \frac{1}{\sqrt{N}} \sum_{k=-N/2}^{N/2-1} s_k e^{j\frac{2\pi k}{N}(1+\Delta)n} e^{j\frac{2\pi k}{T_u}\varepsilon}, \quad (4.9)$$

$$X_1(\ell) = s_\ell c_{\ell,\ell} e^{j\frac{2\pi\ell}{T_u}\varepsilon} + \sum_{\substack{k=-N/2 \\ k \neq \ell}}^{N/2-1} s_k c_{\ell,k} e^{j\frac{2\pi k}{T_u}\varepsilon}. \quad (4.10)$$

In this case, the distortion coefficients $c_{\ell,\ell}$ and $c_{k,\ell}$ are multiplied by the additional phase shift due to STO, resulting in a more severe effect. Moreover, the impact of both SFO and STO depends on the subcarrier index, i.e., each subcarrier experiences a phase shift and an amplitude distortion growing with the index ℓ along with the presence of the ICI from other subcarriers. This explains why OFDM systems are typically sensitive to SFO. Figure 4.3

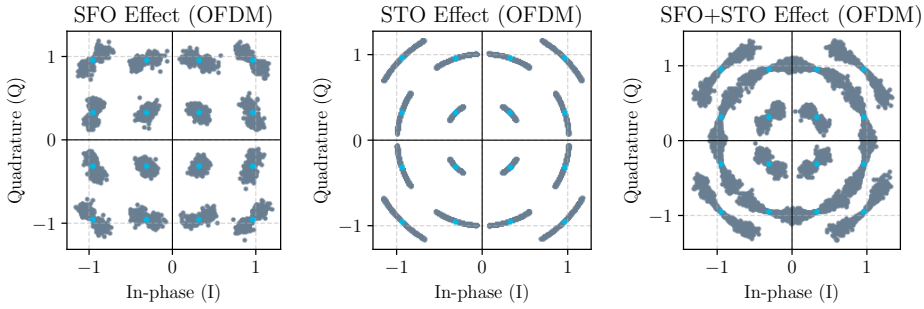


Figure 4.3: The impact of SFO and STO on the constellation diagrams of 10 OFDM symbols with 819 active subcarriers out of 1024 (80% occupied bandwidth) and 16-QAM data symbols. Here, the SFO and STO are $\Delta = 100$ ppm and $\varepsilon = 0.1$, respectively.

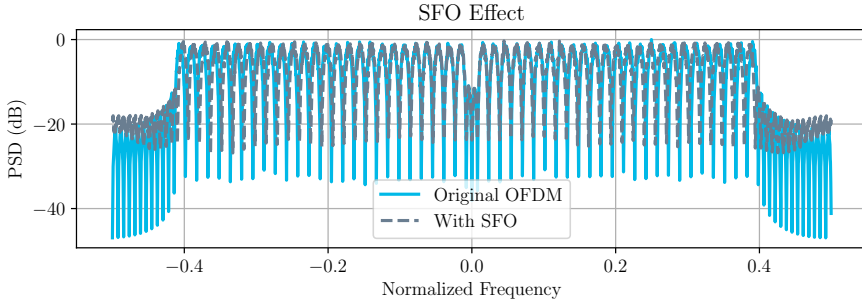


Figure 4.4: The impact of SFO on the spectrum of an OFDM signal with 51 active subcarriers out of 64 (80% occupied bandwidth). Here, $\Delta = 0.01$, and the spectrum is compressed relative to the central (zeroth) carrier frequency due to SFO.

shows the effect of SFO and STO on the constellation diagrams of 16-QAM signals transmitted using an OFDM modulation. The constellations highlight the severe impact of both offsets and the importance of considering them during the clock synchronization stage. Additionally, the OFDM spectrum distortions due to SFO are presented in Fig. 4.4, showing that the spectrum is compressed relative to the central (zeroth) carrier frequency. Since the presence of STO results in subcarrier-dependent phase shift, it does not affect the magnitude spectrum, and thus is not shown here.

4.2.2 Estimation Methods

The SFO estimation methods can be broadly categorized into frequency-domain methods and time-domain methods. For the former, the estimation is carried out using the signal representations in the frequency domain, and majority of the methods target OFDM signals [80, 83–86, 89–91, 94, 173]. Since SFO in OFDM systems appears as subcarrier-dependent phase rotations, most of the methods exploit the phase differences among the subcarriers of transmitted pilot-signals to estimate the phase shift [94, 173]. Some methods rely on blind estimation utilizing the correlation properties of the received OFDM samples, i.e., they exploit second-order statistics to recognize the sampling clock offset from the structured phase terms [170]. Although the frequency-domain estimation methods are quite commonly used in many applications, they have several drawbacks. Firstly, many frequency-domain estimators assume SFO is small so that ICI is negligible. However, SFO occurs in the time domain and in general destroys the orthogonality between the subcarriers for multi-carrier systems after FFT. This means that when SFO is not sufficiently small, the pilot phases are contaminated by more severe distortions, i.e., ICI, and not just amplitude and phase distortions. Secondly, the other impairments such as CFO and phase offset (PO) also affect the pilot phases, making it difficult to obtain accurate estimates of the SFO, unless joint estimation methods are considered [77, 86–91]. Thirdly, these methods are carried out in the frequency domain, that results in complex-valued computations for estimation, leading to higher computational complexity.

On the other hand, the time-domain methods perform estimation based on time-domain sequences, and the existing methods can be applied for different waveforms, including also OFDM signals [169] or any arbitrary waveform [160]. In general, these methods utilize the timing drift occurred due to SFO in their algorithms, that requires to use pilot signals [160] or utilize the structure of CP as in OFDM signals [169]. Importantly, the output of the time-domain estimators can directly be used in the time-domain interpolators to compensate for the SFO, avoiding a feedback from the estimation in the frequency-domain methods, allowing potentially lower-latency implementations. This approach can also prevent the ICI and phase drifts for multi-carrier systems. Additionally, the SFO and STO estimation can be separated from CFO and PO because the clock offsets affect only sampling instants, while the carrier offsets results in phase drifts. Finally, the time-domain SFO estimation can be performed utilizing real-valued signals [160], leading to potentially lower computational complexity compared to frequency-domain methods.

In Paper F, an approach based on time-domain SFO estimation is proposed, allowing for low-complexity joint estimation of SFO and STO even in the presence of other synchronization impairments.

4.2.3 Compensation Methods

SFO compensation can also be carried out in either the frequency domain [77, 94, 175] or time domain [77, 87, 91–94]. The frequency-domain methods can mainly be used for multi-carrier systems by applying subcarrier-dependent phase rotations, and this approach can be efficient only for small offsets, i.e., with negligibly small ICI term as discussed in [77] and [94]. In contrast, the time-domain interpolation methods can generally deal with much larger SFO values by providing precise correction, significantly outperforming the frequency-domain phase correction method, especially, for wideband signals and systems with small subcarrier spacing [77, 94]. Existing time-domain methods typically implement SFO compensation using a VFD filter, specifically, the Farrow structure [92–95] shown in Fig. 3.1, allowing low implementation complexity. In this case, the output of the compensator with the frequency response given by (3.1) is expressed as

$$y(n, d) = \sum_{k=0}^L d^k [x(n) * h_k(n)], \quad (4.11)$$

where $x(n)$ is the input signal, $h_k(n)$ represents the impulse response of the subfilter $H_k(z)$, with $*$ denoting convolution, and d stands for the fractional delay. In the context of the SFO compensation, the fractional delay is time-varying as it accumulates with the sample index. Considering also a fixed fractional STO from (4.3), d can be expressed as

$$d(n, \Delta, \varepsilon) = n\Delta + \varepsilon. \quad (4.12)$$

In Paper F, the proposed SFO estimation algorithms exploit the compensator's structure and use only one real-valued signal component for estimation, thereby reducing the overall implementation complexity.

4.3 Joint Impact of Sampling and Carrier Frequency Offsets

For multi-carrier systems, both SFO and CFO appear as phase rotations per subcarrier. Additionally, the sampling and carrier frequencies can be

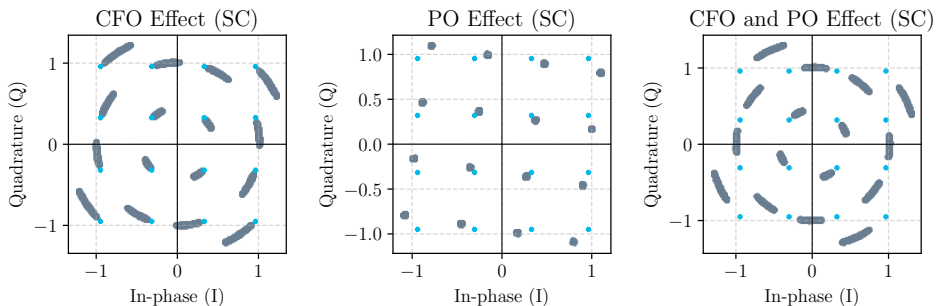


Figure 4.5: The impact of CFO and PO on constellation diagrams of 1024 received 16-QAM symbols using a single carrier transmission with 80% occupied bandwidth. Here, the CFO and PO are $\psi = 600$ ppm and $\phi_0 = 0.05\pi$, respectively.

coupled through a shared reference oscillator, creating frequency dependent drifts. Therefore, SFO and CFO are commonly analyzed and estimated jointly [77, 86–91].

4.3.1 Carrier Frequency Offset Impact

First, the impact of CFO alone is considered here. A sampled signal distorted by an offset Δ_{CFO} between carrier frequencies and an initial phase mismatch ϕ_0 , known as PO, can be expressed as [185]

$$x_2(n) = x_0(n)e^{j(2\pi\psi n + \phi_0)}, \quad (4.13)$$

where $x_0(n)$ is the reference signal and

$$\psi = \frac{\Delta_{\text{CFO}}}{f_0} = \Delta_{\text{CFO}}T \quad (4.14)$$

is the CFO normalized to the sampling frequency. The impact of CFO and PO on a single-carrier transmission of a 16-QAM wide-band signal is illustrated in Fig. 4.5, highlighting that both offsets result in constellation rotations where PO introduces rotations by a fixed angle and CFO leads to rotations increasing with the time index. In the frequency domain, the CFO appears as a shift of the original spectrum (i.e., spectrum of the transmitted signal), while PO results only in a constant phase shift, and thus, does not affect the magnitude spectrum.

In contrast, for a multi-carrier signal, the CFO synchronization stages must account not only for a phase rotation but also for ICI. For example,

a received OFDM signal with CFO and PO after removing the CP can be expressed as [185]

$$\begin{aligned}
 x_2(n) &= \frac{1}{\sqrt{N}} \sum_{k=-N/2}^{N/2-1} s_k e^{j\frac{2\pi}{N}nk} e^{j(2\pi\psi n + \phi_0)} \\
 &\stackrel{(b)}{=} \frac{1}{\sqrt{N}} \sum_{k=-N/2}^{N/2-1} s_k e^{j\left(\frac{2\pi}{N}n\left(k + \frac{\Delta_{\text{CFO}}}{\Delta f_{\text{sub}}}\right) + \phi_0\right)},
 \end{aligned} \tag{4.15}$$

where N is the total number of subcarriers, s_k is a complex data symbol, and in (b) the definition of the normalized CFO in (4.14) and the definition of the sampling frequency in term of the subcarrier spacing Δf_{sub} from (4.8) are used. After the DFT, the ℓ th subcarrier can be expressed as [185]

$$X_2(\ell) = e^{j\phi_0} \left(s_\ell q_{\ell,\ell} + \sum_{\substack{k=-N/2 \\ k \neq \ell}}^{N/2-1} s_k q_{\ell,k} \right) \tag{4.16}$$

with $q_{\ell,\ell}$ being the scaling and rotation coefficient for the ℓ th subcarrier due to CFO given by

$$q_{\ell,\ell} = e^{j\pi(N-1)\psi} \frac{\sin(\pi\psi N)}{N \sin(\pi\psi)}. \tag{4.17}$$

Note that the coefficient $q_{\ell,\ell}$ does not depend on the subcarrier index ℓ , meaning that the CFO causes a common rotation and amplitude distortion for all subcarriers. The second term, $q_{\ell,k}$, denotes the ICI coefficient given by

$$q_{\ell,k} = e^{-j\pi\frac{N-1}{N}(\ell-k-\frac{\Delta_{\text{CFO}}}{\Delta f_{\text{sub}}})} \frac{\sin(\pi(\ell-k-\frac{\Delta_{\text{CFO}}}{\Delta f_{\text{sub}}}))}{N \sin(\pi(\ell-k-\frac{\Delta_{\text{CFO}}}{\Delta f_{\text{sub}}})/N)}. \tag{4.18}$$

As an illustration, the CFO and PO effects on the constellation diagrams of 16-QAM symbols transmitted using the OFDM modulation are shown in Fig. 4.6, and the CFO effect on the OFDM spectrum is shown in Fig. 4.7. Compared with single-carrier QAM constellations in Fig. 4.5, CFO in OFDM causes rotations of the constellation of each subcarrier by the same fixed angle. However, the presence of ICI introduces additional distortion. In the frequency domain, the CFO shifts the original OFDM spectrum relative to the FFT bins used at the reference as shown in Fig. 4.7. As a result, the orthogonality between the subcarriers is lost, resulting in ICI.

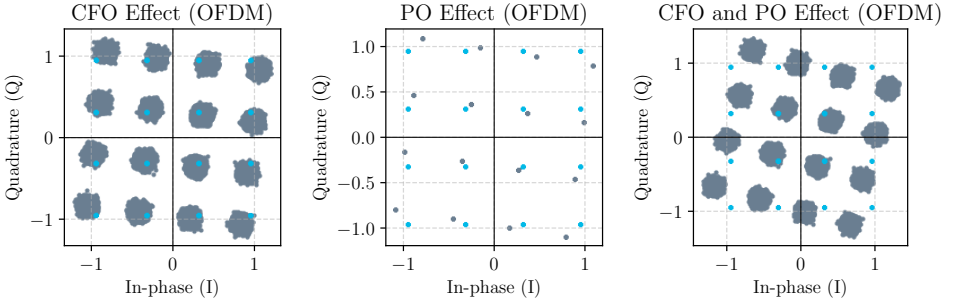


Figure 4.6: The impact of CFO and PO on the constellation diagrams of 10 OFDM symbols with 819 active subcarriers out of 1024 (80% occupied bandwidth) and 16-QAM data symbols. Here, the CFO and PO are $\psi = 600$ ppm and $\phi_0 = 0.05\pi$, respectively.

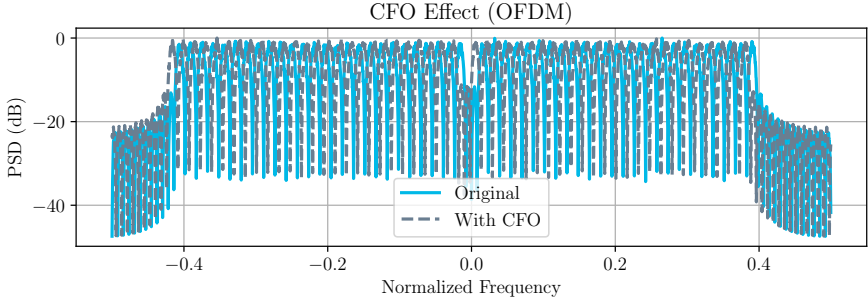


Figure 4.7: Spectrum of an OFDM signal due to CFO with $\psi = 0.01$. Due to CFO all subcarriers are shifted to the left by the same amount.

4.3.2 Joint Impact of SFO and CFO

When both SFO and CFO together with STO and PO are present, the result is

$$x_3(n) = x_a(n(1 + \Delta)T + \varepsilon) e^{j(2\pi\Delta_{\text{CFO}}(n(1+\Delta)T + \varepsilon) + \phi_0)}. \quad (4.19)$$

In OFDM systems, the distorted time-domain signal is given by

$$\begin{aligned} x_3(n) &= \frac{1}{\sqrt{N}} \sum_{k=-N/2}^{N/2-1} s_k e^{j\frac{2\pi k}{N}(1+\Delta)n} e^{j\frac{2\pi k}{T_u}\varepsilon} e^{j2\pi\Delta_{\text{CFO}}n(1+\Delta)T} e^{j(2\pi\Delta_{\text{CFO}}\varepsilon + \phi_0)} \\ &\stackrel{(c)}{=} \frac{1}{\sqrt{N}} e^{j(2\pi\frac{\psi N}{T_u}\varepsilon + \phi_0)} \sum_{k=-N/2}^{N/2-1} s_k e^{j\frac{2\pi k}{N}(1+\Delta)n} e^{j\frac{2\pi k}{T_u}\varepsilon} e^{j2\pi\psi n(1+\Delta)}, \end{aligned} \quad (4.20)$$

where in (c) the definition of the normalized CFO in (4.14) and the definition of the sampling frequency in term of the useful data duration T_u from (4.8) are used. After the DFT, the ℓ th subcarrier can be expressed as

$$\begin{aligned}
 X_3(\ell) = e^{j\left(2\pi\frac{\psi N}{T_u}\varepsilon + \phi_0\right)} & \sum_{k=-N/2}^{N/2-1} s_k e^{j\frac{2\pi k}{T_u}\varepsilon} \\
 & \times \frac{1}{N} \sum_{n=0}^{N-1} e^{-j\frac{2\pi n}{N}(\ell - (1+\Delta)k)} e^{j2\pi\psi n(1+\Delta)}.
 \end{aligned} \tag{4.21}$$

This means that the phase rotation, scaling, and the ICI term coefficients depend on all distortion parameters, making it complicated to utilize a separate SFO or CFO estimation method only relying on phase differences between the subcarriers over several OFDM symbols. For this reason, many joint SFO and CFO estimation approaches have been proposed [77, 86–91].

However, SFO is an inherently time-domain distortion. Therefore, the time-domain SFO estimators can utilize the timing drift to estimate the SFO first, then resample the signal using the time-domain interpolator, and further proceed with the following CFO estimation using available methods [178]. For multi-carrier systems, this approach enables correcting the SFO before performing the FFT, keeping only the impact of CFO for the subcarriers. In Paper F, the proposed time-domain SFO estimation approach demonstrates the effectiveness of the approach even in the presence of CFO and PO.

Chapter 5

Power Amplifier Nonlinearities

This chapter gives an introduction to PAs, their challenges and the effect of using them in cascade.

5.1 Power Amplifier Challenges

In practical communication systems, the achievable communication range is directly determined by the transmitted signal power. PAs are responsible for amplifying the signal before it is transmitted. Therefore, they constitute one of the most critical components in the RF front-end of a communication transceiver. At the same time they represent one of the most power hungry devices in the transmitter chain. Since power consumption is a critical factor in many communication devices, PAs are required to operate in the most efficient regime [187]. The efficiency of a PA shows how effectively the amplifier converts the supplied DC power into useful RF output power. It is commonly evaluated through the drain efficiency metric given by

$$\eta = \frac{P_{\text{out}}}{P_{\text{DC}}}, \quad (5.1)$$

with P_{out} being the average RF output power and P_{DC} being the DC power consumed by the PA [5, 188].

One of the ways to increase the power efficiency of PAs is to utilize the supply power more effectively, for example, operating at a power level closer to their maximum output power, i.e., near the saturation point [188]. However, practical PAs exhibit nonlinear transfer characteristics. Therefore,

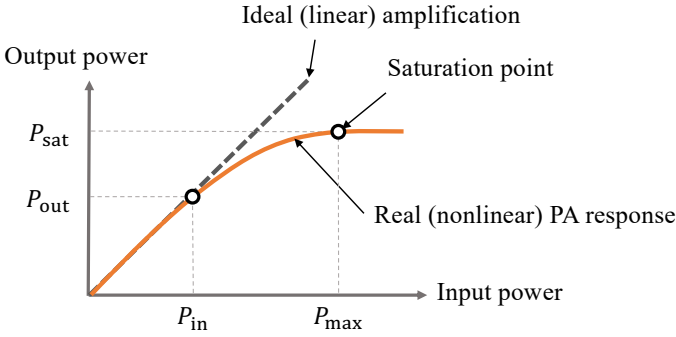


Figure 5.1: A typical PA amplitude characteristic.

operating closer to the saturation region results in a nonlinear regime. A typical PA amplitude characteristic is illustrated in Fig. 5.1, highlighting the difference between a real (nonlinear) and ideal (linear) PA behaviors as the input power increases. This behavior is especially important to consider for waveforms with high PAPR because large variations in the signal envelope can push the PA into its nonlinear operating region. Typically, PAs are either linear and inefficient (for low input powers) or nonlinear and efficient (for high input powers) [187, 188]. This trade-off has been widely investigated for many years, leading to the development of various techniques aiming at improving both linearity and efficiency [189–199].

5.1.1 Behavioral Modeling

To understand the impact of PA nonlinearities to the incoming signal and ensure linear or near-linear operation regime, behavioral modeling of PAs is essential [97, 200–202]. In many communication systems, signals transmitted at a carrier frequency f_c are modeled as narrowband bandpass signals, i.e., the signal bandwidth is much smaller the carrier frequency. Under this assumption, the PA input $x_{\text{RF}}(t)$ and output $y_{\text{RF}}(t)$ passband signals can be conveniently represented using complex baseband equivalent models given respectively by

$$x_{\text{RF}}(t) = \Re\{x(t) \exp(j2\pi f_c t)\}, \quad (5.2)$$

$$y_{\text{RF}}(t) = \Re\{y(t) \exp(j2\pi f_c t)\}, \quad (5.3)$$

where $x(t)$ and $y(t)$ are the corresponding complex baseband signals [5, 201]. Assuming ideal sampling of the baseband signals, the complex envelopes in

the discrete-time form can be expressed using in-phase (I) and quadrature (Q) components as

$$x(n) = x_I(n) + jx_Q(n), \quad (5.4)$$

$$y(n) = y_I(n) + jy_Q(n). \quad (5.5)$$

Measurements on the PA nonlinear effects generally include dynamic amplitude distortion captured via amplitude-to-amplitude modulation (AM/AM) curves and phase distortions captured via amplitude-to-phase modulation (AM/PM) characterization [188]. To model AM/AM and AM/PM simultaneously, numerous models have been proposed, among which polynomial, Rapp, and Volterra series models are the most widely used [5, 97, 201–203].

Memoryless Models

Among various available models, memoryless models provide the simplest form by describing static PA effects.

Memoryless polynomial model: One of the simplest and most commonly used approach is to utilize a memoryless polynomial model. It is expressed as

$$y(n) = \sum_{p=1}^P a_p x(n) |x(n)|^{p-1}, \quad (5.6)$$

where a_p denotes the complex coefficients and P represents the nonlinearity order. In the case of bandpass RF signal transmission, only odd-order terms are typically included in (5.6), i.e., p is odd, because they produce distortions around the carrier frequency, and after downconversion, this falls inside the baseband signal causing in-band distortion and slightly outside the band causing spectral regrowth and adjacent channel interference. In contrast, the appearance of even-order terms is outside the narrowband spectrum of the signal and can often be removed by RF filtering [5, 188]. Polynomial models are often used in system-level simulations because of their their simplicity and ease of parameter estimation [105, 204–206].

Rapp and modified Rapp models: While the original Rapp model in [207] approximated only the amplitude distortion, the modified Rapp model approximates both AM/AM and AM/PM curves [104, 208]. They are given by

$$F_A(|x(n)|) = \frac{g|x(n)|}{\left(1 + \left(\frac{g|x(n)|}{V_{\text{sat}}}\right)^{2p}\right)^{\frac{1}{2p}}}, \quad (5.7)$$

$$F_P(|x(n)|) = \frac{A|x(n)|^{q_1}}{1 + \left(\frac{|x(n)|}{B}\right)^{q_2}}, \quad (5.8)$$

where g denotes the small signal gain, p represents the smoothness factor, V_{sat} stands for the saturation voltage coefficient, and A , B , q_1 , q_2 are AM/PM distortion curve parameters. Then, the PA output can be expressed as

$$y(n) = F_A(|x(n)|)e^{j(F_P(|x(n)|) + \arg\{x(n)\})}. \quad (5.9)$$

The Rapp model or modified Rapp models are often used to evaluate system performance under realistic PA saturation effects [100, 209–211].

Memory-Based Models

While memoryless models capture mainly static effects of PAs, dynamic effects can be modeled using behavioral models with memory [188]. Among many behavioral models available in the literature, memory polynomial and generalized memory polynomial are the most commonly used because they provide a good balance between modeling accuracy and computational complexity.

Memory polynomial model: The memory polynomial model represents one of the simplest forms of behavioral models that incorporate memory effects. It is given by

$$y(n) = \sum_{p=1}^P \sum_{m=0}^{M-1} b_{pm} x(n-m) |x(n-m)|^{p-1}, \quad (5.10)$$

where M and P denote the memory depth and nonlinear order, respectively, while b_{pm} represent the model coefficients [5, 190].

Generalized memory polynomial: This is an extension of the memory polynomial model, providing better accuracy for modeling PAs exhibiting strong memory effects by additionally accounting for cross-memory terms. It is represented by

$$\begin{aligned} y(n) = & \sum_{p=1}^{P_a} \sum_{m=0}^{M_a-1} a_{pm} x(n-m) |x(n-m)|^{p-1} \\ & + \sum_{p=1}^{P_b} \sum_{m=0}^{M_b-1} \sum_{\ell=1}^{L_b} b_{pm\ell} x(n-m) |x(n-m-\ell)|^{p-1} \\ & + \sum_{p=1}^{P_c} \sum_{m=0}^{M_c-1} \sum_{\ell=1}^{L_c} c_{pm\ell} x(n-m) |x(n-m+\ell)|^{p-1}, \end{aligned} \quad (5.11)$$

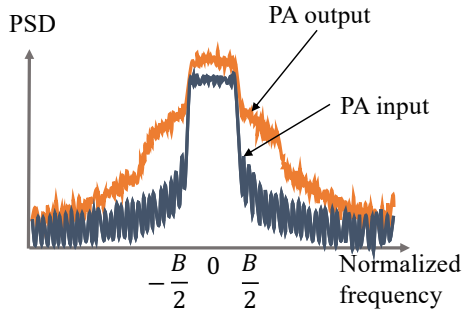


Figure 5.2: A typical spectrum at the output of a PA.

where P_a and M_a are the number of coefficients associated with the aligned signal-envelope terms (as in the memory polynomial model). Specifically, P_a denotes the nonlinear order and M_a represents the memory depth. Further, P_b , M_b , and L_b are the number of coefficients associated with the lagging cross-memory terms, where the signal interacts with the envelope of the delayed signal, with L_b being the lagging envelope memory depth. Similarly, P_c , M_c , and L_c determine the number of coefficients for signal and leading envelope. Correspondingly, a_{pm} , b_{pml} , and c_{pml} represent the model coefficients [190].

Volterra series: The Volterra series is a more general model that can capture both linear and nonlinear memory effects of PAs. However, it is computationally complex and often not practical for real-time applications. Therefore, it is typically used for theoretical analysis and system-level simulations [5].

5.1.2 Linearization Techniques

The nonlinear behavior of PAs near the saturation point can be also seen as spectral regrowth in the frequency domain, caused by intermodulation between frequency components of the signal. These nonlinear products appear both within the signal band and outside the allocated bandwidth, leading to adjacent channel interference [188]. A typical output spectrum of a PA, illustrating spectral regrowth caused by nonlinear amplification, is shown in Fig. 5.2.

To reduce the distortions and prevent interference with adjacent channels, it is common to back-off the output power of the PA [187, 188, 193], which is

known as *output power back-off* and given by

$$\text{OBO} = 10 \log_{10} \left(\frac{\text{OP1dB}}{P_{\text{out}}} \right), \quad (5.12)$$

where OP1dB is the output power at the 1 dB compression point, i.e., the output power at which the gain of the PA is compressed by 1 dB compared to the ideal linear gain. This can force the amplifier operating within a more linear regime [185]. Alternatively, *input power back-off* measures the reduction of the input power $P_{\text{in, sat}}$ relative to IP1dB, which is the input power level producing OP1dB, as

$$\text{IBO} = 10 \log_{10} \left(\frac{\text{IP1dB}}{P_{\text{in}}} \right). \quad (5.13)$$

However, power back-off generally leads to reduction of PA efficiency [188].

PA linearization techniques are employed to improve the linearity while maintaining an acceptable level of power efficiency [5]. This can be also seen as extension of the effective linear operating region of the amplifier towards its saturation point. As a result, a smaller back-off is needed for the PA compared to the initial (nonlinearized) case, leading to improving the power efficiency.

Among various linearization techniques that have been extensively studied over the years, digital predistortion (DPD) has received most attention and is widely adopted in many practical systems. The main idea of DPD is to digitally pre-compensate the signal incoming to the PA so that the cascade of the predistorter and the amplifier produces the overall linear response [5]. Numerous DPD techniques have been proposed in the literature for efficient linearization of PAs [190, 191, 194–198, 212–216], but since this is not the focus of this thesis, this topic will not be discussed further here.

5.1.3 Performance Metrics

To evaluate the impact of PA nonlinearities, it is common to use the normalized mean squared error (NMSE), which provides a general indication of the overall distortions. It is defined as

$$\text{NMSE} = \frac{\sum_{n=0}^{N-1} |d(n) - y(n)|^2}{\sum_{n=0}^{N-1} |d(n)|^2}, \quad (5.14)$$

where $d(n) = Gx(n)$ is the desired output with the ideal linear gain G , and $y(n)$ is the PA output signal. However, this metric does not distinguish

between the distortions occurring within the signal bandwidth and outside the signal bandwidth. Therefore, additional in-band and out-of-band performance metrics are also used [5].

The adjacent channel leakage ratio (ACLR) characterizes the out-of-band distortions and quantifies the amount of unwanted power leaked into adjacent frequency bands. It is measured as the ratio between the power in the adjacent channel with the largest power and power measured in the main channel, i.e.,

$$\text{ACLR} = \frac{\int_{\text{max. adj.}} |Y(f)|^2}{\int_{\text{ch.}} |Y(f)|^2}, \quad (5.15)$$

where $Y(f)$ is the power spectrum of the signal $y(n)$ [212].

The error vector magnitude (EVM) quantifies the distortions introduced within the signal bandwidth and is defined as

$$\text{EVM} = \frac{\sum_{n=0}^{N-1} |d_n - s_n|^2}{\sum_{n=0}^{N-1} |d_n|^2}, \quad (5.16)$$

where d_n and s_n are the n th transmitted and received symbols after down-sampling [212].

5.2 Cascaded Power Amplifiers Challenges

The challenges associated with a single PA become substantially more complex when a number of PAs are used in cascade. Specifically, nonlinear distortions from each amplifier accumulate with those from preceding stages, resulting in more severe nonlinear behavior and greater spectral regrowth after several stages. This leads to the need of a larger back-off, thereby significantly reducing the PA efficiency, i.e., the trade-off between linearity and efficiency is more difficult to maintain.

Systems involving cascaded amplifiers have been known for several years [94, 108–110, 217], but the effect of cascaded nonlinearities has not been fully studied in these areas. Moreover, many papers assumed that the nonlinear effect is negligible. This thesis focuses on cascaded PAs, particularly, Paper H addresses this issue by modeling the cascaded PAs, analyzing the total nonlinearities and optimizing the parameters of the PAs to mitigate the severe effect of their cascade connection.

Chapter 6

Concluding Remarks and Thesis Contributions

This doctoral thesis investigates efficient signal processing techniques for reconfigurable communication system front-ends and presents contributions in three areas, specifically, design and implementation of VDFs, efficient sampling clocks synchronization, and analysis of cascaded PA nonlinearities.

In the area of VDFs, Paper A proposes implementations and systematic design procedures for RLPE based on minimax optimization, while Paper B investigates an analysis of chip area and power consumption for an ASIC implementation of the RLPE. Further, Paper C presents low-complexity frequency-domain implementations of VDFs designed in the time domain, while Papers D and E introduce efficient frequency-sampling-based design approaches for a variable-bandwidth FIR filter implemented in the frequency domain using minimax and LS optimization methods, respectively.

In the area of sampling clocks synchronization, Paper F proposes a joint SFO estimation and compensation framework based on a VFD filter, while Paper G introduces a generalized accumulator-based approach for efficient computation of the components in the proposed SFO estimation algorithm.

In the area of cascaded PAs, Paper H presents the results of modeling, analysis, and optimization of cascaded PA parameters to mitigate the severe effect of the accumulated distortions.

Bibliography

- [1] V. K. Madiseti, *The Digital Signal Processing Handbook*. CRC Press, 1999.
- [2] P. Prandoni and M. Vetterli, *Signal Processing for Communications*. EPFL Press, 2008.
- [3] S. K. Mitra, *Digital Signal Processing: A Computer-Based Approach*, 3rd ed. McGraw-Hill, 2006.
- [4] A. Oppenheim and R. Schaffer, *Discrete-Time Signal Processing*, 3rd ed. Pearson, 2010.
- [5] F.-L. Luo, *Digital Front-Ends in Wireless Communications and Broadcasting Circuits and Signal Processing*. Cambridge, UK: Cambridge University Press, 2011.
- [6] M. Z. Chowdhury, M. Shahjalal, S. Ahmed, and Y. M. Jang, “6G wireless communication systems: Applications, requirements, technologies, challenges, and research directions,” *IEEE Open J. Commun. Society*, vol. 1, pp. 957–975, 2020.
- [7] G. Callebaut, L. Liu, T. Eriksson, L. Van der Perre, O. Edfors, and C. Fager, “6G radio testbeds: Requirements, trends, and approaches,” *IEEE Microwave Mag.*, vol. 25, no. 4, pp. 14–31, 2024.
- [8] C.-X. Wang, X. You, X. Gao, X. Zhu, Z. Li, C. Zhang, H. Wang, Y. Huang, Y. Chen, H. Haas, J. S. Thompson, E. G. Larsson, M. D. Renzo, W. Tong, P. Zhu, X. Shen, H. V. Poor, and L. Hanzo, “On the road to 6G: Visions, requirements, key technologies, and testbeds,” *IEEE Commun. Surveys Tuts.*, vol. 25, no. 2, pp. 905–974, 2023.
- [9] F. Hamdar, C. M. G. Gussen, J. Nadal, C. A. Nour, and A. Baghdadi, “FBMC/OQAM transceiver for future wireless communication systems: Inherent potentials, recent advances, research challenges,” *IEEE Open J. Vehicular Technology*, vol. 4, pp. 652–666, 2023.
- [10] R. Akeela and B. Dezfouli, “Software-defined radios: Architecture, state-of-the-art, and challenges,” *Computer Commun.*, vol. 128, pp. 106–125, 2018.
- [11] M. Kumm, A. Volkova, and S.-I. Filip, “Design of optimal multiplierless FIR filters with minimal number of adders,” *IEEE Trans. Comput.-Aided Design of Integr. Circuits Syst.*, vol. 42, no. 2, pp. 658–671, Feb. 2023.
- [12] R. Garcia, A. Volkova, M. Kumm, A. Goldsztejn, and J. Kühle, “Hardware-aware design of multiplierless second-order IIR filters with minimum adders,” *IEEE Trans. Signal Process.*, vol. 70, pp. 1673–1686, Mar. 2022.
- [13] A. Kovalev, O. Gustafsson, and M. Garrido, “Implementation approaches for 512-tap 60 GSa/s chromatic dispersion FIR filters,” in *Proc. 51st Asilomar Conf. Signals Systems Computers*, Oct. 29–Nov. 1, 2017, pp. 1779–1783.
- [14] X. X. Zheng, J. Yang, S. Y. Yang, W. Chen, L. Y. Huang, and X. Y. Zhang, “Synthesis of linear-phase FIR filters with a complex exponential impulse response,” *IEEE Trans. Signal Process.*, vol. 69, pp. 6101–6115, Sep. 2021.
- [15] S. Yergaliyev and M. T. Akhtar, “A systematic review on distributed arithmetic-based hardware implementation of adaptive digital filters,” *IEEE Access*, vol. 11, pp. 85 165–85 183, 2023.
- [16] D. Pakiyarajah and C. U. S. Edussooriya, “Minimax design of computationally-efficient FIR graph filters using semidefinite programming,” *IEEE Trans. Circuits Syst. II: Exp. Briefs*, vol. 69, no. 9, pp. 3655–3659, 2022.

-
- [17] L. Aksoy, P. Flores, and J. Monteiro, "A tutorial on multiplierless design of FIR filters: Algorithms and architectures," *Circuits Syst. Signal Process.*, vol. 33, p. 1689–1719, Jun. 2014.
- [18] Z. Liwen, F. Qamar, M. Liaqat, M. Nour Hindia, and K. Akram Zainol Ariffin, "Toward efficient 6G IoT networks: A perspective on resource optimization strategies, challenges, and future directions," *IEEE Access*, vol. 12, pp. 76 606–76 633, 2024.
- [19] H. Zhang, Z. Ghassemlooy, M. Wang, and T. Zhang, "Flexible double-layer optical OFDM for IM/DD-based visible light communications," *IEEE Commun. Letters*, vol. 28, no. 5, pp. 1151–1155, 2024.
- [20] J. Zhang, X. Xu, S. Han, K. Zhang, P. Zhang, and T. Q. S. Quek, "Intelligent ultrareliable and low-latency communications: Flexibility and adaptation," *IEEE Internet of Things J.*, vol. 9, no. 17, pp. 16 140–16 153, 2022.
- [21] A. Loulou, J. Yli-Kaakinen, and M. Renfors, "Advanced low-complexity multicarrier schemes using fast-convolution processing and circular convolution decomposition," *IEEE Trans. Signal Process.*, vol. 67, no. 9, pp. 2304–2319, 2019.
- [22] I. Shallari, I. S. Leal, S. Krug, A. Jantsch, and M. O’Nils, "Design space exploration for an IoT node: Trade-offs in processing and communication," *IEEE Access*, vol. 9, pp. 65 078–65 090, 2021.
- [23] B. Mao, F. Tang, Y. Kawamoto, and N. Kato, "AI models for green communications towards 6G," *IEEE Commun. Surveys Tuts.*, vol. 24, no. 1, pp. 210–247, 2022.
- [24] O. Moryakova, Y. Wang, and H. Johansson, "Low-complexity reconfigurable FIR lowpass equalizers for polynomial channel models," *J. Digital Signal Process.*, vol. 150, pp. 1–13, 2024.
- [25] O. Moryakova and H. Johansson, "Frequency-domain implementations of variable digital FIR filters using the overlap-save technique," in *Proc. 24th Int. Conf. Digital Signal Process. (DSP)*, Rhodes, Greece, Jun. 11–13, 2023, pp. 1–5.
- [26] K. Sreelekha and T. Bindiya, "Design of cost effective variable bandwidth 2D low-pass, high-pass and band-pass filters with improved circularity," *J. Digital Signal Process.*, vol. 133, pp. 1–14, Mar. 2023.
- [27] L. Canese, G. C. Cardarilli, L. Di Nunzio, R. Fazzolari, D. Giardino, M. Re, and S. Spanò, "Efficient digital implementation of a multirate-based variable fractional delay filter for wideband beamforming," *IEEE Trans. Circuits Syst. II: Exp. Briefs*, vol. 70, no. 6, pp. 2231–2235, Jun. 2023.
- [28] X. Liu, G. Ren, W. Zhang, and S. Liang, "Optimized design of a variable fractional delay filter with delay error constraints," *IEEE Trans. Circuits Syst. II: Exp. Briefs*, vol. 70, no. 8, pp. 3164–3168, Aug. 2023.
- [29] T. Ma, Y. Wei, and X. Lou, "Reconfigurable nonuniform filter bank for hearing aid systems," *IEEE/ACM Trans. Audio Speech Language Process.*, vol. 30, pp. 758–771, 2022.
- [30] S. Roy and A. Chandra, "On the design of variable filtered-OFDM based LDACS for future generation air-to-ground communication system," *IEEE Trans. Circuits Syst. II: Exp. Briefs*, vol. 69, no. 2, pp. 644–648, Feb. 2022.
- [31] J. Sun, Y. Wang, Y. Shen, and S. Lu, "Design of variable fractional delay FIR filter using the high-order derivative sampling method," *J. Digital Signal Process.*, vol. 123, pp. 1–10, Apr. 2022.

- [32] R. Zhao and D. Tay, "A complex exponential structure for low-complexity variable fractional delay FIR filters," *Circuits Syst. Signal Process.*, vol. 42, p. 1105–1141, Feb. 2023.
- [33] T. O. Otunniyi and H. C. Myburgh, "Low-complexity filter for software-defined radio by modulated interpolated coefficient decimated filter in a hybrid Farrow," *Sensors*, vol. 22, no. 3, Feb. 2022.
- [34] O. Moryakova, Y. Wang, and H. Johansson, "Reconfigurable FIR lowpass equalizers," in *Proc. IEEE Workshop Signal Process. Syst. (SiPS)*, Rennes, France, Nov. 2–4, 2022, pp. 1–6.
- [35] S. Roy and A. Chandra, "A survey of FIR filter design techniques: Low-complexity, narrow transition-band and variable bandwidth," *Integration*, vol. 77, pp. 193–204, Mar. 2021.
- [36] S. Dhabu, A. Ambede, N. Agrawal, K. G. Smitha, S. Darak, and A. Vinod, "Variable cutoff frequency FIR filters: A survey," *SN Applied Sciences*, vol. 2, no. 3, Feb. 2020.
- [37] T. Ma, C. Shen, and Y. Wei, "Adjustable filter bank design for hearing aids system," in *Proc. IEEE Int. Symp. Circuits Syst. (ISCAS)*, May 26–29, 2019, pp. 1–5.
- [38] R. Zhao and X. Hong, "Matrix-based algorithms for the optimal design of variable fractional delay FIR filters," *IEEE Trans. Circuits Syst. I: Reg. Papers*, vol. 66, no. 12, pp. 4740–4752, Dec. 2019.
- [39] I. Raghu and E. Elias, "Low complexity spectrum sensing technique for cognitive radio using Farrow structure digital filters," *Eng. Science and Technology, Int. J.*, vol. 22, no. 1, pp. 131–142, Feb. 2019.
- [40] J. Yli-Kaakinen and M. Renfors, "Optimized reconfigurable fast convolution-based transmultiplexers for flexible radio access," *IEEE Trans. Circuits Syst. II: Exp. Briefs*, vol. 65, no. 1, pp. 130–134, 2018.
- [41] X. Huang, B. Zhang, H. Qin, and W. An, "Closed-form design of variable fractional-delay FIR filters with low or middle cutoff frequencies," *IEEE Trans. Circuits Syst. I: Reg. Papers*, vol. 65, no. 2, pp. 628–637, Feb. 2018.
- [42] S. Koshita, M. Abe, and M. Kawamata, "Recent advances in variable digital filters," in *Digital Systems*, V. Asadpour, Ed. Rijeka: IntechOpen, Nov. 2018, ch. 2.
- [43] T. Bindima and E. Elias, "Design and implementation of low complexity 2-D variable digital FIR filters using single-parameter-tunable 2-D Farrow structure," *IEEE Trans. Circuits Syst. I: Reg. Papers*, vol. 65, no. 2, pp. 618–627, Feb. 2018.
- [44] R. Indrakanti, N. Haridas, and E. Elias, "High performance continuous variable bandwidth digital filter design for hearing aid application," *AEÜ - Int. J. Electron. Commun.*, vol. 92, pp. 36–53, Aug. 2018.
- [45] N. Haridas and E. Elias, "Reconfigurable Farrow structure-based FRM filters for wireless communication systems," *J. Circuits Syst. Signal Process.*, vol. 36, no. 1, p. 315–338, Jan. 2017.
- [46] —, "Design of reconfigurable low-complexity digital hearing aid using Farrow structure based variable bandwidth filters," *J. Applied Research and Technology*, vol. 14, no. 2, pp. 154–165, 2016.
- [47] A. Ambede, S. Shreejith, A. P. Vinod, and S. A. Fahmy, "Design and realization of variable digital filters for software-defined radio channelizers using an improved

- coefficient decimation method,” *IEEE Trans. Circuits Syst. II: Exp. Briefs*, vol. 63, no. 1, pp. 59–63, Jan. 2016.
- [48] S. J. Darak, S. Dhabu, C. Moy, H. Zhang, J. Palicot, and A. Vinod, “Low complexity and efficient dynamic spectrum learning and tunable bandwidth access for heterogeneous decentralized cognitive radio networks,” *J. Digital Signal Process.*, vol. 37, pp. 13–23, Feb. 2015.
- [49] W. J. Xu, Y. J. Yu, and H. Johansson, “Improved filter bank approach for the design of variable bandedge and fractional delay filters,” *IEEE Trans. Circuits Syst. I: Reg. Papers*, vol. 61, no. 3, pp. 764–777, Mar. 2014.
- [50] M. Renfors, J. Yli-Kaakinen, and F. J. Harris, “Analysis and design of efficient and flexible fast-convolution based multirate filter banks,” *IEEE Trans. Signal Process.*, vol. 62, no. 15, pp. 3768–3783, Aug. 2014.
- [51] H. Johansson and A. Eghbali, “A realization of FIR filters with simultaneously variable bandwidth and fractional delay,” *Proc. 20th European Signal Process. Conf. (EUSIPCO)*, pp. 2178–2182, Aug. 27–31, 2012.
- [52] Y. J. Yu and W. J. Xu, “Mixed-radix fast filter bank approach for the design of variable digital filters with simultaneously tunable bandedge and fractional delay,” *IEEE Trans. Signal Process.*, vol. 60, no. 1, pp. 100–111, Jan. 2012.
- [53] H. Johansson and E. Hermanowicz, “Two-rate based low-complexity variable fractional-delay FIR filter structures,” *IEEE Trans. Circuits Syst. I: Reg. Papers*, vol. 60, no. 1, pp. 136–149, Jan. 2013.
- [54] C.-C. Tseng and S.-L. Lee, “Efficient design and implementation of variable fractional delay filters using differentiators,” *IEEE Trans. Circuits Syst. I: Reg. Papers*, vol. 58, no. 6, pp. 1311–1322, Jun. 2011.
- [55] H. Lee and Z. Bien, “A variable bandwidth filter for estimation of instantaneous frequency and reconstruction of signals with time-varying spectral content,” *IEEE Trans. Signal Process.*, vol. 59, no. 5, pp. 2052–2071, May 2011.
- [56] Y. J. Yu, Y. C. Lim, and D. Shi, “Low-complexity design of variable bandedge linear phase FIR filters with sharp transition band,” *IEEE Trans. Signal Process.*, vol. 57, no. 4, pp. 1328–1338, Apr. 2009.
- [57] T.-B. Deng and Y. Lian, “Weighted-least-squares design of variable fractional-delay FIR filters using coefficient symmetry,” *IEEE Trans. Signal Process.*, vol. 54, no. 8, pp. 3023–3038, Aug. 2006.
- [58] P. Löwenborg and H. Johansson, “Minimax design of adjustable-bandwidth linear-phase FIR filters,” *IEEE Trans. Circuits Syst. I: Reg. Papers*, vol. 53, no. 2, pp. 431–439, Feb. 2006.
- [59] T.-B. Deng, “Closed-form design and efficient implementation of variable digital filters with simultaneously tunable magnitude and fractional delay,” *IEEE Trans. Signal Process.*, vol. 52, no. 6, pp. 1668–1681, 2004.
- [60] P. Löwenborg and H. Johansson, “Linear programming design of linear-phase FIR filters with variable bandwidth,” in *Proc. Int. Symp. Circuits Syst. (ISCAS)*, vol. 3, Bangkok, Thailand, May 25–28, 2003, pp. 554–557.
- [61] C.-C. Tseng, “Design of variable fractional delay FIR filter using differentiator bank,” in *Proc. IEEE Int. Symp. Circuits Syst. (ISCAS)*, vol. 4, 2002, pp. IV–IV.

- [62] C. Pun, S. Chan, K. Yeung, and K. Ho, "On the design and implementation of FIR and IIR digital filters with variable frequency characteristics," *IEEE Trans. Circuits Syst. II: Analog and Digital Signal Process.*, vol. 49, no. 11, pp. 689–703, 2002.
- [63] T.-B. Deng, "Weighted least-squares design of variable 1-D FIR filters with arbitrary magnitude responses," in *Proc. IEEE Asia-Pacific Conf. Circuits Syst. (APCCAS)*, 2000, pp. 288–291.
- [64] —, "Design of recursive 1-D variable filters with guaranteed stability," *IEEE Trans. Circuits Syst. II: Analog and Digital Signal Process.*, vol. 44, no. 9, pp. 689–695, 1997.
- [65] G. Stoyanov and M. Kawamata, "Variable digital filters," *J. Signal Process. Japan*, vol. 1, 01 1997.
- [66] R. Zarour and M. Fahmy, "A design technique for variable digital filters," *IEEE Trans. Circuits Syst.*, vol. 36, no. 11, pp. 1473–1478, 1989.
- [67] P. Jarske, S. Mitra, and Y. Neuvo, "Variable linear phase FIR filters," in *Proc. IEEE International Conf. Acoust. Speech Signal Process. (ICASSP)*, 1988, pp. 1463–1466 vol.3.
- [68] C. W. Farrow, "A continuously variable delay element," in *Proc. IEEE Int. Symp. Circuits Syst. (ISCAS)*, vol. 3, Espoo, Finland, Jun. 7–9, 1988, pp. 2641–2645.
- [69] S. Hazra, "Linear phase bandpass digital filters with variable cutoff frequencies," *IEEE Trans. Circuits Syst.*, vol. 31, no. 7, pp. 661–663, 1984.
- [70] K. Steiglitz, "A note on variable recursive digital filters," *IEEE Trans. Acoust. Speech Signal Process.*, vol. 28, no. 1, pp. 111–112, 1980.
- [71] S. Ahuja and S. Dutta Roy, "Linear phase variable digital bandpass filters," *Proc. IEEE*, vol. 67, no. 1, pp. 173–174, 1979.
- [72] S. Roy and S. Ahuja, "Frequency transformations for linear-phase variable-cutoff digital filters," *IEEE Trans. Circuits Syst.*, vol. 26, no. 1, pp. 73–75, 1979.
- [73] D. Johnson, "Variable digital filters having a recursive structure," *IEEE Trans. Acoust. Speech Signal Process.*, vol. 27, no. 1, pp. 98–99, 1979.
- [74] A. Oppenheim, W. Mecklenbrauker, and R. Mersereau, "Variable cutoff linear phase digital filters," *IEEE Trans. Circuits Syst.*, vol. 23, no. 4, pp. 199–203, 1976.
- [75] N. M. Sarband, O. Moryakova, H. Johansson, and O. Gustafsson, "Low-complexity implementation of real-time reconfigurable low-pass equalizers," *IEEE Trans. Very Large Scale Integr. (VLSI) Syst.*, vol. 33, no. 9, pp. 2462–2473, Jul. 2025.
- [76] T. W. Parks and C. S. Burrus, *Digital Filter Design*. Wiley, 1987.
- [77] Y. Son, H. Jeon, and J. Kim, "Tackling the coupled frequency offset impairments for IEEE 802.11be wideband WLANs," *IEEE Trans. Wireless Commun.*, vol. 25, pp. 865–882, Jul. 2025.
- [78] K. Wang, Y. Ma, S. Liu, J. Loo, W. Lin, Z. Deng, and J. Li, "Sampling frequency offset analysis and compensation for OFDM-based LEO satellite communication system," *IEEE Trans. Commun.*, vol. 73, no. 9, pp. 8362–8376, Sep. 2025.
- [79] M. Morelli and M. Moretti, "Fine carrier and sampling frequency synchronization in OFDM systems," *IEEE Trans. Wireless Commun.*, vol. 9, no. 4, pp. 1514–1524, Apr. 2010.

- [80] L. Li, Z. Zhan, Z. Pang, Q. Yang, X. Liu, B. Huang, and S. Wei, "A sampling frequency offset estimation method for high-speed power line communication system," in *Proc. 9th Int. Conf. Comput. Commun. Sys. (ICCCS)*, Xi'an, China, 19–22 Apr., 2024, pp. 1094–1099.
- [81] S. A. Matin and L. B. Milstein, "OFDM system performance, variability and optimality with design imperfections and channel impediments," *IEEE Trans. Veh. Tech.*, vol. 70, no. 1, pp. 381–397, 2021.
- [82] X. Wang, T. Tjhung, Y. Wu, and B. Caron, "SER performance evaluation and optimization of OFDM system with residual frequency and timing offsets from imperfect synchronization," *IEEE Trans. Broadcast.*, vol. 49, no. 2, pp. 170–177, 2003.
- [83] L. Giroto de Oliveira, Y. Li, S. Mandelli, D. Brunner, M. Henninger, X. Wan, T. Jun Cui, T. Zwick, and B. Nuss, "Pilot-based SFO estimation for bistatic integrated sensing and communication," *IEEE Trans. Microwave Theory Techn.*, vol. 73, no. 7, pp. 4143–4161, Jul. 2025.
- [84] D. Brunner, L. Giroto de Oliveira, C. Muth, S. Mandelli, M. Henninger, A. Diewald, Y. Li, M. Basim Alabd, L. Schmalen, T. Zwick, and B. Nuss, "Bistatic OFDM-based ISAC with over-the-air synchronization: System concept and performance analysis," *IEEE Trans. Microwave Theory Techn.*, vol. 73, no. 5, pp. 3016–3029, May 2025.
- [85] Y. Hou, X. Chen, and K. Du, "Comparison and analysis of SFO estimation methods based on OFDM," in *Proc. 5th Int. Conf. Comput. Commun. Syst. (ICCCS)*, Shanghai, China, 15–18 May. 2020, pp. 640–644.
- [86] H. Nguyen-Le, T. Le-Ngoc, and C. C. Ko, "RLS-based joint estimation and tracking of channel response, sampling, and carrier frequency offsets for OFDM," *IEEE Trans. Broadcast.*, vol. 55, no. 1, pp. 84–94, 2009.
- [87] P.-Y. Tsai, H.-Y. Kang, and T.-D. Chiueh, "Joint weighted least-squares estimation of carrier-frequency offset and timing offset for OFDM systems over multipath fading channels," *IEEE Trans. Veh. Technol.*, vol. 54, no. 1, pp. 211–223, 2005.
- [88] Y.-H. Kim and J.-H. Lee, "Joint maximum likelihood estimation of carrier and sampling frequency offsets for OFDM systems," *IEEE Trans. Broadcast.*, vol. 57, no. 2, pp. 277–283, 2011.
- [89] X. Wang and B. Hu, "A low-complexity ML estimator for carrier and sampling frequency offsets in OFDM systems," *IEEE Commun. Lett.*, vol. 18, no. 3, pp. 503–506, 2014.
- [90] Y. Wu, R. Mei, and J. Xu, "Non pilot data-aided carrier and sampling frequency offsets estimation in fast time-varying channel," *Big Data Res.*, vol. 36, p. 100461, 2024.
- [91] C. Oberli, "ML-based tracking algorithms for MIMO-OFDM," *IEEE Trans. Wireless Commun.*, vol. 6, no. 7, pp. 2630–2639, Jul. 2007.
- [92] R. Hamila, J. Vesma, H. Vuolle, and M. Renfors, "Effect of frequency offset on carrier phase and symbol timing recovery in digital receivers," in *Proc. URSI Int. Symp. Signals Syst., and Electron. Conf.*, Pisa, Italy, 1998, pp. 247–252.
- [93] Q. Hu, X. Jin, and Z. Xu, "Compensation of sampling frequency offset with digital interpolation for OFDM-based visible light communication systems," *J. Light. Technol.*, vol. 36, no. 23, pp. 5488–5497, 2018.

- [94] X. Gao, M. Chen, J. Zhou, J. Xu, H. Li, Y. Cai, and D. Wang, "Sampling frequency offset estimation and compensation for asynchronous optical IMDD FBMC systems," *J. Light. Technol.*, vol. 42, no. 9, pp. 3099–3106, 2024.
- [95] L. Erup, F. Gardner, and R. Harris, "Interpolation in digital modems. II. implementation and performance," *IEEE Trans. Commun.*, vol. 41, no. 6, pp. 998–1008, 7–9 Jun. 1993.
- [96] O. Hammi, S. Carichner, B. Vassilakis, and F. M. Ghannouchi, "Power amplifiers' model assessment and memory effects intensity quantification using memoryless post-compensation technique," *IEEE Trans. Microw. Theory Techn.*, vol. 56, no. 12, pp. 3170–3179, 2008.
- [97] A. S. Tehrani, H. Cao, S. Afsardoost, T. Eriksson, M. Isaksson, and C. Fager, "A comparative analysis of the complexity/accuracy tradeoff in power amplifier behavioral models," *IEEE Trans. Microw. Theory Techn.*, vol. 58, no. 6, pp. 1510–1520, Jun. 2010.
- [98] T. R. Cunha, E. G. Lima, and J. C. Pedro, "Validation and physical interpretation of the power-amplifier polar Volterra model," *IEEE Trans. Microw. Theory Techn.*, vol. 58, no. 12, pp. 4012–4021, Dec. 2010.
- [99] J. C. Pedro, P. M. Cabral, T. R. Cunha, and P. M. Lavrador, "A multiple time-scale power amplifier behavioral model for linearity and efficiency calculations," *IEEE Trans. Microw. Theory Techn.*, vol. 61, no. 1, pp. 606–615, Jan. 2013.
- [100] S. Glock, J. Rascher, B. Sogl, T. Ussmueller, J.-E. Mueller, and R. Weigel, "A memoryless semi-physical power amplifier behavioral model based on the correlation between AM–AM and AM–PM distortions," *IEEE Trans. Microw. Theory Techn.*, vol. 63, no. 6, pp. 1826–1835, Jun. 2015.
- [101] Y. Khawam, O. Hammi, L. Albasha, and H. Mir, "Behavioral modeling of GaN Doherty power amplifiers using memoryless polar domain functions and deep neural networks," *IEEE Access*, vol. 8, pp. 202 707–202 715, 2020.
- [102] M. H. Moghaddam, S. R. Aghdam, N. Mazzali, and T. Eriksson, "Statistical modeling and analysis of power amplifier nonlinearities in communication systems," *IEEE Trans. Commun.*, vol. 70, no. 2, pp. 822–835, 2022.
- [103] J. He, S. Huang, Y. Huang, S. Chang, S. Ying, B.-Z. Shen, and Z. Feng, "A unified power amplifier representation-based receiver equalization technique for nonlinear OFDM signal detection," *IEEE Trans. Commun.*, vol. 72, no. 4, pp. 2260–2274, 2024.
- [104] L. Samara, S. Haussmann, E. Tufa, A. A. D'Amico, T. Zugno, I. Kallfass, and T. Kürner, "Sub-THz power amplifiers: Measurements, behavioral modeling, and predistortion algorithms," *IEEE Trans. Terahertz Science Techn.*, vol. 15, no. 6, pp. 1007–1019, Nov. 2025.
- [105] D. Kong, D. P. M. Osorio, and E. G. Larsson, "Radio over fiber with cascaded structure: Algorithm for uplink positioning," *IEEE Tran. Wireless Commun.*, vol. 25, pp. 9000–9014, Dec. 2025.
- [106] L. Van der Perre, G. Callebaut, T. Eriksson, M. Sarajlic, C. Fager, F. Tufvesson, B. K. Lau, and E. G. Larsson, "Distributed deployment and dual-frequency concepts to strengthen sub-THz wireless systems," *IEEE Wireless Commun.*, pp. 1–8, 2025.
- [107] Y.-S. Hurh, K.-W. Shin, S.-H. Lee, and J.-S. Lee, "Weather-insensitive optical free-space communication using gain-saturated optical fiber amplifiers," *J. Lightwave Technol.*, vol. 23, no. 12, pp. 4022–4025, 2005.

-
- [108] S. Wannemacher and G. Bauer, "Optimum configuration for cascaded fiber amplifiers in attenuation limited transmission systems," *J. Lightwave Technol.*, vol. 16, no. 4, pp. 509–514, 1998.
- [109] Y. Awaji, H. Sotobayashi, and F. Kubota, "Transmission of 80 Gb/s \times 6 WDM over 100 km using linear optical amplifiers," *IEEE Photonics Techn. Lett.*, vol. 17, no. 3, pp. 699–701, Mar. 2005.
- [110] F. Francis and R. Manivasakan, "A performance limit estimation framework for multihop repeated/regenerated optical links," *IEEE Access*, vol. 10, pp. 70 016–70 031, 2022.
- [111] O. Hammi, S. Boumaiza, J. Kim, S. Hong, I. Kim, B. Kim, and F. Ghannouchi, "RF power amplifiers for emerging wireless communications: Single branch vs. multi-branch architectures," in *Canadian Conf. Electric. Comput. Eng.*, 2006, pp. 598–601.
- [112] P. N. Landin and U. Gustavsson, "Distortion mitigation in RF transmitters with cascaded nonlinear and efficient power amplifiers," in *WAMICON 2014*, 2014, pp. 1–4.
- [113] M. Renfors and Y. Neuvo, "The maximum sampling rate of digital filters under hardware speed constraints," *IEEE Trans. Circuits Syst.*, vol. 28, no. 3, pp. 196–202, 1981.
- [114] M. G. Bellanger, *Digital Processing of Signals*. John Wiley and Sons, 1984.
- [115] A. V. Oppenheim and R. W. Schaffer, *Discrete-Time Signal Processing*. Prentice Hall, 1989.
- [116] L. Wanhammar and H. Johansson, *Digital Filters Using MATLAB*. Linköping University, 2013.
- [117] L. Wanhammar, *DSP Integrated Circuits*, ser. Academic Press Series in Engineering. Academic Press, 1999.
- [118] L. R. Rabiner and B. Gold, *Theory and Application of Digital Signal Processing*. Prentice-Hall, Englewood Cliffs, NJ, 1975.
- [119] K. Ichige, M. Iwaki, and R. Ishii, "Accurate estimation of minimum filter length for optimum FIR digital filters," *IEEE Trans. Circuits Syst. II: Analog and Digital Signal Process.*, vol. 47, no. 10, pp. 1008–1016, Oct. 2000.
- [120] F. Harris, "On the use of windows for harmonic analysis with the discrete Fourier transform," *Proc. IEEE*, vol. 66, no. 1, pp. 51–83, 1978.
- [121] T. W. Parks and C. S. Burrus, *Digital Filter Design*. John Wiley and Sons, 1987.
- [122] P. P. Vaidyanathan, *Multirate Systems and Filter Banks*. USA: Prentice-Hall, Inc., 1993.
- [123] S. Harris and E. Ifeakor, "Automatic design of frequency sampling filters by hybrid genetic algorithm techniques," *IEEE Trans. Signal Process.*, vol. 46, no. 12, pp. 3304–3314, Dec. 1998.
- [124] S. Salcedo-Sanz, F. Cruz-Roldan, C. Heneghan, and X. Yao, "Evolutionary design of digital filters with application to subband coding and data transmission," *IEEE Trans. Signal Process.*, vol. 55, no. 4, pp. 1193–1203, Apr. 2007.
- [125] L. Rabiner, B. Gold, and C. McGonegal, "An approach to the approximation problem for nonrecursive digital filters," *IEEE Trans. Audio and Electroacoust.*, vol. 18, no. 2, pp. 83–106, Jun. 1970.

- [126] R. Y. Belorutsky and I. S. Savinykh, "Modified technique of FIR filter design by the frequency sampling method," in *Proc. 11th Int. Forum on Strategic Technology (IFOST)*, Jun. 1-3, 2016, pp. 259–262.
- [127] J. J. Shynk, "Frequency-domain and multirate adaptive filtering," *IEEE Signal Process. Mag.*, vol. 9, no. 1, pp. 14–37, Jan. 1992.
- [128] K. Ishihara, R. Kudo, T. Kobayashi, A. Sano, Y. Takatori, T. Nakagawa, and Y. Miyamoto, "Frequency-domain equalization for coherent optical transmission systems," in *Proc. Optical Fiber Commun. Conf. and Exposition and the National Fiber Optic Engineers Conf.*, Mar. 6-10, 2011, pp. 1–3.
- [129] H. Johansson and O. Gustafsson. (2023, Feb.) On frequency-domain implementation of digital FIR filters using overlap-add and overlap-save techniques. Doi: 10.48550/ARXIV.2302.08845.
- [130] H. Sorensen, D. Jones, M. Heideman, and C. Burrus, "Real-valued fast Fourier transform algorithms," *IEEE Trans. Acoustics Speech Signal Process.*, vol. 35, no. 6, pp. 849–863, June 1987.
- [131] S. A. Alam and O. Gustafsson, "Design of finite word length linear-phase FIR filters in the logarithmic number system domain," *VLSI Design*, vol. 2014, no. 1, p. 217495, Apr. 2014.
- [132] Y. Wang, M. Deng, H. Johansson, Z. Li, and Q. Li, "Unified filter order estimate for minimax-designed linear-phase FIR wideband and lowpass digital differentiators," *J. Circuits Syst. Signal Process.*, pp. 1–22, Jul. 2023.
- [133] Z. U. Sheikh and H. Johansson, "A class of wide-band linear-phase FIR differentiators using a two-rate approach and the frequency-response masking technique," *IEEE Trans. Circuits Syst. I: Reg. Papers*, vol. 58, no. 8, pp. 1827–1839, Aug. 2011.
- [134] S. J. Darak, S. K. P. Gopi, V. A. Prasad, and E. Lai, "Low-complexity reconfigurable fast filter bank for multi-standard wireless receivers," *IEEE Trans. Very Large Scale Integr. (VLSI) Syst.*, vol. 22, no. 5, pp. 1202–1206, 2014.
- [135] Y. Wei and Y. Wang, "Design of low complexity adjustable filter bank for personalized hearing aid solutions," *IEEE/ACM Trans. Audio Speech Language Process.*, vol. 23, no. 5, pp. 923–931, 2015.
- [136] M. Borgerding, "Turning overlap-save into a multiband mixing, downsampling filter bank," *IEEE Signal Process. Mag.*, vol. 23, no. 2, pp. 158–161, 2006.
- [137] A. Mehr and T. Chen, "Representations of linear periodically time-varying and multirate systems," *IEEE Trans. Signal Process.*, vol. 50, no. 9, pp. 2221–2229, 2002.
- [138] T. Laas, L. G. Baltar, and J. A. Nossek, "Frequency-domain analysis of linear periodically time-varying FBMC systems," in *Proc. IEEE Sensor Array and Multichannel Signal Process. Workshop (SAM)*, 2016, pp. 1–5.
- [139] T. Chen and L. Qiu, "Linear periodically time-varying discrete-time systems: Aliasing and LTI approximations," in *Proc. 35th IEEE Conf. Decision Control*, vol. 3, 1996, pp. 2677–2682 vol.3.
- [140] G. Brown, "Exploring 5G new radio : Use cases , capabilities & timeline," Qualcomm Technologies, Inc., Tech. Rep., 2016. [Online]. Available: https://www.qualcomm.com/content/dam/qualcomm-martech/dm-assets/documents/heavyreading_whitepaper_-_exploring_5g_new_radio_use_cases_capabilities_and_timeine.pdf

- [141] C. B. Mwakwata, H. Malik, M. Mahtab Alam, Y. Le Moullec, S. Parand, and S. Mumtaz, "Narrowband internet of things (NB-IoT): From physical (PHY) and media access control (MAC) layers perspectives," *Sensors*, vol. 19, no. 11, 2019. [Online]. Available: <https://www.mdpi.com/1424-8220/19/11/2613>
- [142] G. Deep, S. J. Darak, and P. Garg, "Spectral parameter approximation based tunable digital filters on Zynq SoC," in *Proc. IEEE Int. Symp. Circuits Syst. (ISCAS)*, Florence, Italy, May 27–30, 2018, pp. 1–5.
- [143] N. Haridas and E. Elias, "Efficient Farrow structure based bank of variable bandwidth filters for digital hearing aids," in *Proc. IEEE Int. Conf. Signal Processing, Informat., Commun., Energy Syst. (SPICES)*, Feb. 19–21, 2015, pp. 1–5.
- [144] A. Constantinides, "Spectral transformations for digital filters," *Proc. Institution of Electrical Engineers*, vol. 117, pp. 1585–1590, 01 1970.
- [145] H. Johansson and P. Löwenborg, "On the design of adjustable fractional delay FIR filters," *IEEE Trans. Circuits Syst. II: Exp. Briefs*, vol. 50, no. 4, pp. 164–169, Apr. 2003.
- [146] H. Zhao and J. Yu, "A simple and efficient design of variable fractional delay FIR filters," *IEEE Trans. Circuits Syst. II: Exp. Briefs*, vol. 53, no. 2, pp. 157–160, 2006.
- [147] T.-B. Deng, "Coefficient-symmetries for implementing arbitrary-order lagrange-type variable fractional-delay digital filters," *IEEE Trans. Signal Process.*, vol. 55, no. 8, pp. 4078–4090, Aug. 2007.
- [148] S. Dhabu and A. P. Vinod, "A new time-domain approach for the design of variable FIR filters using the spectral parameter approximation technique," *Circuits Syst. Signal Process.*, vol. 36, May 2017.
- [149] T. Laakso, V. Valimäki, M. Karjalainen, and U. Laine, "Splitting the unit delay [FIR/all pass filters design]," *IEEE Signal Process. Mag.*, vol. 13, no. 1, pp. 30–60, 1996.
- [150] V. Välimäki and T. I. Laakso, "Fractional delay filters—design and applications," in *Nonuniform Sampling: Theory and Practice*, F. Marvasti, Ed. Springer US, 2001, pp. 835–895.
- [151] H. Liu, J. Lin, S. Xu, T. Bi, and Y. Lao, "A resampling method based on filter designed by window function considering frequency aliasing," *IEEE Trans. Circuits Syst. I: Reg. Papers*, vol. 67, no. 12, pp. 5018–5030, 2020.
- [152] J. Rämö and V. Välimäki, "Optimizing a high-order graphic equalizer for audio processing," *IEEE Signal Process. Lett.*, vol. 21, no. 3, pp. 301–305, Mar. 2014.
- [153] P. Regalia and S. Mitra, "Tunable digital frequency response equalization filters," *IEEE Trans. Acoust. Speech Signal Process.*, vol. 35, no. 1, pp. 118–120, 1987.
- [154] H. Johansson, "Sampling and quantization," in *Signal Processing and Machine Learning Theory*, P. S. Diniz, Ed. Academic Press, 2024, ch. 5, pp. 185–265.
- [155] E. Lai, "Converting analog to digital signals and vice versa," in *Practical Digital Signal Processing*, E. Lai, Ed. Oxford: Newnes, 2003, ch. 2, pp. 14–49.
- [156] P. Löwenborg and H. Johansson, "Minimax design of adjustable-bandwidth linear-phase FIR filters," *IEEE Trans. Circuits Syst. I: Reg. Papers*, vol. 53, no. 2, pp. 431–439, Feb. 2006.

- [157] Y. Lim and B. Farhang-Boroujeny, "Fast filter bank (FFB)," *IEEE Trans. Circuits Syst. II: Analog and Digital Signal Process.*, vol. 39, no. 5, pp. 316–318, 1992.
- [158] S. Dikmese, M. Renfors, and I. Guvenc, "Flexible filter bank based spectrum sensing and waveform processing for mission critical communications," in *Proc. IEEE Military Commun. Conf. (MILCOM)*, 2017, pp. 174–179.
- [159] X. Lin, L. Mei, F. Labeau, X. Sha, and X. Fang, "Efficient fast-convolution based hybrid carrier system," *IEEE Trans. Wireless Commun.*, vol. 21, no. 5, pp. 3508–3522, 2022.
- [160] K. Pärilin, T. Riihonen, V. Le Nir, and M. Adrat, "Estimating and tracking wireless channels under carrier and sampling frequency offsets," *IEEE Trans. Signal Process.*, vol. 71, pp. 1053–1066, Mar. 2023.
- [161] Y. Qi, T. Zhang, Y. Feng, Z. Qin, and D. He, "Design and implementation of spectrally efficient frequency division multiplexing receiver," *IEEE Access*, vol. 11, pp. 121 482–121 491, Oct. 2023.
- [162] D. Cherkassky and S. Gannot, "Blind synchronization in wireless acoustic sensor networks," *IEEE/ACM Trans. Audio Speech Language Process.*, vol. 25, no. 3, pp. 651–661, Mar. 2017.
- [163] D. Hu, H. Zhang, F. Bao, and R. Wang, "Distributed sampling rate offset estimation over acoustic sensor networks based on asynchronous network Newton optimization," *IEEE/ACM Trans. Audio Speech Language Process.*, vol. 31, pp. 301–312, Nov. 2023.
- [164] J. Tian, Y. Han, Z. Jin, X. Yang, J. Yang, W. Tang, X. Li, W. Wang, and S. Jin, "Pioneering scalable prototype for mid-band XL-MIMO systems: Design and implementation," *IEEE J. Sel. Areas Commun.*, vol. 44, pp. 3365–3381, Jan. 2026.
- [165] M. Arikawa and K. Hayashi, "Performance of adaptive MIMO filter and adaptive interference canceller for SDM transmission at sub-symbol rate sampling," *Opt. Express*, vol. 34, no. 2, pp. 1626–1638, Jan. 2026.
- [166] D. K. Kim, S. H. Do, H. B. Cho, H. J. Chol, and K. B. Kim, "A new joint algorithm of symbol timing recovery and sampling clock adjustment for OFDM systems," *IEEE Trans. Consumer Electron.*, vol. 44, no. 3, pp. 1142–1149, Aug. 1998.
- [167] H. Minn, V. Bhargava, and K. Letaief, "A robust timing and frequency synchronization for OFDM systems," *IEEE Trans. Wireless Commun.*, vol. 2, no. 4, pp. 822–839, Jul. 2003.
- [168] K. Shi and E. Serpedin, "Coarse frame and carrier synchronization of OFDM systems: a new metric and comparison," *IEEE Trans. Wireless Commun.*, vol. 3, no. 4, pp. 1271–1284, Jul. 2004.
- [169] E. Oswald, "NDA based feedforward sampling frequency synchronization for ofdm systems," in *Proc., IEEE 59th. Veh. Technol. Conf. (VTC-Spring)*, vol. 2, Milan, Italy, 2004, pp. 1068–1072 Vol.2.
- [170] A. Laourine, A. Stephenne, and S. Affes, "Blind sampling clock offset estimation in OFDM systems based on second order statistics," in *Proc. Fortieth Asilomar Conf. Signals Syst. Computers*, 29 Oct.–1 Nov. 2006, pp. 1782–1785.
- [171] G. Ren, Y. Chang, H. Zhang, and H. Zhang, "An efficient frequency offset estimation method with a large range for wireless OFDM systems," *IEEE Trans. Veh. Tech.*, vol. 56, no. 4, pp. 1892–1895, 2007.

- [172] D.-C. Chang, "Effect and compensation of symbol timing offset in OFDM systems with channel interpolation," *IEEE Trans. Broadcasting*, vol. 54, no. 4, pp. 761–770, Dec. 2008.
- [173] Y.-H. You, S.-T. Kim, K.-T. Lee, and H.-K. Song, "An improved sampling frequency offset estimator for OFDM-based digital radio mondiale systems," *IEEE Trans. Broadcast.*, vol. 54, no. 2, pp. 283–286, Jun. 2008.
- [174] Y. Wang and X. Dong, "Comparison of frequency offset and timing offset effects on the performance of SC-FDE and OFDM over UWB channels," *IEEE Trans. Veh. Tech.*, vol. 58, no. 1, pp. 242–250, 2009.
- [175] C. Harish, R. Mohan, and R. Shashank, "Sampling clock offset estimation and correction in frequency domain for OFDM receivers," in *Proc. TENCON - IEEE Region 10 Conf.*, Penang, Malaysia, 5–8 Nov., 2017, pp. 1583–1587.
- [176] Y.-A. Jung, M.-Y. Kim, H.-K. Song, and Y.-H. You, "Blind weighted least-squares frequency offset estimation method for LTE machine-type communications," *IEEE Internet Things J.*, vol. 6, no. 6, pp. 9806–9815, 2019.
- [177] Y. Liu, W. Yang, Z. Wang, and Y. Xu, "Easy-hardware-implementation algorithm of carrier and sampling frequency offset estimation in OFDM systems," in *OES China Ocean Acoust. (COA)*, 2024, pp. 1–4.
- [178] S. Singh, S. Kumar, S. Majhi, U. Satija, and C. Yuen, "Blind carrier frequency offset estimation techniques for next-generation multicarrier communication systems: Challenges, comparative analysis, and future prospects," *IEEE Commun. Surv. Tutor.*, vol. 27, no. 1, pp. 1–36, 2025.
- [179] D. Salwan, S. Agarwal, and B. Kumbhani, "Design and analysis of low-complexity communication receiver for PSK-LFM joint sensing and communication waveform," *IEEE Trans. Intelligent Vehic.*, vol. 11, no. 1, pp. 236–248, 2026.
- [180] H. Meyr, M. Moeneclaey, and S. A. Fechtel, *Digital Communication Receivers: Synchronization, Channel Estimation, and Signal Processing*. New York, NY, USA: John Wiley & Sons, 1997.
- [181] D. Wang, Z. Mei, H. Zhang, and H. Li, "A novel PSS timing synchronization algorithm for cell search in 5G NR system," *IEEE Access*, vol. 9, pp. 5870–5880, Jan. 2021.
- [182] M.-H. Jeong, T.-J. Lee, M.-J. Kim, and Y.-C. Ko, "Effect of phase noise in IEEE 802.11ad MIMO-OFDM systems with common/independent local oscillators," in *Proc. Int. Conf. Informat. Commun. Tech. Convergence (ICTC)*, 28-30 Oct. 2015, pp. 1332–1335.
- [183] C.-Y. Wu, Y.-K. Lin, C.-K. Wu, and C.-H. Lee, "Deep learning-based end-to-end design for OFDM systems with hardware impairments," *IEEE Open J. Commun. Society*, vol. 4, pp. 2468–2482, Oct. 2023.
- [184] B. Ai, Y. Shen, Z. D. Zhong, and B. H. Zhang, "Enhanced sampling clock offset correction based on time domain estimation scheme," *IEEE Trans. Consum. Electron.*, vol. 57, no. 2, pp. 696–704, 2011.
- [185] L. Smaini, *RF Analog Impairments Modeling for Communication Systems Simulation: Application to OFDM-Based Transceivers*. Chichester, UK: John Wiley & Sons, 2012.

- [186] Y.-H. You, Y.-A. Jung, and J.-H. Paik, "Joint estimation of symbol timing and sampling frequency offset for CDD-OFDM-based DRM systems," *IEEE Trans. Broadcast.*, vol. 65, no. 2, pp. 333–339, Jun. 2019.
- [187] J. Vuolevi and T. Rahkonen, *Distortion in RF Power Amplifiers*. Norwood, MA: Artech House, 2003.
- [188] S. C. Cripps, *RF Power Amplifiers for Wireless Communications*, 2nd ed. Norwood, MA: Artech House, 2006.
- [189] P. Kenington, "Linearized transmitters: an enabling technology for software defined radio," *IEEE Commun. Magazine*, vol. 40, no. 2, pp. 156–162, Feb. 2002.
- [190] D. Morgan, Z. Ma, J. Kim, M. Zierdt, and J. Pastalan, "A generalized memory polynomial model for digital predistortion of RF power amplifiers," *IEEE Trans. Signal Process.*, vol. 54, no. 10, pp. 3852–3860, 2006.
- [191] B. Ai, Z.-x. Yang, C.-y. Pan, S.-g. Tang, and T.-t. Zhang, "Analysis on LUT based predistortion method for HPA with memory," *IEEE Trans. Broadcast.*, vol. 53, no. 1, pp. 127–131, March 2007.
- [192] S. Chen, "An efficient predistorter design for compensating nonlinear memory high power amplifiers," *IEEE Trans. Broadcast.*, vol. 57, no. 4, pp. 856–865, Dec. 2011.
- [193] S. Boumard, M. Lasanen, O. Apilo, A. Hekkala, C. Cassan, J.-P. Verdeil, J. David, and L. Pichon, "Power consumption trade-off between power amplifier OBO, DPD, and clipping and filtering," in *Proc. 26th Int. Teletraffic Congress (ITC)*, 9–11 Sep. 2014, pp. 1–5.
- [194] S. Wang, M. Roger, and C. Lelandais-Perrault, "Impacts of crest factor reduction and digital predistortion on linearity and power efficiency of power amplifiers," *IEEE Trans. Circuits Syst. II: Expr. Briefs*, vol. 66, no. 3, pp. 407–411, Mar. 2019.
- [195] S. Wang, M. Roger, J. Sarrazin, and C. Lelandais-Perrault, "An efficient method to study the tradeoff between power amplifier efficiency and digital predistortion complexity," *IEEE Microw. Wireless Components Lett.*, vol. 29, no. 11, pp. 741–744, Nov. 2019.
- [196] J. Zanen, E. Klumperink, and B. Nauta, "Power efficiency model for MIMO transmitters including memory polynomial digital predistortion," *IEEE Trans. Circuits Syst. II: Expr. Briefs*, vol. 68, no. 4, pp. 1183–1187, Apr. 2021.
- [197] M. Abdelaziz, L. Anttila, S. Dikmese, M. Renfors, A. M. Wyglinski, and M. Valkama, "Flexible digital predistortion for future spectrally-agile waveforms and 5G radio systems," in *Proc. IEEE 82nd Vehic. Techn. Conf. (VTC2015-Fall)*, 6–9 Sep. 2015, pp. 1–7.
- [198] H. Le Duc, B. Feuvrie, M. Pastore, and Y. Wang, "An adaptive cascaded ILA- and DLA-based digital predistorter for linearizing an RF power amplifier," *IEEE Trans. Circuits Syst. I: Reg. Papers*, vol. 66, no. 3, pp. 1031–1041, Mar. 2019.
- [199] L. Golard, Y. Agram, F. Rottenberg, F. Quitin, D. Bol, and J. Louveaux, "A parametric power model of multi-band sub-6 GHz cellular base stations using on-site measurements," in *Proc. IEEE 35th Int. Symp. Personal Indoor Mobile Radio Commun. (PIMRC)*, 2–5 Sep. 2024, pp. 1–7.
- [200] W. J., *Behavioral Modeling and Linearization of RF Power Amplifiers*. Norwood, MA: Artech House, 2006.

-
- [201] M. Isaksson, D. Wisell, and D. Ronnow, "A comparative analysis of behavioral models for RF power amplifiers," *IEEE Trans. Microw. Theory Tech.*, vol. 54, no. 1, pp. 348–359, Jan. 2006.
- [202] O. Hammi, M. Younes, and F. M. Ghannouchi, "Metrics and methods for benchmarking of RF transmitter behavioral models with application to the development of a hybrid memory polynomial model," *IEEE Trans. Broadcast.*, vol. 56, no. 3, pp. 350–357, 2010.
- [203] X. Ling, X. Zhang, J. Sun, P. Ge, J. Wang, C. Zhao, and X. Gao, "When Hammerstein meets Wiener: Nonlinearity modeling for end-to-end visible light communication links," *IEEE Trans. Commun.*, vol. 71, no. 1, pp. 310–323, 2023.
- [204] O. B. H. Belkacem, M. L. Ammari, and R. Dinis, "Performance analysis of NOMA in 5G systems with HPA nonlinearities," *IEEE Access*, vol. 8, pp. 158 327–158 334, Aug. 2020.
- [205] G. Wei, A. Li, and C. Masouros, "Exploiting power amplifier nonlinearities through symbol-level interference exploitation precoding in the MU-MIMO downlink," *IEEE Trans. Wireless Commun.*, vol. 23, no. 8, pp. 8432–8446, Aug. 2024.
- [206] U. Kayikci and E. Aktas, "Downlink performance of MU-MIMO-FBMC in power amplifier nonlinearity," *IEEE Wireless Commun. Lett.*, vol. 13, no. 1, pp. 198–202, Jan. 2024.
- [207] C. Rapp, "Effects of HPA-nonlinearity on 4-DPSK/OFDM-signal for a digital sound broadcasting system," in *2nd Europ. Conf. Satellite Commun.*, Oct. 1991, pp. 179–184.
- [208] 3GPP, "Realistic power amplifier model for the new radio evaluation," 3GPP, Sophia Antipolis, France, TSG RAN WG4 Meeting Contribution R4-163314, May 2016, tSG RAN WG4 Meeting 79.
- [209] T. Pratt, N. Jones, L. Smee, and M. Torrey, "OFDM link performance with companding for PAPR reduction in the presence of non-linear amplification," *IEEE Trans. Broadcast.*, vol. 52, no. 2, pp. 261–267, Jun. 2006.
- [210] H. Shaiek, R. Zayani, Y. Medjahdi, and D. Roviras, "Analytical analysis of SER for beyond 5G post-OFDM waveforms in presence of high power amplifiers," *IEEE Access*, vol. 7, pp. 29 441–29 452, Feb. 2019.
- [211] T. Feys, L. V. d. Perre, and F. Rottenberg, "Toward energy-efficient massive MIMO: Graph neural network precoding for mitigating non-linear PA distortion," *IEEE Trans. Cognitive Commun. Networking*, vol. 11, no. 1, pp. 184–201, Feb. 2025.
- [212] J. Chani-Cahuana, P. N. Landin, C. Fager, and T. Eriksson, "Iterative learning control for RF power amplifier linearization," *IEEE Trans. Microwave Theory and Techniques*, vol. 64, no. 9, pp. 2778–2789, 2016.
- [213] M. Noweir, Q. Zhou, A. Kwan, R. Valivarthi, M. Helaoui, W. Tittel, and F. M. Ghannouchi, "Digitally linearized radio-over fiber transmitter architecture for cloud radio access network's downlink," *IEEE Trans. Microw. Theory Techn.*, vol. 66, no. 7, pp. 3564–3574, 2018.
- [214] Y. Yu, L. Yu, R. Liu, X.-W. Zhu, P. Chen, and C. Yu, "Digital predistortion of millimeter-wave GaN power amplifiers for 6G integrated communication, sensing, and power transfer scenarios," *IEEE Trans. Microw. Theory Techn.*, vol. 73, no. 1, pp. 26–37, 2025.

- [215] L. Chen, W. Chen, Y.-J. Liu, Y. He, X. Liu, T. Cao, F. M. Ghannouchi, and Z. Feng, “Linearization of a directional modulation transmitter using low-complexity cascaded digital predistortion,” *IEEE Trans. Microw. Theory Techn.*, vol. 67, no. 11, pp. 4467–4478, 2019.
- [216] R. Criado, W. Li, G. Montoro, and P. L. Gilabert, “Smart digital predistortion: Leveraging cascaded and artificial neural network models with pruning for next-generation challenges,” *IEEE Microw. Mag.*, vol. 27, no. 1, pp. 64–75, Jan. 2026.
- [217] M. Q. Nguyen, S. Dubey, S. Rao, and C. Chiao, “Wireless power transfer via air and building materials using multiple repeaters,” in *Texas Symp. Wireless Microw. Circuits Syst.*, 2014, pp. 1–4.

Part II

Included Papers

Papers

The papers associated with this thesis have been removed for copyright reasons. For more details about these see:

<https://doi.org/10.3384/9789181185379>

Other Recently Published Theses From
The Division of Communication Systems
Department of Electrical Engineering (ISY)
Linköping University, Sweden

Deijany Rodríguez Linares *Contributions to Low-Complexity Linearization, Equalization, and Synchronization*, Linköping Studies in Science and Technology. Dissertations, No. 2514, 2026.

Dexin Kong, *Aspects of Terahertz Radio-over-Fiber Stripes*, Linköping Studies in Science and Technology. Licentiate Thesis, No. 2029, 2026.

Chung-Hsuan Hu, *Wireless Federated Learning: Efficient Communication and Resource Management*, Linköping Studies in Science and Technology. Dissertations, No. 2498, 2026.

Jianan Bai, *Enabling Technologies for Latency-Critical Wireless Systems*, Linköping Studies in Science and Technology. Dissertations, No. 2481, 2025.

Zakir Hussain Shaik, *Distributed Signal Processing for Cell-Free Massive MIMO*, Linköping Studies in Science and Technology. Dissertations, No. 2418, 2024.

Daniel Pérez Herrera, *Communication-Efficient Scheduling Designs for Distributed Consensus and Optimization over Wireless Networks*, Linköping Studies in Science and Technology. Licentiate Thesis, No. 2004, 2024.

Oksana Moryakova, *Contributions to Efficient Design and Implementation of Variable Digital Filters*, Linköping Studies in Science and Technology. Licentiate Thesis, No. 2002, 2024.

Unnikrishnan Kunnath Ganesan, *Beyond Boundaries: Evolving Connectivity with Massive MIMO*, Linköping Studies in Science and Technology. Dissertations, No. 2395, 2024.

Olle Abrahamsson, *On Aggregation and Dynamics of Opinions in Complex Networks*, Linköping Studies in Science and Technology. Licentiate Thesis, No. 1990, 2024.

Ahmet Kaplan, *Signal Processing Aspects of Bistatic Backscatter Communication*, Linköping Studies in Science and Technology. Licentiate Thesis, No. 1989, 2024.

Ziya Gülgün, *GNSS and Massive MIMO: Spoofing, Jamming and Robust Receiver Design for Impulsive Noise*, Linköping Studies in Science and Technology. Dissertations, No. 2310, 2023.

FACULTY OF SCIENCE AND ENGINEERING

Linköping Studies in Science and Technology, Dissertations, No. 2517, 2026
Department of Electrical Engineering (ISY)

Linköping University
SE-581 83 Linköping, Sweden

www.liu.se

